TKK Dissertations 22
Espoo 2006

ULTIMATE STRENGTH OF HULL GIRDER FOR PASSENGER SHIPS

Doctoral Dissertation

Hendrik Naar

Helsinki University of Technology
Department of Mechanical Engineering
Ship Laboratory

TKK Dissertations 22
Espoo 2006

ULTIMATE STRENGTH OF HULL GIRDER FOR PASSENGER SHIPS

Doctoral Dissertation

Hendrik Naar

Dissertation for the degree of Doctor of Science in Technology to be presented with due permission of the Department of Mechanical Engineering for public examination and debate in Auditorium 216 at Helsinki University of Technology (Espoo, Finland) on the 10th of March, 2006, at 12 noon.

Helsinki University of Technology
Department of Mechanical Engineering
Ship Laboratory

Teknillinen korkeakoulu
Konetekniikan osasto
Laivalaboratorio

Distribution:
Helsinki University of Technology
Department of Mechanical Engineering
Ship Laboratory
P.O. Box 5300 (Tietotie 1)
FI - 02015 TKK
FINLAND
URL: http://www.tkk.fi/Units/Ship/
Tel. +358-(0)9-4511
Fax +358-(0)9-451 4173
E-mail: leila.silonsaari@tkk.fi

ISBN 951-22-8028-0
ISBN 951-22-8029-9 (PDF)
ISSN 1795-2239
ISSN 1795-4584 (PDF)
URL: http://lib.tkk.fi/Diss/2006/isbn9512280299/

TKK-DISS-2101

Picaset Oy
Helsinki 2006

HELSINKI UNIVERSITY OF TECHNOLOGY P. O. BOX 1000, FI-02015 TKK http://www.tkk.fi	ABSTRACT OF DOCTORAL DISSERTATION

Author Hendrik Naar

Name of the dissertation

Ultimate Strength of Hull Girder for Passenger Ships

Date of manuscript 12.09.2005	Date of the dissertation 10.03.2006
☒ Monograph	☐ Article dissertation (summary + original articles)

Department	Department of Mechanical Engineering
Laboratory	Ship Laboratory
Field of research	Strength of materials
Opponent(s)	Preben Terndrup Pedersen, Ivo Senjanović
Supervisor	Petri Varsta
(Instructor)	Petri Varsta

Abstract

The ultimate strength of the hull girder for large passenger ships with numerous decks and openings was investigated. The collapse of the hull girder, composed of the hull itself and the superstructure, as compared to a single deck ship with a continuous structure, involves several important structural phenomena that complicate understanding of this process. In this study, a theory of a non-linear coupled beam method was created. This method enables one to estimate the non-linear response of a passenger ship with a large multi-deck superstructure subjected to longitudinal bending. The method is based on the assumption that the ship structure can be modelled as a set of coupled beams. Each deck in the superstructure and also in the main hull can be considered as a thin-walled beam with non-linear structural behaviour. These beams are coupled to adjacent beams with non-linear springs called vertical and shear members, modelling the stiffness properties of the longitudinal bulkheads, side shells and pillars. Special emphasis was placed on the modelling of the shear members. A semi-analytic formula of the load-displacement curve was developed by help of the non-linear finite element analysis. Also, the load-end shortening curves under axial load taken from the literature were validated with the finite element method. The reverse loading options are included into the behaviour of the structural members. The created approach allows the calculation of the normal stresses and vertical deflections in the arbitrary location of the whole hull girder. Average longitudinal displacements and deflections of deck structures and shear stresses in the side structures can be estimated as well. The method is a further development of the linear coupled beam method. The ultimate strength of the hull girder was studied also with the non-linear finite element method. This required an investigation of the element mesh configuration in order to find an optimum mesh type and size. The prismatic hull girder of a post-Panamax passenger ship was chosen as a case study. The ultimate strength was estimated both in hogging and sagging loading with the coupled beam method and with the finite element method. The results of these two different methods, presented in the form of the bending moment versus the deflection of the hull girder, show good correlation up to the area where the moment starts to decrease. In both loading cases, the failure starts by the shear collapse in the longitudinal bulkhead. The ultimate stage of the strength was reached in the sagging loading when the failure progressed to the lower decks and correspondingly, in the hogging loading when the bottom structures failed in compression. The results on the structural failure modes show clearly that the shear strength of the longitudinal bulkheads and side structures is a very important issue on the ultimate strength problem of a passenger ship.

Keywords	coupled beam, finite element, superstructure, passenger ship, ultimate strength		
ISBN (printed)	951-22-8028-0	ISSN (printed)	1795-2239
ISBN (pdf)	951-22-8029-9	ISSN (pdf)	1795-4584
ISBN (others)		Number of pages	102
Publisher	Helsinki University of Technology, Ship Laboratory		
Print distribution	Helsinki University of Technology, Ship Laboratory		
☒ The dissertation can be read at http://lib.tkk.fi/Diss/2006/isbn9512280299/			

PREFACE

This research was carried out within the framework of the European Union project of Development of Innovative Structural Concepts for Advanced Passenger Ships (DISCO), (G3RD-CT2000-00290). The financial support by the European Commission is gratefully acknowledged.

I am grateful to my supervisor, professor Petri Varsta from Helsinki University of Technology for his encouragement, support and guidance that I have received over the years. The possibility to concentrate on my thesis work and good working conditions are acknowledged. I am also grateful to Dr. Pentti Kujala whose management work in Helsinki University of Technology and in the DISCO project made this thesis possible. His optimistic attitude is appreciated as well. Special thanks are due to Leila Silonsaari whose help in daily problems is recognised.

I would like to express my sincere thanks to professor Jaan Metsaveer from Tallinn University of Technology who provided support and was a source for many helpful discussions.

I would like to thank my colleagues and friends in Helsinki University of Technology: Heikki Remes, Kristjan Tabri, Jani Romanoff, Tommi Mikkola, Alan Klanac, and Sören Ehlers for their support, helpfulness and a pleasant working atmosphere.

I am grateful to my friend and colleague Meelis Mäesalu whose help and support is greatly appreciated. Also, I would like to thank my friend Juha Schweighofer whose knowledge and research experience, endless optimism, and a very good sense of humour helped me during hard times and were a source of strength for this task.

Aker Finnyards is thanked for providing information of the structural design of a post-Panamax passenger ship. Special thanks are due to Ari Niemelä and Juhani Siren for their assistance.

MEC-Insenerilahendused is thanked for providing the hardware and software for analyses, especially in the final stage of the thesis.

Finally, I would like to thank my wife, Rista, and my son Mikk, for their encouragement during the entire project, especially in the final stage of the preparation of this thesis.

Tallinn, December 2005

Hendrik Naar

TABLE OF CONTENTS

LIST OF SYMBOLS

A_e	net section area of stiffener
A_{ii}	cross-section area of beam i
A_{ii}^S	effective cross-section area in shear
A_S	cross-section area of a stiffener
$a_1 \ldots a_4$	constants
$B(\xi)$	shape function
$[B_u]$	shape functions matrix of axial displacement
$[B_v^M]$	shape functions matrix of deflection induced by bending deformation
$[B_v^Q]$	shape functions matrix of deflection induced by shear deformation
b	breadth of the plate strip
b_e	effective breadth of the plate
C_{ij}	coupling distance for beam i attached to beam j
C_0	stiffness constant
$c_1 \ldots c_m$	constants
$\{c_v^M\}$	vector of constants for deflections induced by bending deformation
$\{c_v^Q\}$	vector of constants for deflections induced by shear deformation
$\{c_u\}$	vector of constants for axial displacements
d_{ik}	coupling distance for beam i attached to beam k, where $k > i$
$[D]$	tangent stiffness matrix for the total coupled system
E	Young's modulus
E_t	tangent modulus of the strength member
EA_{ii}^t	axial tangent stiffness of beam i
EI_{ii}^t	bending tangent stiffness of beam i
EX_{ii}^t	cross-term tangent stiffness of beam i
e_{ij}	coupling distance for beam i attached to beam j, where $j < i$
$\{F\}$	external force vector for the coupled system
$\{F^A\}$	internal force vector for the coupled system

$\{F^B\}$ coupling force vector for the coupled system

G shear modulus

$GA_{ii}^{S,t}$ tangent shear stiffness of beam i

H_{ij} effective height of shear member for coupling between beams i and j

I_{ii} moment of inertia of beam i

I_p net polar moment of inertia

I_t St Venant's net moment of inertia

I_w sectional moment of inertia

i, j, k integers

k_i shear factor for cross-section of beam i

K_{ij} vertical elongation stiffness of coupling between beams i and j

K_{ij}^t tangent stiffness of vertical elongation for coupling between beams i and j

$K_{ij}^{A,t}$ modified vertical tangent elongation stiffness matrix

L total length of ship

l span

M_i bending moment in beam i

m_i number of strength members in the cross-section of beam i

N_i axial force in beam i

n number of beams used in the ship cross-section

$\{P\}$ resultant vertical coupling force vector

p_{ij} vertical distributed coupling force between beam i and j

Q_i shear force in beam i

q_i external distributed load for beam i

r_1, r_2 shape parameters for a modified edge function

$\{S\}$ resultant longitudinal shear flow vector

$\{S^C\}$ resultant longitudinal shear flow vector weighted with coupling distance

s_{ij} shear flow between beam i and j

T_{ij} shear stiffness of coupling between beams i and j

T_{ij}^t tangent shear stiffness of coupling between beams i and j

$T^{A,t}, T^{B,t}, T_{ij}^{C,t}$	modified shear tangent stiffness matrices
t	plate thickness
u_i	axial displacement of beam i
v_i	total deflection of beam i
v_i^M	deflection of beam i induced by bending deformation
v_i^Q	deflection of beam i induced by shear deformation
x	local axial co-ordinate for a beam
X_{ii}	first moment of area of beam i with respect to reference line
y	local vertical co-ordinate for a beam
Δ	increment
δ^u	relative axial displacement
δ^v	relative deflection
β	slenderness parameter
ε	axial strain
ε_R	relative strain
Φ	edge function
κ	wave parameter for shape functions
λ	load proportionality factor
σ	normal stress
σ_C	critical stress
σ_E	elastic buckling stress
σ_{CP}	buckling stress of attached plating
σ_{CR}	averaged stress in a member
σ_Y	yield stress
τ	shear stress
ξ	dimensionless co-ordinate

ORIGINAL FEATURES

A modern passenger ship is a complex structure containing all essential facilities for convenient voyage and at the same time capable of sustaining safely possible extreme sea loads. Passenger ships are multi-layer structures, creating an idea that if the hull girder strength is ensured, no need exists to study the ultimate strength problem in detail. So far no studies have been reported that could prove this approach. The present work concentrates on the behaviour of large passenger ships in load cases, where the hull girder reaches its ultimate stage.

The following features of this thesis are believed to be original:

1. The non-linear equations of the Coupled Beams (CB) method for multi-deck structures were developed and are presented. The method is based on the assumption that the ship structure can be modelled as a set of coupled beams.

2. The coupled beams method enables one to estimate not only the ultimate strength of the hull girder, but also its deflections, average strains and stresses for the whole loading path.

3. The structural members describing coupling in shear between beams were developed to consider the behaviour of stiffened plate panels.

4. The reverse loading was included into the structural members of the CB-method.

5. The ultimate hull girder strength of a post-Panamax passenger ship was estimated both for hogging and for sagging loading conditions with the developed CB-method, taking into account the possibility of shear and compression collapse in the stiffened plate panels of the hull girder.

6. The non-linear finite element analyses included an estimation of the proper mesh used for the analysis of the ultimate strength of the hull girder composed of stiffened plate panels.

7. The prismatic type Finite Element model was analysed on a full scale both in the sagging and hogging loading conditions. The buckling of deck, bottom and bulkheads structures in compression and in shear were considered. As a result, the Finite Element Analyses allowed for a description of the collapse behaviour of the hull girder as a function of the deflection both in the hogging and sagging loading cases. The results were exploited in the validation of the CB-method.

1 INTRODUCTION

1.1 GENERAL

During the last decades, passenger ships have seen drastic changes. The superstructure volume in relation to that of a hull has increased significantly due to a growing need for open spaces in restaurants, theatres and atriums. Also, the size of ships has increased, based on the advantage offered by the scale of economy. This all has caused a concern of whether the global longitudinal strength of the hull girder is sufficient. A modern passenger ship is a complicated structure, which has a high and long superstructure with several decks supported by pillars, longitudinal and transverse bulkheads on the hull, see Figure 1. The complexity of structural behaviour is increased by large openings in the longitudinal structures and by the need to transfer internal loads from one longitudinal structure to another, for instance, in the area of lifeboat recess.

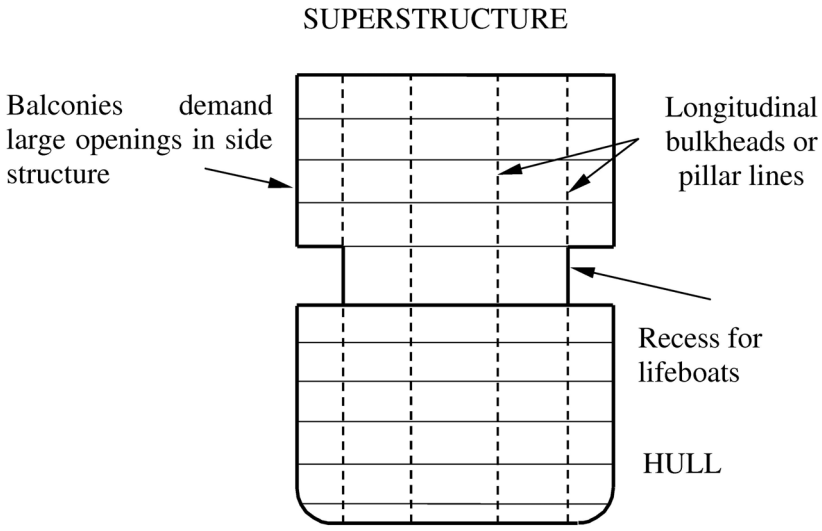

Figure 1. Modern passenger ship's cross-section of the hull girder composed of the hull and superstructure.

Due to this complex structural behaviour, the ultimate strength of the passenger ship is hardly predictable. Today, no information is available about this phenomenon. The design codes for passenger ships are based on elastic analysis, where buckling, yield or fatigue limits determine scantlings. This approach inherently implies an assumption that there exists an excessive ultimate strength capacity in the hull girder. This situation results from structural considerations, i.e. a modern passenger ship hull with a superstructure is a high beam with numerous decks, which can produce a sufficient internal moment even when some of the decks have collapsed. However, a

typical superstructure has low shear stiffness, reducing the effect of the upper decks in the longitudinal bending. In addition, the shear buckling reduces this shear stiffness and as a result, the shear lag effects become stronger. Thus, the structure may collapse at the load level close to the design load. The loads at see are caused by the forces of nature and are statistically determined, therefore the ship can sail into waves, where the design bending moment may be exceeded. Consequently, in order to keep safety at an acceptable level, a better understanding of the ultimate strength of a passenger ship is required.

Today a practical tool to solve the response of a passenger ship is the three-dimensional (3D) Finite Element (FE) method. However, the drawback of this method is that it is time-consuming, moreover, it is difficult to acquire a deeper understanding of the structural behaviour. A prismatic non-linear FE-model of the passenger ship can be created in two or three weeks. If the interest lies only in the linear behaviour, the computation time can be measured in hours. For the ultimate strength analysis, the corresponding time will extend to weeks. Additionally, the time spent on creating the proper mesh must be included, as certain structural components need a very dense mesh. Therefore, simplified and fast analytic methods are useful in the concept design stage and also to improve the physical understanding.

1.2 SCOPE OF THE WORK

The background of the present work is based on the linear theory meant for the estimation of the hull girder response of ships with large superstructures. This theory called the Coupled Beams (CB) method is presented in reference Naar et. al. [23]. In the present work, this theory was enlarged in order to cover also the ultimate strength of the hull girder composed of stiffened panels. This method allows for a better explanation of the effects of various parameters on the ultimate strength of the hull girder in the passenger ships. Also, a practical requirement set up was that the method should be fast and easy to use.

The basic beam theory is not directly applicable to the problem of hull girder bending in the case of ships with a large superstructure. This fact is due to the axial bending strains, which are non-linearly distributed in the cross-section of the hull girder. The CB-method approximates these strains with a piecewise linear and non-continuous distribution. According to the CB-method, the whole structural behaviour can be described with so-called coupled beams. For this purpose, the whole ship's cross-section was divided into beams, presenting the structural components participating in the longitudinal strength of the hull girder. Each beam was coupled to neighbouring beams with distributed springs, presenting the side shells, pillars, and longitudinal bulkheads and

transferring the loads between different decks. These distributed springs were named also as vertical elongation and longitudinal shear members.

The non-linear CB-method required some additional assumptions to enable the loading up to the ultimate strength of the hull girder. The stiffness of beams and coupling springs might be reduced locally due to the structural collapse during the loading. These springs were assumed also to behave non-linearly. Thus, the assumption of a non-prismatic beam must be applied. The stiffness of beams and couplings is based on the relation between the normal stress and strain called also as the load-end shortening curve. These curves can be determined analytically, based on the literature. However, the relation of stress-strain curves in shear must be separately studied due to lack of knowledge in the literature. Thus, in the present study, emphasis was placed on the development of the shear members. The determination of axial and bending stiffness for each individual beam in the cross-section is based on the method presented by Smith [35], where the linear strain distribution in the cross-section is assumed. To solve this non-linear problem, an incremental approach was needed.

The aim of the thesis was also to study the ultimate strength of the hull girder of a large passenger ship. Up to now, mainly single-deck ships have been studied. Thus, there is lack of knowledge about the structural behaviour of large passenger ships under extreme conditions. The non-linear Finite Element (FE) method offered the only tool for the validation, as no ultimate strength test results for hull girders of passenger ships exist. However, the calculation resources, especially for non-linear FE-analyses, are normally limited. To obtain reliable results, a large amount of basic knowledge for the FE-modelling is required. For example, the global FE-model has to be refined in critical structural areas and thus, several local test structures with various mesh combinations have to be analysed to determine the collapse modes. The FE-method was also used for the validation of the behaviour of stiffened panels in compression and in shear needed in the CB-method.

As the object of the case study, an actual post-Panamax passenger ship was chosen. It had all the typical structural features present in modern passenger ships. The hull and the superstructure were of equal length and had prismatic geometry and thus, the effect of the fore and after body structures was not considered. In addition to this, local structural strengthening outside the midship region was not included. The shape of the external loading of the hull girder was based on the classification society's rules. The problem was considered as quasi-static. This case study was intended to point out that the low shear stiffness of typical post-Panamax passenger ships, see reference Naar et. al. [23], might reduce remarkably the ultimate strength in bending. Therefore, the relevant ultimate strength estimation could not be done without taking into consideration the shear strength.

1.3 STATE OF ART

Full-scale tests will probably produce information that would be most valuable to describe the ultimate behaviour of ship structures. Unfortunately these are difficult and extremely expensive to conduct. Therefore, only few tests have been conducted with full-scale ships and little data are available. Vasta [38] analysed several full-scale tests that have been carried out in the past. He made many important conclusions. According to the test results, the hull girder of a ship with deckhouses does not behave according to the simple beam theory. Normal stresses may not reach their maximum at the top deck. Vasta claimed also that the deckhouse-hull interaction depended on several factors, such as on the relative stiffness of the hull and superstructure and on the spring stiffness between them. Also, the length of the deckhouse was an important parameter.

In contrast to full-scale tests, numerous small-scale tests have been conducted, such as those by Dowling [13], Dow [12], Reckling [33], Ostapenko [26], and Mansour et al. [21]. These can be divided into ultimate strength tests done with exact small-scale models and those done with stiffened box-girders. The small scale-tests do not correspond exactly to real ship structures, as the scaling of dimensions and material properties is difficult. Also, the option of several decks is not considered. However, the results are still of great importance, as they improve the understanding of the failure mechanisms and offer a possibility for validation with theoretical models.

The linear response of the multi-layer structure is one of the sub-problems when studying the ultimate strength of the passenger ship. Main attention in linear analysis has to be paid to the shear lag effects, hull-superstructure interaction and to the large side openings. At present, two basic approaches exist to estimate the linear response of a ship with a superstructure in the longitudinal bending. These are based on the beam or on the plane stress theory. An excellent literature survey has been made by de Oliveira [25]. Crawford [8] was the first to develop a method based on the two-beam theory, taking into account the longitudinal shear force and vertical force due to the hull-superstructure interaction. Bleich [4] has presented a similar approach, which proposes a straightforward computation of stresses for prismatic beams. Terazawa and Yagi [36] introduced the shear lag correction to the two-beam theory. The stresses were calculated by the energy approach and by assuming certain stress patterns for the structure. Terazawa and Yagi also considered the effect of side openings on the structural behaviour. A further development of Bleich's idea based on the coupled beam approach was presented by Naar et. al. [23]. There, the whole cross-section is divided into beams coupled to each other with distributed springs. In addition to the beam methods, there exists another approach for the estimation of the ship hull and

superstructure interaction. This is based on the plane stress theory and it enables one to include the shear lag phenomenon in the response model, see Caldwell [5] and Fransman [14].

Several direct methods have been developed to estimate the ultimate strength of single deck ship girders. Based on an assumed stress distribution, Caldwell [6] obtained the ultimate strength of a hull girder under longitudinal bending. He proved that the buckling strength of stiffened panels has an important influence on the ultimate strength. Similar methods have been developed by Nishihara [24], Mansour et al. [21] and Paik & Mansour [27]. Smith [35] demonstrated that the strength reduction of stiffened panels beyond the ultimate load plays an important role in the ultimate strength of hull girders. In this method, the cross-section of the hull girder was divided into plate-stiffener members. In addition, average stress-strain relations were provided for each member in the progressive collapse analysis of the cross-section. Several modifications and applications of the Smith's method are available, see references Ostapenko [26], Gordo and Guedes Soares [16], Gordo et al. [17], Beghin and Jastrzebski [3], and Yao and Nikolov [40].

The FE-method offers several possibilities for analysing the ultimate strength problem. The material behaviour can be considered in a more exact way. Geometrically non-continuous structures can be well described. The effect of stiffeners can be taken into account with a high accuracy. The material fracture and the contact between elements can be modelled as well. In their paper, Kutt et al. [20] used the FE-method to estimate the ultimate longitudinal strength for four different types of ship structures.

The Idealised Structural Unit Method (ISUM) is another example of a simplified approach. The basic idea of the ISUM is to exploit large structural units in the element mesh. This reduces significantly the computation time. The elements must be able to describe the influence of buckling and yielding. Ueda et al. [37] have proposed the elements of an idealised plate and a stiffened plate, accurately simulating the buckling and plastic collapse under combined bi-axial compression, tension and shear loads. Similar approaches and their applications are presented in references Paik & Lee [28], Paik [29], Paik et al. [30], Paik [31], and Bai et al. [1].

Today's simplified incremental methods to estimate the ultimate strength of hull girders are mostly suitable for single deck ships, as there the bending strains are linearly distributed in the ship's cross-section. In the case of passenger ships, this is not necessarily valid. Therefore, together with the FE-method the only approach that can be directly applied might be the ISUM. However, both methods are fully numerical and need experience and much time for model construction and analysis. The plane stress theory seems to be very potential in order to determine stresses and deflections in the structure. However, in the case of the ultimate strength analysis, the plane stress theory may produce difficulties, as the stiffness parameters of the ship cross-section will change in

the case of structural buckling or yield. In conclusion, it can be claimed that the beam-based methods, such as developed by Bleich [4], are most promising. These allow for the estimation of stresses and deflections and inclusion of non-linear effects caused by structural collapses. In addition, some ideas from the routines developed, like Smith's approach [35], can be made good use of.

2 NON-LINEAR COUPLED BEAM THEORY

2.1 EQUILIBRIUM EQUATIONS FOR A BEAM

Each beam in a coupled system has to satisfy the force and moment equilibrium. In the segment of beam i presented in Figure 2, internal forces, coupling forces and external loads are acting. The internal forces are well known from the basic beam theory. These are axial force N_i, shear force Q_i and bending moment M_i acting in the cross-section. The coupling forces are composed of the vertical distributed force p_{ij} and the longitudinal shear flow s_{ij}, where the subscripts describe the interaction of beam i with its adjacent beam j. The only external force is the distributed vertical line load q_i, which arises from the load induced by weights and water pressure. The position of the reference line, see Figure 2, is fixed to the deck and it can differ from the centroid of the cross-section. In Figure 2 it is assumed that the coupling is affecting the upper and lower edge. The distances from the reference line to the upper and lower edge of the beam are therefore denoted by d_{ik} and e_{ij}. In general, these distances define the vertical position of coupling between beam i and adjacent beams j and k.

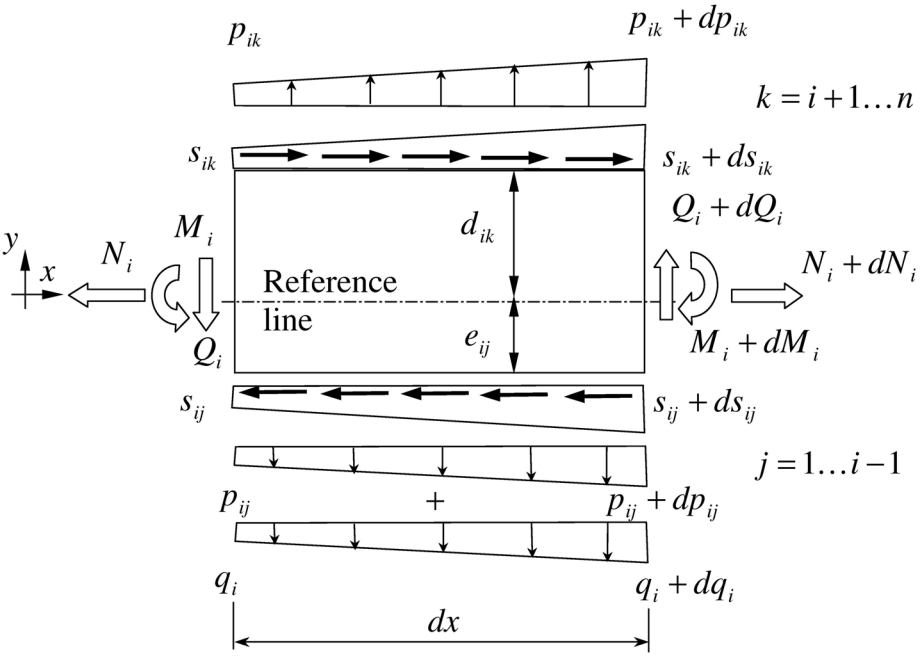

Figure 2. Segment of beam i with internal forces, coupling forces and external load.

In the simplest case, the coupling between beams is vertical, as shown in Figure 3, where an arbitrary deck is coupled only with the upper and lower neighbor. However, for more sophisticated ship structures, a mixed coupling is needed, where the cross-section is divided into beam sections not only in the vertical direction, but for some decks also in the horizontal direction, see Figure 3.

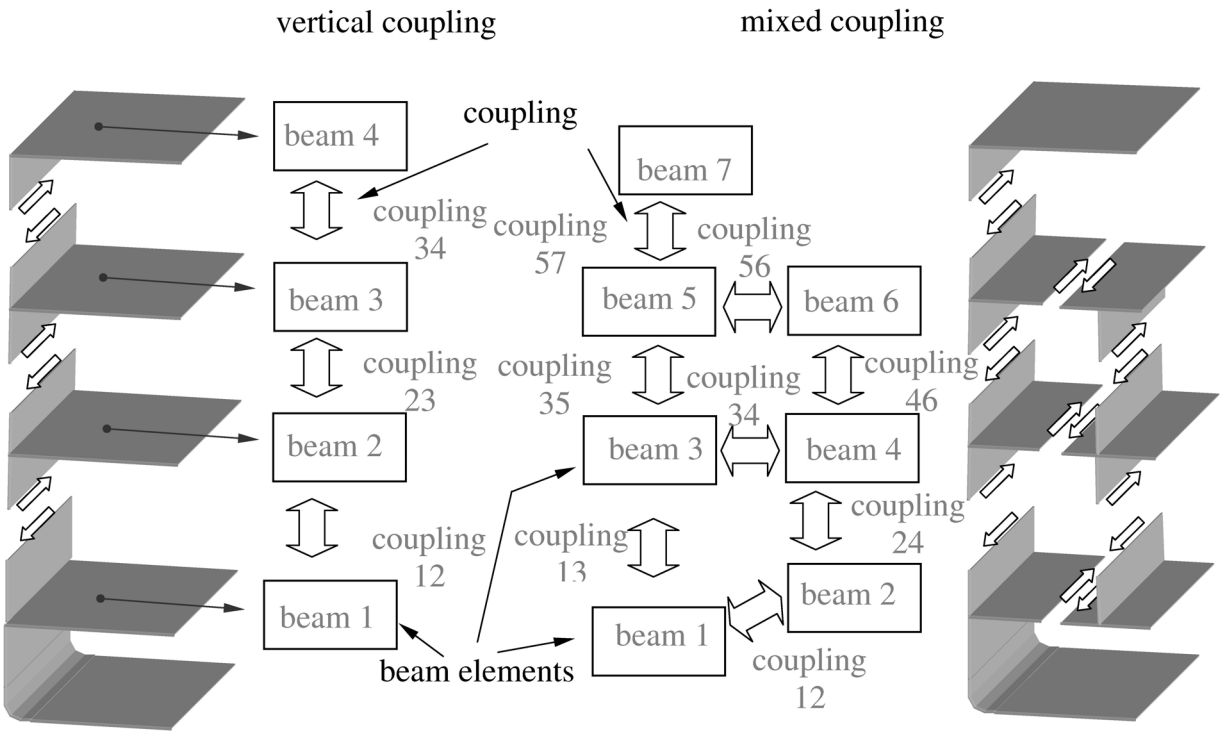

Figure 3. Types of coupling between beams.

Mixed coupling affects the equilibrium equations. In vertical coupling, the beam has two coupling forces as the maximum, one in the upper and another in the lower layer of the beam. In the case of a mixed coupling, the total coupling force for a beam segment can be a sum of more than two individual coupling forces. The following equilibrium equations are written so that an arbitrary coupling could be used. The equation of longitudinal equilibrium for beam i with n couplings is therefore

$$\frac{\partial N_i}{\partial x} + \sum_{j=1}^{n} s_{ij} = 0\,, \tag{1}$$

where the shear force matrix s_{ij} is

$$s_{ij} = \begin{cases} s_{ij} & if \quad j > i \\ 0 & if \quad j = i \\ -s_{ji} & if \quad j < i. \end{cases} \tag{2}$$

The equilibrium of vertical forces gives

$$\frac{\partial Q_i}{\partial x} + \sum_{j=1}^{n} p_{ij} = q_i\,, \tag{3}$$

where q_i is the external force vector and p_{ij} is the matrix of vertical coupling forces

$$p_{ij} = \begin{cases} p_{ij} & if \quad j > i \\ 0 & if \quad j = i \\ -p_{ji} & if \quad j < i. \end{cases} \tag{4}$$

If beams are vertically coupled, the matrices (2) and (4) have values only at diagonals next to the main diagonal. The equilibrium of moments about z-axis gives

$$\frac{\partial M_i}{\partial x} - Q_i + \sum_{j=1}^{n} C_{ij} s_{ij} = 0\,, \tag{5}$$

where matrix C is

$$C_{ij} = \begin{cases} d_{ij} & if \quad j > i \\ 0 & if \quad j = i \\ -e_{ij} & if \quad j < i. \end{cases} \tag{6}$$

After differentiation of Eq. (5) and substitution of Eq. (3), the relation can be written as

$$\frac{\partial^2 M_i}{\partial x^2} + \sum_{j=1}^{n} p_{ij} + \frac{\partial}{\partial x}\left(\sum_{j=1}^{n} C_{ij} s_{ij} \right) = q_i , \tag{7}$$

The second summation term in Eq. (7) corresponds to the moment caused by the longitudinal shear flows $s_{i,j}$.

To estimate the ultimate strength, the non-linear behaviour of structures has to be considered. Therefore, equilibrium Eqs. (1), (3) and (7) must be given in an incremental form, see Appendix A, where the derivation is given. For the axial equilibrium, the incremental form is

$$\frac{\partial \Delta N_i}{\partial x} + \sum_{j=1}^{n} \Delta s_{ij} = 0 . \tag{8}$$

For the vertical equilibrium,

$$\frac{\partial \Delta Q_i}{\partial x} + \sum_{j=1}^{n} \Delta p_{ij} = \Delta\lambda \cdot q_i , \tag{9}$$

where $\Delta\lambda$ is the load proportionality factor for the load increment. The incremental equilibrium of moments about z axis gives

$$\frac{\partial^2 \Delta M_i}{\partial x^2} + \sum_{j=1}^{n} \Delta p_{ij} + \frac{\partial}{\partial x}\left(\sum_{j=1}^{n} C_{ij} \Delta s_{ij} \right) = \Delta\lambda \cdot q_i . \tag{10}$$

As the co-ordinate system is fixed to the reference line, which differs from that of the neutral axis, the matrix C_{ij} is constant during the loading.

2.2 RELATIONS BETWEEN INTERNAL FORCES AND DISPLACEMENTS

2.2.1 Bending and axial force due to displacements

Using the beam theory, the relations between the internal forces and the displacements are defined so that the axial strain in the cross-section of the beam varies linearly. If the axial displacement u_i and the deflection induced by the bending deformation v_i^M are known for beam i, then the bending moment M_i is, see Crisfield [9]

$$M_i = (-1)EI_{ii}\frac{\partial^2 v_i^M}{\partial x^2} + EX_{ii}\frac{\partial u_i}{\partial x}, \tag{11}$$

where E is the Young's modulus of the material, I_{ii} is the moment of inertia and X_{ii} is the first moment of the area of beam i calculated with respect to the reference axis. In the same way, the axial internal force in beam i is approximated as

$$N_i = EA_{ii}\frac{\partial u_i}{\partial x} + (-1)EX_{ii}\frac{\partial^2 v_i^M}{\partial x^2}, \tag{12}$$

where A_{ii} is the cross-section area of beam i.

Also, those relations must be presented in the incremental form due to the non-linear behaviour. Therefore, the incremental increase of the bending moment due to the deflection and axial displacement is

$$\Delta M_i = (-1)EI_{ii}^t\frac{\partial^2 \Delta v_i^M}{\partial x^2} + EX_{ii}^t\frac{\partial \Delta u_i}{\partial x}, \tag{13}$$

where EI_{ii}^t and EX_{ii}^t are now tangent stiffness values. In a similar way, the relation for the axial force increment is expressed as

$$\Delta N_i = EA_{ii}^t\frac{\partial \Delta u_i}{\partial x} + (-1)EX_{ii}^t\frac{\partial^2 \Delta v_i^M}{\partial x^2}, \tag{14}$$

where EA_{ii}^t is the axial tangent stiffness of the beam. The derivation of tangent stiffness parameters is given below in Chapter 3.3.

2.2.2 Shear force due to deflection

The shape of the hull girder deflection for a modern passenger ship, see Fransman [14], proves that shear deformations are important. The ratio between the length and the height of the hull girder is close to six in these ships. According to the beam theory, the shear deformation is important when the ratio is less than ten. Therefore, the present method must consider also the deflections induced by the shear deformations. The relation between shear force Q_i and deflection due to shear v_i^Q is

$$Q_i = GA_{ii}^S \cdot \frac{\partial v_i^Q}{\partial x}, \tag{15}$$

where G is the shear modulus of the material, A_{ii}^S is the effective cross-section area of the beam in shear. The typical cross-section of a beam is shown in Figure 4, where the shear area of the cross-section A_{ii}^S consists of the vertical plating of that. This approach for describing shear stiffness is also proposed for an I-beam and box beam by Gere & Timoshenko [15]. Comparing these cross-sections to those presented in Figure 3, a conclusion can be drawn that as a first estimation, this approach is possible. The shear stiffness k_i can be expressed more accurately on the basis of the shear factor

$$k_i = \frac{A_{ii}}{Q^2} \int_A \tau_i^2 dA, \tag{16}$$

where τ_i is the shear stress in the cross-section of beam i. However, this stress depends on the unknown shear flow values at the lower and upper edge of the beam, see Figure 4. Thus, the solution procedure of the CB-method would become non-linear with respect to the shear factor. A rough study of the shear factor Eq. (16) indicates that the simplified shear factor given as A_{ii} / A_{ii}^s-ratio differs from the exact value by 20 % at the maximum. In the incremental form, Eq. (15) can be presented as

$$\Delta Q_i = GA_{ii}^{S,t} \cdot \frac{\partial \Delta v_i^Q}{\partial x}, \tag{17}$$

where $GA_{ii}^{S,t}$ is the tangential shear stiffness.

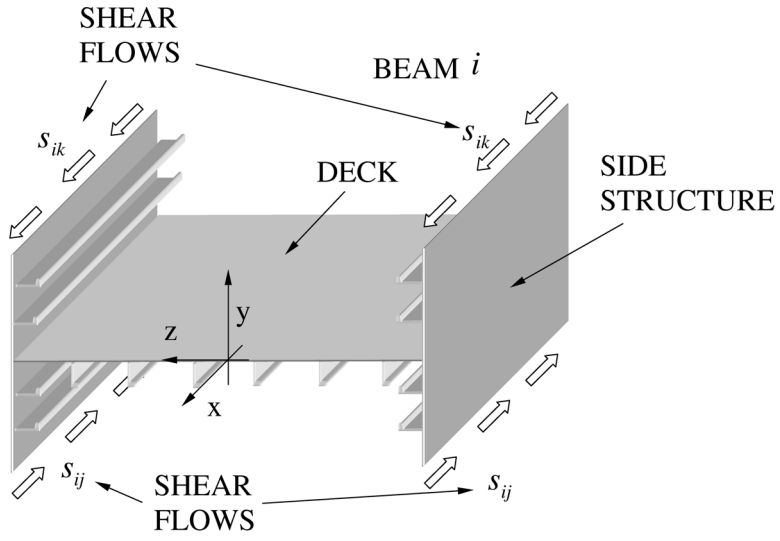

Figure 4. Typical cross-section of a beam used in the CB-method.

2.2.3 Forces caused by shear coupling

The coupling equations define the interaction between the beams. According to the presented assumption, the shear and the vertical coupling are considered important. The shear coupling between beams i and j is shown in Figure 5. In the case of linear structural behavior, the shear member with shear stiffness T_{ij} and relative displacement δ_{ij}^{u} causes shear flow s_{ij} between the beams, see Naar et al. [23]. This shear flow is assumed to be constant over length dx and thus, the force can be described as the response of distributed horizontal springs. The shear stiffness depends on the effective height H_{ij} of the shear member and of the effective shear area. In the case presented in Figure 5, the effective height equals the deck spacing.

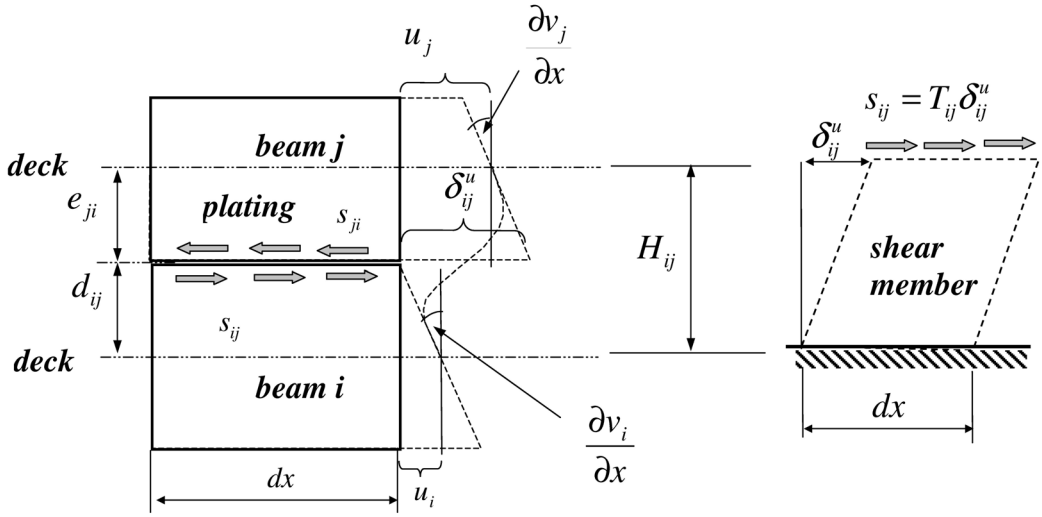

Figure 5. Shear coupling between beams.

The relative displacement between beam i and j can be obtained through the axial displacement u and the bending induced deflection v^M of the beams as follows:

$$\delta_{ij}^{u} = u_j + e_{ji} \cdot \frac{\partial v_j^M}{\partial x} - u_i + d_{ij} \cdot \frac{\partial v_i^M}{\partial x}. \tag{18}$$

By taking into account Eq. (6), this relative displacement becomes

$$\delta_{ij}^{u} = u_j - C_{ji} \cdot \frac{\partial v_j^M}{\partial x} - u_i + C_{ji} \cdot \frac{\partial v_i^M}{\partial x}. \tag{19}$$

If the structural behaviour is non-linear, the shear flow s_{ij} can be given also as a function of relative displacement

$$s_{ij} = s_{ij}\left(\delta_{ij}^{u}\right). \tag{20}$$

The incremental form of Eq. (20) is obtained by differentiating by parts with respect to displacement u_i and deflection v_i^M. At this point, one should note that the term C_{ij} is constant. Therefore,

$$\Delta s_{ij} = T_{ij}^{t}\left(\Delta u_j - C_{ji}\cdot\frac{\partial\Delta v_j^M}{\partial x} - \Delta u_i + C_{ij}\cdot\frac{\partial\Delta v_i^M}{\partial x}\right), \tag{21}$$

where T_{ij}^{t} is now the longitudinal tangent shear stiffness

$$T_{ij}^{t} = \begin{cases} T_{ij}^{t} & if \quad j \neq i \\ 0 & if \quad j = i. \end{cases} \tag{22}$$

2.2.4 Forces caused by vertical coupling

Another coupling type is the vertical coupling of the beams. This becomes substantial when the superstructure is weakly supported. Thus, the curvature of the upper structure differs from that of the supporting structure, as shown in Figure 6. This phenomenon was well described by Bleich [4].

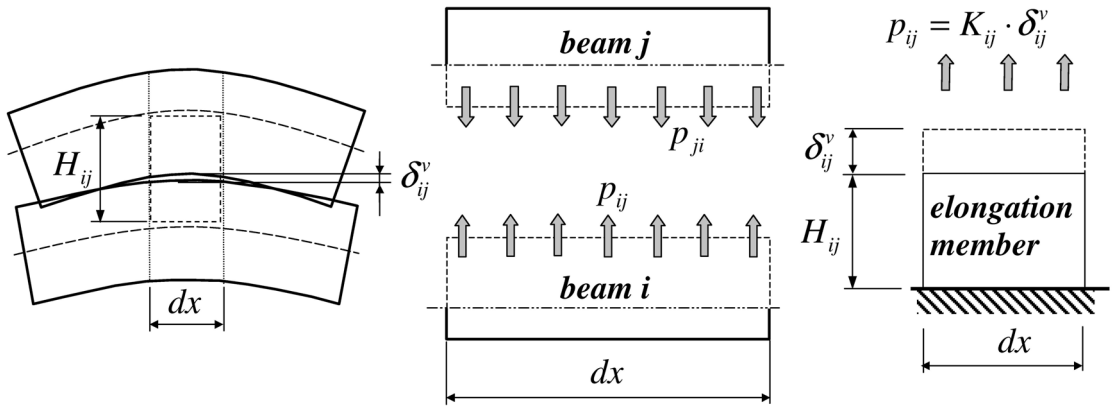

Figure 6. Vertical coupling between beams.

According to Bleich, the vertical coupling force p_{ij} depends on the vertical elongation stiffness K_{ij} and on the relative deflection δ_{ij}^{v}, which is approximated by the difference between beam deflections v_i and v_j as follows:

$$\delta_{ij}^{v} = v_j - v_i . \tag{23}$$

If the elongation member behaves non-linearly, the vertical coupling force is as in Eq. (20) a function of relative deflection δ_{ij}^{v}

$$p_{ij} = p_{ij}\left(\delta_{ij}^{v}\right). \tag{24}$$

The coupling force increment is then again obtained by differentiating Eq. (24) by parts with respect to deflection variables v_i^M and v_i^Q. Accordingly,

$$\Delta p_{ij} = K_{ij}^{t}\left(\Delta v_j - \Delta v_i\right), \tag{25}$$

where K_{ij}^{t} is now the tangent stiffness of the vertical coupling. The tangent stiffness matrix for all coupling members is expressed by

$$K_{ij}^{t} = \begin{cases} K_{ij}^{t} & if \quad j \neq i \\ 0 & if \quad j = i. \end{cases} \tag{26}$$

2.3 TANGENT STIFFNESS MATRIX FOR A COUPLED SYSTEM

The tangent stiffness matrix of the hull girder was needed for the non-linear progressive collapse analysis. It describes the relations between the displacement increments and external load increment and it has to be updated during the calculation.

The set of the equilibrium equations consists of Eqs. (8), (9) and (10) given in the incremental form. The unknown variables are the incremental axial displacement vector Δu, the incremental beam deflection vector due to bending Δv^M and due to shear Δv^Q. The tangent stiffness matrix was derived with Galerkin's method. There, the dimensionless co-ordinate ξ was used in the integration. This co-ordinate is related to a ship's longitudinal co-ordinate x as

$$\xi = (x - L/2)/(L/2), \tag{27}$$

where L is the total length of the ship. The boundary conditions for a single beam are shown in Figure 7. It is assumed that no internal forces exist at the beam boundaries $\xi = -1$ and $\xi = 1$. This is due to the vertical line load, which is self-balanced. Thus, there are no supports needed at the boundaries.

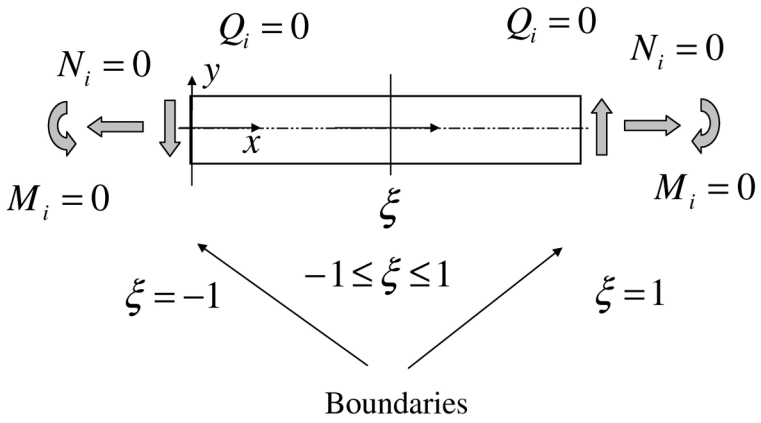

Figure 7. Boundary conditions for the single beam.

As the internal forces will vanish at the boundaries, it can be concluded that the incremental forces have to do the same. The functional form of equations required by Galerkin's method was obtained by multiplying the equilibrium equations with the weight function and by integrating the result over the beam length. Therefore, the axial equilibrium equation, see Eq. (8), will obtain the form

$$\int_{-1}^{1} u_i \frac{\partial \Delta N_i}{\partial x} d\xi + \int_{-1}^{1} u_i \sum_{j=1}^{n} \Delta s_{ij} d\xi = 0, \tag{28}$$

where u_i is the unknown axial displacement considered as the weight function. Similarly, the equation describing vertical force equilibrium, see Eq. (9) is

$$\int_{-1}^{1} v_i^Q \frac{\partial \Delta Q_i}{\partial x} d\xi + \int_{-1}^{1} v_i^Q \sum_{j=1}^{n} \Delta p_{i,j} d\xi = \int_{-1}^{1} v_i^Q \Delta\lambda \cdot q_i d\xi, \tag{29}$$

where v_i^Q is the weight function. The incremental moment equilibrium, see Eq. (10), can be expressed by

$$\int_{-1}^{1} v_i^M \frac{\partial}{\partial x}\left(\frac{\partial \Delta M_i}{\partial x} + \sum_{j=1}^{n} C_{ij} \cdot \Delta s_{ij} \right) d\xi + \int_{-1}^{1} v_i^M \sum_{j=1}^{n} \Delta p_{ij} d\xi = \int_{-1}^{1} v_i^M \Delta\lambda \cdot q_i d\xi, \tag{30}$$

where v_i^M is the corresponding weight function. By integrating Eqs. (28), (29) and (30) by parts, the boundary conditions can be used and the resulting equations will have symmetric form. The

unknown displacements were approximated as the linear combination of the known shape functions $B(\xi)_1 \ldots B(\xi)_m$ and unknown constants $\Delta c_1 \ldots \Delta c_m$. Thus, the displacement increments are

$$\{\Delta u\} = [B_u]\{\Delta c^u\}, \tag{31}$$

$$\{\Delta v^Q\} = [B_v^Q]\{\Delta c_v^Q\} \tag{32}$$

and

$$\{\Delta v^M\} = [B_v^M]\{\Delta c_v^M\}, \tag{33}$$

where Eq. (31), for example, can be written in an open form as

$$\begin{Bmatrix} \Delta u_1 \\ \vdots \\ \Delta u_n \end{Bmatrix} = \begin{bmatrix} B(\xi)_1 & \cdots & B(\xi)_m & \cdots & 0 & \cdots & 0 \\ \vdots & \ddots & \vdots & \ddots & \vdots & \ddots & \vdots \\ 0 & \cdots & 0 & \cdots & B(\xi)_1 & \cdots & B(\xi)_m \end{bmatrix} \begin{Bmatrix} \Delta c_1^{u_1} \\ \vdots \\ \Delta c_m^{u_1} \\ \vdots \\ \Delta c_1^{u_n} \\ \vdots \\ \Delta c_m^{u_n} \end{Bmatrix}. \tag{34}$$

Thus, the stiffness matrix in a compact form will be

$$\begin{bmatrix} D_{11} & D_{12} & 0 \\ D_{12}{}^T & D_{22} & D_{23} \\ 0 & D_{23}{}^T & D_{33} \end{bmatrix} \begin{Bmatrix} \Delta c_u \\ \Delta c_v^M \\ \Delta c_v^Q \end{Bmatrix} = \Delta\lambda \begin{Bmatrix} 0 \\ F^M \\ F^Q \end{Bmatrix}, \tag{35}$$

where the derivation of the sub-matrices $[D_{ij}]$ and sub-vectors $\{F^M\}$, $\{F^Q\}$ are presented in more detail in Appendix A.

2.4 EQUILIBRIUM EQUATIONS FOR A COUPLED SYSTEM

In the present approach, the arc-length method was applied and thus, the equilibrium equations for the coupled system were used to correct the solution approximated with tangent stiffness. Before the new load increment is applied, the internal forces N_i, M_i, Q_i, the coupling forces s_{ij}, p_{ij} and the external load $\lambda \cdot q_i$ are in equilibrium. The new equilibrium state has to be

reached after the increase of the external load $(\lambda + \Delta\lambda) \cdot q_i$. This is possible only if the internal forces and coupling forces have incremental changes ΔN_i, ΔM_i, ΔQ_i, Δs_{ij}, Δp_{ij} and are determined through incremental displacements. For a straightforward analysis, rearrangement of the equilibrium equations as in the tangential stiffness matrix is helpful, see Eq. (35). The equilibrium equations, see Eqs. (28)-(30), can be used also in the case of a coupled system. To find the new equilibrium state, the internal and coupling force increments are replaced by total forces $N_i + \Delta N_i$, $M_i + \Delta M_i$, $Q_i + \Delta Q_i$, $s_{ij} + \Delta s_{ij}$, and $p_{ij} + \Delta p_{ij}$. Now again, the boundary conditions can be utilised and by substituting displacements (31)-(33) into equilibrium equations (28)-(30), then

$$\int_{-1}^{1} \frac{\partial}{\partial x} [B_u]^T \{N + \Delta N\} d\xi + (-1) \int_{-1}^{1} [B_u]^T \{S + \Delta S\} d\xi = 0, \tag{36}$$

$$\int_{-1}^{1} \frac{\partial}{\partial x} [B_v^Q]^T \{Q + \Delta Q\} d\xi + (-1) \int_{-1}^{1} [B_v^Q]^T \{P + \Delta P\} d\xi = (\lambda + \Delta\lambda)(-1) \int_{-1}^{1} [B_v^Q]^T \{q\} d\xi \tag{37}$$

and

$$\begin{aligned} &(-1) \int_{-1}^{1} \frac{\partial^2}{\partial x^2} [B_v^M]^T \{M + \Delta M\} d\xi + \int_{-1}^{1} \frac{\partial}{\partial x} [B_v^M]^T \{S^C + \Delta S^C\} d\xi + \\ &+ (-1) \int_{-1}^{1} [B_v^M]^T \{P + \Delta P\} d\xi = (\lambda + \Delta\lambda)(-1) \int_{-1}^{1} [B_v^M]^T \{q\} d\xi, \end{aligned} \tag{38}$$

where the vector components are

$$\Delta S_i = \sum_{j=1}^{n} \Delta s_{ij} \tag{39}$$

$$\Delta S_i^C = \sum_{j=1}^{n} C_{ij} \Delta s_{ij}, \tag{40}$$

and

$$\Delta P_i = \sum_{j=1}^{n} \Delta p_{ij}, \tag{41}$$

are the incremental changes of summed coupling forces and where S, S^C, P, N, M *and* Q are the total summed forces. The final form of the equilibrium equations is

$$\begin{Bmatrix} F_1^A \\ F_2^A \\ F_3^A \end{Bmatrix} + \begin{Bmatrix} F_1^B \\ F_2^B \\ F_3^B \end{Bmatrix} = (\lambda + \Delta\lambda) \begin{Bmatrix} 0 \\ F^M \\ F^Q \end{Bmatrix}, \tag{42}$$

where the sub-vectors $\{F_i^A\}$ and $\{F_i^B\}$ are presented in Appendix B.

3 IMPLEMENTATION OF THE THEORY

3.1 SHAPE FUNCTIONS FOR DISPLACEMENTS

The approximation of displacements was an important issue, as the accuracy of the solution depends on it. The two main parameters, which could be varied, were the type and the number of shape functions used in the approximation. According to the boundary conditions, the forces had to vanish at the boundaries, see Figure 7. This requirement could be used for the determinations of shape functions. These functions have the following form:

$$B(\xi)_i = a_1 \sin\left(\kappa_i \frac{\xi+1}{2}\right) + a_2 \sinh\left(\kappa_i \frac{\xi+1}{2}\right) + a_3 \cos\left(\kappa_i \frac{\xi+1}{2}\right) + a_4 \cosh\left(\kappa_i \frac{\xi+1}{2}\right). \tag{43}$$

where a_1, a_2, a_3 and a_4 are the constants, which can be determined in order to satisfy the predefined boundary conditions. The parameter κ_i is the wave number. According to the boundary conditions of the beam, axial force N_i, moment M_i and shear force Q_i will vanish at the boundaries, see Figure 7. The first two boundary conditions are described by the axial displacements and deflections, see Eqs. (11) and (12). Thus,

$$\left.\frac{\partial u_i}{\partial x}\right|_{x=0}^{x=L} = \left.\frac{\partial^2 v_i^M}{\partial x^2}\right|_{x=0}^{x=L} = 0. \tag{44}$$

The shear force Q_i at the boundary can be defined by Eq. (5). Accordingly, the shear force Q_i will vanish at the boundary if the first derivative of the bending moment and the longitudinal shear flow s_{ij} are zero at the boundaries. However, this longitudinal shear flow has also to disappear at the free boundaries, otherwise shear stress will also be present, see Figure 8. On the other hand, Eq. (1)

shows that the longitudinal shear flow will disappear at the free boundary only if the first derivative of the axial force is zero.

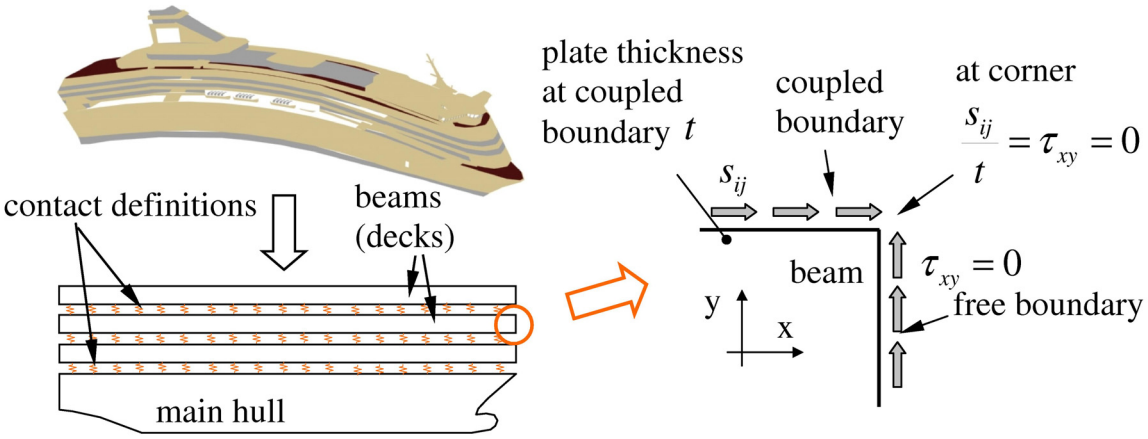

Figure 8. Longitudinal shear flow s_{ij} at the free boundary.

Thus, the requirement that the first derivative of the axial force and of the bending moment have to be zero can be applied in Eqs. (11) and (12), and the boundary conditions for the shear force are expressed by

$$\left.\frac{\partial^2 u_i}{\partial x^2}\right|_{x=0}^{x=L} = \left.\frac{\partial^3 v_i^M}{\partial x^3}\right|_{x=0}^{x=L} = 0\,. \tag{45}$$

An additional boundary condition for the deflection induced by shear deformation can be constructed with Eq. (15). Therefore, shear force Q_i at the boundary will disappear only if

$$\left.\frac{\partial v_i^Q}{\partial x}\right|_{x=0}^{x=L} = 0\,. \tag{46}$$

Now a total of four boundary conditions exist for the axial displacement u_i given in Eqs. (44) and (45). Similarly, four boundary conditions for the deflection induced by bending v_i^M, are available, see Eqs. (44) and (45). Two boundary conditions given in Eq. (46) are used for the deflection induced by shear v_i^Q. The form of shape functions suitable for the approximation of the bending deflections can be obtained by substituting Eq. (43) into the second boundary condition presented in Eqs. (44) and (45). As a result, the set of four equations becomes

$$\begin{cases} a_3(-1)+a_4=0 \\ a_1(-1)\sin(\kappa_i)+a_2\sinh(\kappa_i)+a_3(-1)\cos(\kappa_i)+a_4\cosh(\kappa_i)=0 \\ a_1(-1)+a_2=0 \\ a_1(-1)\cos(\kappa_i)+a_2\cosh(\kappa_i)+a_3\sin(\kappa_i)+a_4\sinh(\kappa_i)=0 \end{cases}. \tag{47}$$

This homogeneous set of equations with arbitrary constants $a_1 \ldots a_4$ is satisfied only when the determinant of this set has a zero value. Therefore,

$$\cos(\kappa_i)\cosh(\kappa_i)-1=0. \tag{48}$$

This equation had no analytical solution and so the parameter κ_i was solved numerically. The first twelve values are

$$\kappa_i = \begin{Bmatrix} 4.730040744862700 \\ 7.853204624095840 \\ 10.995607838001700 \\ 14.137165491257500 \\ 17.278759657399500 \\ 20.420352245626100 \\ 23.561944902040500 \\ 26.703537555508200 \\ 29.845130209103300 \\ 32.986722862692800 \\ 36.128315516282600 \\ 39.269908169872400 \end{Bmatrix}. \tag{49}$$

All the constants from a_2 to a_4 could be written by help of a_1, which itself was taken as a unit. Using Eq. (43), the shape functions for the deflection induced by bending can be presented in the following way:

$$\begin{aligned} B(\xi)_i^{v^M} &= \left[\sin\left(\kappa_i\frac{\xi+1}{2}\right)+\sinh\left(\kappa_i\frac{\xi+1}{2}\right)\right]+ \\ &+(-1)\frac{\sin(\kappa_i)-\sinh(\kappa_i)}{\cos(\kappa_i)-\cosh(\kappa_i)}\left[\cos\left(\kappa_i\frac{\xi+1}{2}\right)+\cosh\left(\kappa_i\frac{\xi+1}{2}\right)\right]. \end{aligned} \tag{50}$$

The first four shape functions are shown in Figure 9. The shape functions with odd index numbers are symmetric and those with even numbers are anti-symmetric functions. Together they should be able to describe an arbitrary beam deflection.

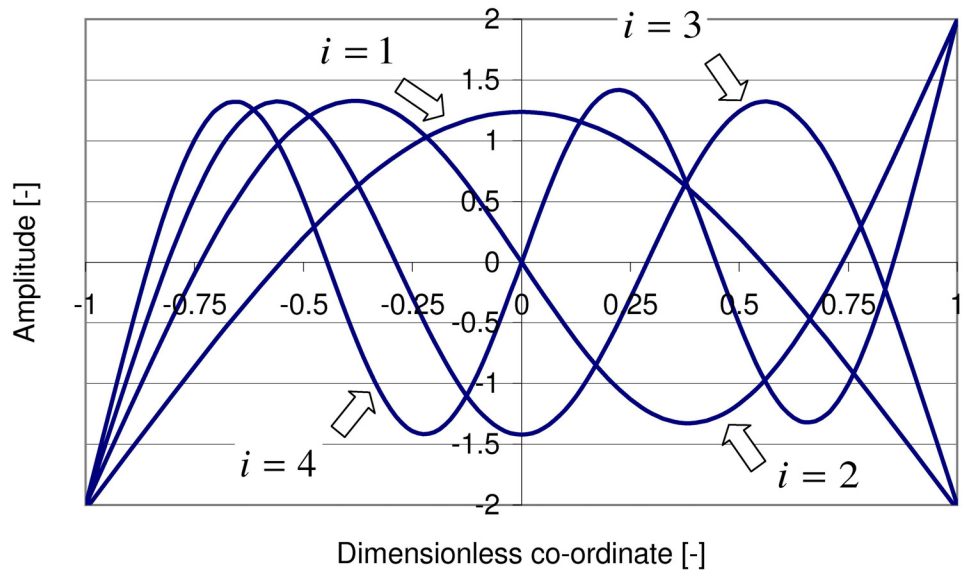

Figure 9. Shape functions for deflection induced by bending deformation.

Shape functions for the axial displacement could be obtained in the similar way. Thus, substituting Eq. (43) into the first part of Eqs. (44) and (45), the set of equations will be

$$\begin{cases} a_1 + a_2 = 0 \\ a_1 \cos(\kappa_i) + a_2 \cosh(\kappa_i) + (-1) a_3 \sin(\kappa_i) + a_4 \sinh(\kappa_i) = 0 \\ (-1) a_3 + a_4 = 0 \\ (-1) a_1 \sin(\kappa_i) + a_2 \sinh(\kappa_i) + (-1) a_3 \cos(\kappa_i) + a_4 \cosh(\kappa_i) = 0 \end{cases} . \tag{51}$$

The determinant for this equation set is the same as in the previous case, which means that the same κ values can be used for the approximation of the axial displacement. Representing again all the constants by help of constant a_1, the shape functions for the axial displacement can be written as

$$B(\xi)_i^u = \left[\sin\left(\kappa_i \frac{\xi+1}{2} \right) - \sinh\left(\kappa_i \frac{\xi+1}{2} \right) \right] + \\ + \frac{\cos(\kappa_i) - \cosh(\kappa_i)}{\sin(\kappa_i) - \sinh(\kappa_i)} \left[\cos\left(\kappa_i \frac{\xi+1}{2} \right) + \cosh\left(\kappa_i \frac{\xi+1}{2} \right) \right]. \tag{52}$$

The first four shape functions are again presented in Figure 10.

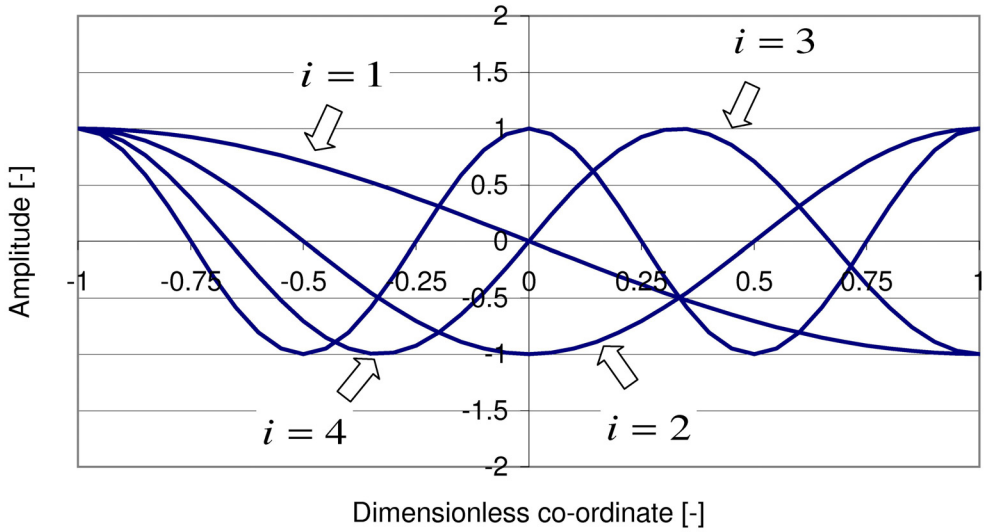

Figure 10. Shape functions for axial displacement.

For the estimation of the deflections induced by shear deformation, the boundary conditions presented in Eq. (46) were used. Additionally, it could be assumed that the third derivative of the deflection induced by shear was zero. This condition was chosen in order to determine all four constants and it had no theoretical background. Therefore, the set of equation becomes

$$\begin{cases} a_1 + a_2 = 0 \\ a_1 \cos(\kappa_i) + a_2 \cosh(\kappa_i) + (-1) a_3 \sin(\kappa_i) + a_4 \sinh(\kappa_i) = 0 \\ (-1) a_1 + a_2 = 0 \\ (-1) a_1 \cos(\kappa_i) + a_2 \cosh(\kappa_i) + a_3 \sin(\kappa_i) + a_4 \sinh(\kappa_i) = 0 \end{cases}, \tag{53}$$

where κ_i is now related to the shear. The determinant gives

$$\sin(\kappa_i) \cdot \sinh(\kappa_i) = 0, \tag{54}$$

where

$$\kappa_i = i\pi. \tag{55}$$

The shape function for shear deflection is defined as

$$B(\xi)_i^{v^Q} = \left[\cos\left(\pi i \frac{\xi + 1}{2} \right) + \frac{\sin(\pi i)}{\sinh(\pi i)} \cosh\left(\pi i \frac{\xi + 1}{2} \right) \right]. \tag{56}$$

Figure 11 presents these functions for four i values.

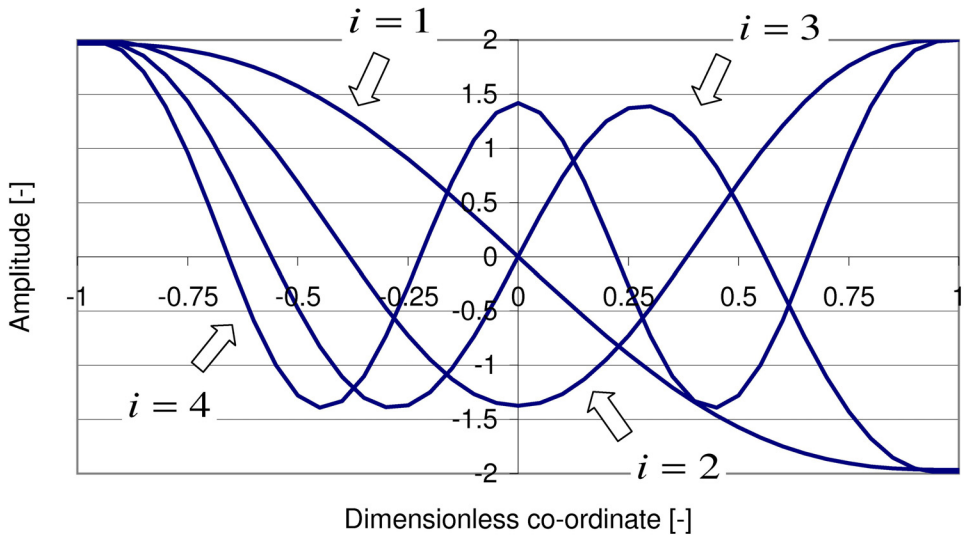

Figure 11. Shape functions for the deflection induced by shear deformation.

3.2 AXIAL LOAD-END SHORTENING CURVES

3.2.1 Definition

Axial load-end shortening curves define the behaviour of structural elements in axial compression or tension. They can also be called averaged stress-strain curves. A sketch of a typical load-end shortening curve for stiffened structures in compression is presented in Figure 12. These curves for different structural members can be defined numerically, analytically or using regression curves based on structural tests.

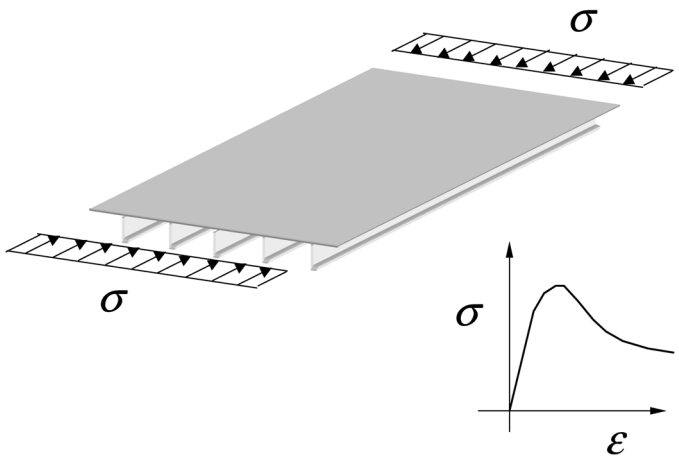

Figure 12. Load-end shortening curve for a stiffened panel.

Load-end shortening curves of various strength members have been formulated in different ways. The analytically defined load-end shortening curves used in this investigation are presented in the Bureau Veritas rules [2]. These load-end shortening curves have an advantage of easy use in practice. Typical structural members are hard corner, longitudinally or transversally stiffened plate members. All of these members are presented in Figure 13.

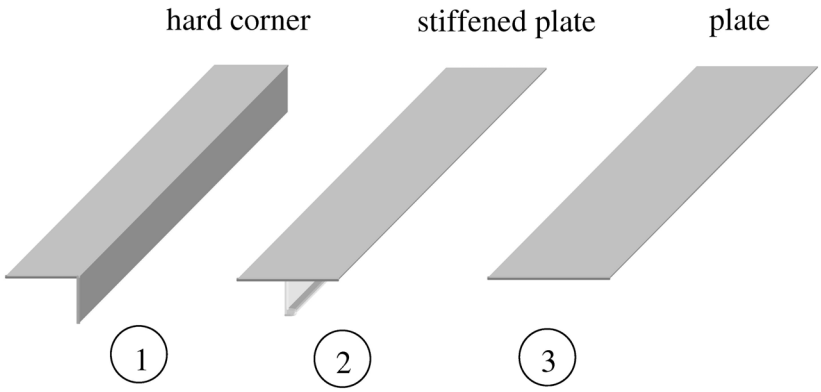

Figure 13. Typical structural members used in a hull girder cross-section.

The load-end shortening curves given in reference [2] typically have the form

$$\sigma_{CR} = \sigma_C \cdot \Phi \cdot \mu, \tag{57}$$

where Φ is the edge function, σ_C is the critical stress for the structural member and μ is the area ratio showing the relative cross-section area effective in loading. The edge function presents the material behaviour in compression or tension. An assumption of an elastic, ideally plastic material without rupture is used for the load-end shortening curves. Therefore,

$$\Phi = \begin{cases} -1 & if \quad \varepsilon_R < -1 \\ \varepsilon_R & if \quad -1 \le \varepsilon_R \le 1, \\ 1 & if \quad \varepsilon_R > 1 \end{cases} \tag{58}$$

where ε_R is the relative strain which can be defined as follows:

$$\varepsilon_R = \frac{\varepsilon}{\sigma_Y} E, \tag{59}$$

where E and σ_Y are the Young's modulus and yield stress for the material and ε is the average strain in a member. The formulae given in reference [2] are based on the discontinuous edge function, but in the present study continuous curves were preferred to avoid numerical problems. The new modified continuous edge function based on the curve fitting is

$$\Phi = sign(\varepsilon_R)\left[|\varepsilon_R| - (|\varepsilon_R| - 1)\cdot\left(1 - e^{-|\varepsilon_R|\cdot r_1}\right)^{r_2}\right], \tag{60}$$

where the constants r_1 and r_2 with values 5.0 and 70.0 give sufficient curve fitting. Both edge functions are presented in Figure 14.

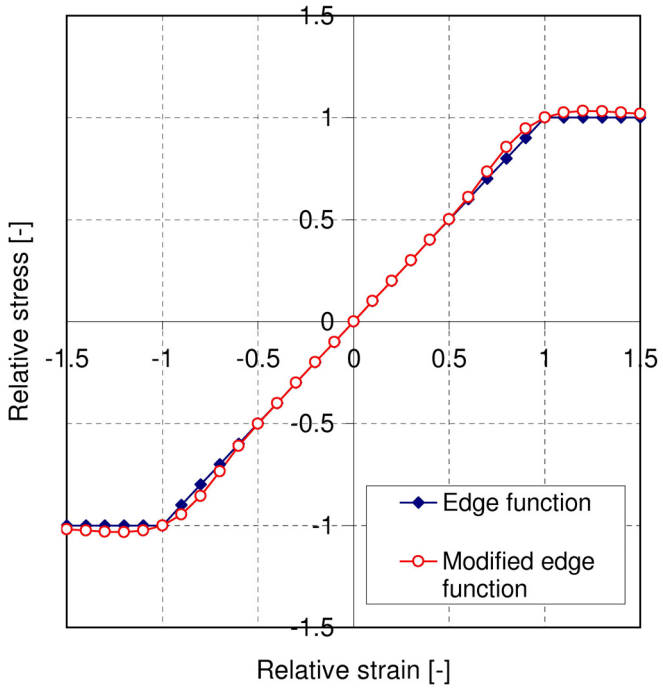

Figure 14. Discontinuous and continuous edge functions.

The critical stress σ_C depends on the loading, the type of the member, and the failure mode. The hard corner has only one failure mode by elasto-plastic collapse in compression and tension. A longitudinally stiffened structural member has a single failure mode in tension by elasto-plastic collapse and several failure modes in compression. This failure is due to beam column buckling, lateral-flexural buckling of the stiffener, or local buckling of the stiffener web. The mode producing the lowest resistance will be the actual failure mode for the structure. A transversally stiffened structural member can fail also by single mode in tension at elasto-plastic-collapse and in compression by elasto-plastic plate buckling.

The critical stress in tension is assumed to be equal to yield stress for all structural members. In compression the critical stress varies due to different collapse modes. For the hard corners, the only failure mode is the elasto-plastic collapse with the critical stress equal to the yield stress. In the case of stiffened members, the yield stress will not be reached often, as the elastic or elasto-plastic buckling will take place first. The effective area ratio μ also depends on the type of the structural

member, on loading and on the failure mode. Table 1 presents the critical stresses and effective area ratios for various structural members with respect to the loading type and to failure mode. More detailed definitions are given in Appendix E.

Table 1. Definition of load-end shortening curves for various structural members.

Member	***Loading***	***Buckling stress*** σ_E ***(Eq.)***	***Critical stress*** σ_C ***(Eq.)***	***Effective area ratio*** μ
Hard corner	Tension	-	σ_Y	1
	Compression	-	σ_Y	1
Longitudinally stiffened plate	Tension	-	σ_Y	1
	Compression Beam column buckling	σ_{E1} (E.4)	σ_{C1} (E.3)	$\frac{A_S + b_e t}{A_S + bt}$
	Compression Lateral-flexural buckling of ordinary stiffeners	σ_{E2} (E.11)	σ_{C2} (E.3)	$\frac{A_S + bt\frac{\sigma_{CP}}{\sigma_{C2}}}{A_S + bt}$
	Compression Web local buckling of flanged ordinary stiffeners	-	σ_Y	$\frac{b_e t + h_{we} t_w + b_f t_f}{bt + h_w t_w + b_f t_f}$
	Compression Web local buckling of flat bar ordinary stiffeners	σ_{E4} (E.26)	σ_{C4} (E.3)	$\frac{bt\frac{\sigma_{CP}}{\sigma_{C4}} + h_w t_w}{bt + h_w t_w}$
Transversally stiffened plate	Tension	-	σ_Y	1
	Compression	-	σ_Y	$\frac{b}{L}\left(\frac{2.25}{\beta_e} - \frac{1.25}{\beta_e^2}\right) + 0.1\left(1 - \frac{b}{L}\right)\left(1 + \frac{1}{\beta_e^2}\right)^2$

3.2.2 Effect of reverse loading

The reverse loading of structural members in the hull girder might be an important issue for the problem of ultimate strength, when the redistribution of stresses during the loading occurs. This stress redistribution is a phenomenon, where in some parts of the cross-section, a change between compression and tension takes place under monotonically increasing external loading. This change of stresses can be observed through the shift of the neutral axis. In the case of single deck ships, the location of the neutral axis will not move significantly until the deck or bottom structure collapses. In spite of the fact that the collapse influences strongly the ultimate strength, the effect of stress redistribution can be normally discarded, as it starts to affect after the ultimate strength has been reached. However, in the case of large passenger ships, several upper decks may collapse before the ultimate strength is reached and due to this the location of the neutral axis can move remarkably. If this happens, then that of the cross-section area where the neutral axis moves will experience reverse loading. If this particular area is large, the redistributed stresses may have a strong influence on the ultimate bending moment.

In the present study, analytically defined stress-strain curves were used. Therefore, the stress in the structural member is simply defined as a function of strain

$$\sigma = f(\varepsilon). \tag{61}$$

The reverse can be considered only, if the incremental stress-strain relation is used, as for large strain values, the loading path may differ from the unloading path. Based on Eq. (61), the incremental form of the stress can be given as

$$\Delta\sigma = \frac{\partial f(\varepsilon)}{\partial \varepsilon}\Delta\varepsilon \text{ or } \Delta\sigma = E_t \Delta\varepsilon, \tag{62}$$

where $\Delta\sigma$, $\Delta\varepsilon$ are the stress and strain increments and E_t is the tangent stiffness of the structural member. This stress-strain relation is valid only for initial loading and due to this not directly useful for unloading. In order to include unloading or reverse loading, some additional assumptions had to be made. The FE-method could be exploited to validate the simplified loading models.

The typical stress-strain curve of a structural member has an elastic behaviour in tension and in compression up to a certain load level, see Figure 15. Loading in tension will cause yielding and hardening, which means that a stress increase after a certain strain point will be small or simply zero. The structural behaviour is stable without any strength reduction up to the failure strain. After the failure strain, the structural member was eliminated. The behaviour of the structural member is different in compression. After the maximum stress is reached, the load level starts to decrease and

a further strain increase reduces the stresses. The member maintains residual strength after the loss of stability. In order to determine the path for reverse loading in tension and in compression, two strain parameters ε_t and ε_c were introduced, see Figure 15 and Figure 16. The initial stress-strain curves are presented in the same figures with the black curve. Figure 15 presents the case where the structural member is subjected first to tension and then to compression. In tension, the strength member follows the initial stress-strain curve marked as path 1 and 2, see Figure 15. In the case of reverse loading, the stress starts to reduce linearly, which is marked as path 3. The parameter ε_t equals to inelastic strain in tension. Under further reverse loading the curve, which describes initial stress-strain relations, will be shifted according to ε_t as shown with the yellow line in Figure 15. This path is marked as 4 and 5.

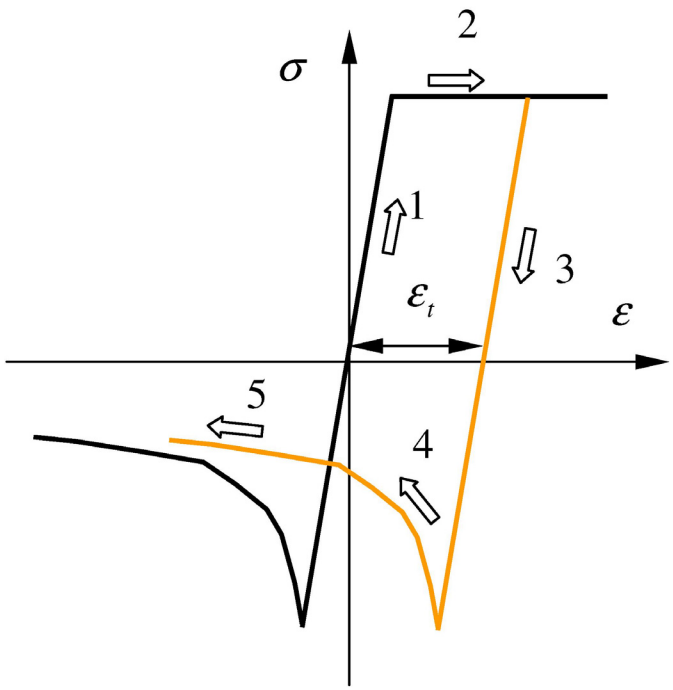

Figure 15. Sketch of the behaviour of a structural member in tension-compression loading.

Figure 16 presents the case where a structural member is subjected first to compression and then to tension loading. Now in compression, the member behaves according to the initial stress-strain curve, marked as path 1 and 2, see Figure 16. In the case of reverse loading, the behaviour of the structural member is described by curved paths 3 and 4 up to the yield point. Thereafter, the member behaves again according to the initial stress-strain curve. The parameter ε_c defines the point where the unloading in compression starts. The whole loading path is presented as a yellow line in Figure 16.

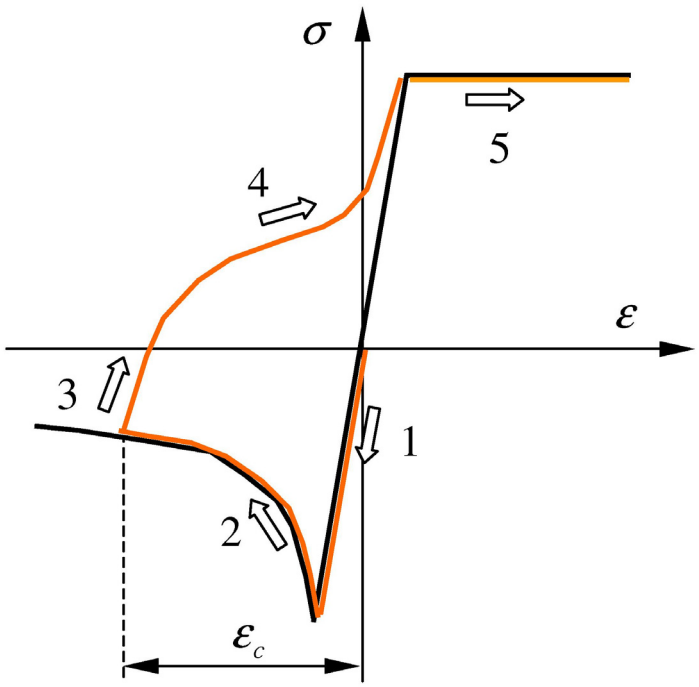

Figure 16. Sketch of the behaviour of a structural member in compression-tension loading.

The tangent stiffness value E_t of the structural member depends on the loading path. The important indicators showing the state of loading or unloading are the stress value σ and strain increment $\Delta\varepsilon$, which point out the direction of the following loading increment. The tangent stiffness can be defined separately for four different loading-unloading situations. If $\sigma \geq 0$ and $\Delta\varepsilon > 0$ the structural member is in tension and the strain increment is increasing. Two stress levels have to be calculated in order to decide whether the initial stress-strain curve (subscript 1) or pre-strained stress-strain curve (subscript 2) will be used in the stiffness estimation. They are calculated from

$$\begin{cases} \sigma_1 &= f(\varepsilon + \Delta\varepsilon) \\ \sigma_2 &= E(\varepsilon + \Delta\varepsilon - \varepsilon_t) \end{cases}. \tag{63}$$

If $\sigma_1 < \sigma_2$ and $\varepsilon \geq 0$, the original curve will be used and the tangential stiffness of the cross-section member E_t and parameter ε_t are approximated as

$$\begin{cases} E_t &= \dfrac{f(\varepsilon + \Delta\varepsilon) - f(\varepsilon)}{\Delta\varepsilon} \\ \varepsilon_t &= \varepsilon + \Delta\varepsilon - \dfrac{\sigma_1}{E} \end{cases}. \tag{64}$$

If $\sigma_2 \leq \sigma_1$ and $\varepsilon_c = 0$ and $\varepsilon \geq 0$, the pre-strained curve will be used and the tangential stiffness together with strain parameter are estimated as

$$\begin{cases} E_t &= E \\ \varepsilon_t &= \varepsilon_t \end{cases}. \tag{65}$$

If the structural member has been previously in compression, the loading path will follow the curve described by the third order polynomial, marked with numbers 3 and 4, see Figure 16. This curve is described by two points, which present the starting and end-point of load path 3 and 4. The starting point is given by the strain value $\varepsilon_3 = -\varepsilon_c$ and by the stress value $\sigma_3 = |f(-\varepsilon_c)|$. The end point is determined by the maximum deformation that the strength member has reached in previously occurred tension. If the member has not been previously under tension loading, the strain value equal to strain at yield will be used. Otherwise, the point is defined by the strain value $\varepsilon_4 = \varepsilon_t + \frac{\sigma_Y}{E}$ and by the stress value $\sigma_4 = f\left(\varepsilon_t + \frac{\sigma_Y}{E}\right)$. Thus, the tangent stiffness and the strain parameter are given as

$$\begin{cases} E_t &= 3c_1(\varepsilon)^2 + 2c_2(\varepsilon) + c_3 \\ \varepsilon_t &= \varepsilon_t \end{cases}, \tag{66}$$

where

$$\begin{cases} c_1 = & 2(c_5 - 1)c_4 \\ c_2 = & 3\left(\varepsilon_c - 2\varepsilon_t - \frac{\sigma_Y}{E}\right)(c_5 - 1)c_4 \\ c_3 = & \left[(\varepsilon_c - \varepsilon_t)\left(\varepsilon_t + \frac{\sigma_Y}{E}\right)(6 - 4c_5) + \left((\varepsilon_c - \varepsilon_t)^2 + \left(\varepsilon_t + \frac{\sigma_Y}{E}\right)^2\right)c_5\right]c_4 \end{cases}, \tag{67}$$

and where

$$c_4 = (\sigma_3 + \sigma_4) \Big/ \left(\frac{\sigma_Y}{E} + \varepsilon_c\right)^3, \tag{68}$$

and c_5 is the shape parameter equal to 2.5. Constants c_1, c_2 and c_3 are determined from the condition that the cubic polynomial has to connect the point where the loading path starts $[-(\varepsilon_c - \varepsilon_t), \sigma_3]$ and ends at the point where the member has been stretched in the previous loading cycle, which is $[\varepsilon_t + \sigma_Y/E, \sigma_4]$, see Figure 15 and Figure 16. If the previous cycle is missing, the stretching point will be the yield point. The comparison with the results of the FE-analysis in the next chapter shows that the cubic polynomial offers a sufficient fit for this loading path.

If the stress in the strength member is $\sigma > 0$ and the strain increment is negative $\Delta\varepsilon < 0$, the tensioned member is under unloaded condition. In that case, the tangent stiffness is defined as

$$\begin{cases} E_t &= E \\ \varepsilon_t &= \varepsilon_t \end{cases}. \tag{69}$$

In compression loading $\sigma < 0$ and $\Delta\varepsilon < 0$. For this case, stress values are also calculated in order to distinguish whether the original or pre-strained curve will be used. Thus, the stresses are

$$\begin{cases} \sigma_1 &= f(\varepsilon + \Delta\varepsilon - \varepsilon_t) \\ \sigma_2 &= \sigma + E\Delta\varepsilon \end{cases}, \tag{70}$$

If $\sigma_1 \geq \sigma_2$, the tangential stiffness E_t and parameter ε_c can be approximated as

$$\begin{cases} E_t &= \dfrac{f(\varepsilon + \Delta\varepsilon - \varepsilon_t) - f(\varepsilon - \varepsilon_t)}{\Delta\varepsilon} \\ \varepsilon_c &= \varepsilon_c + |\Delta\varepsilon| \end{cases}. \tag{71}$$

Otherwise, the structure has been in compression and in this case the tangential stiffness is

$$\begin{cases} E_t &= E \\ \varepsilon_c &= \varepsilon_c \end{cases}. \tag{72}$$

If unloading occurs in compression $\sigma < 0$ and $\Delta\varepsilon > 0$, then Eq. (66) can be used again for the estimation of the tangent stiffness.

3.2.3 Validation with 3D FEM

To validate load-end shortening curves the 3D FE-method was used. Three typical deck structures were chosen for this study. All of these three structures were longitudinally stiffened panels having scantlings typical of those for passenger ships. The deck structures are presented in Figure 17, Figure 18 and Figure 19. The first two deck panels A and B are typical of the upper decks of the superstructure. The deck plate thickness is $5.0\,mm$, the spacing between the longitudinals is $680\,mm$ and the web frame spacing is $2730\,mm$. These web frames have the height of $480\,mm$ in structure A and $440\,mm$ in structure B. The third deck panel is referred to as the strength deck of the ship with a plate thickness of $12.0\,mm$, spacing between longitudinals $825\,mm$ and web frame spacing $3625\,mm$. In passenger ships, normal strength steel is often used because

structures A and B are made of steel material with a yield strength of $235\,MPa$. In the third structure C, the high strength steel is used with a yield strength of $360\,MPa$.

For the validation of the reverse behaviour, the deck structure D shown in Figure 20 was used. This panel has dimensions similar to panel A, except the HP-stiffeners have a larger web thickness, which is 8 mm. Also, the yield stress was taken slightly higher, which was $250\,MPa$.

The validation analysis was conducted using the explicit dynamic FE-code called LS-DYNA. In all three cases, the FE-model covered the whole structure. The web frames, longitudinal girders and the plating were modelled with four-node shell elements and longitudinals were modelled using both shell elements and beam elements. The loading was given in the direction of the longitudinals as in time prescribed axial displacement of the boundaries. In order to avoid dynamic effects, loading speed was taken so low that the kinetic energy was less than five percent of the total internal energy. All the structures included additional pillars placed at every second web frame. Pillars had a height of $3000\,mm$ and were clamped at the ends. The total reaction forces at the boundaries gave the load, and average strain was calculated from the relative displacements between the web frames bounding the collapsed region.

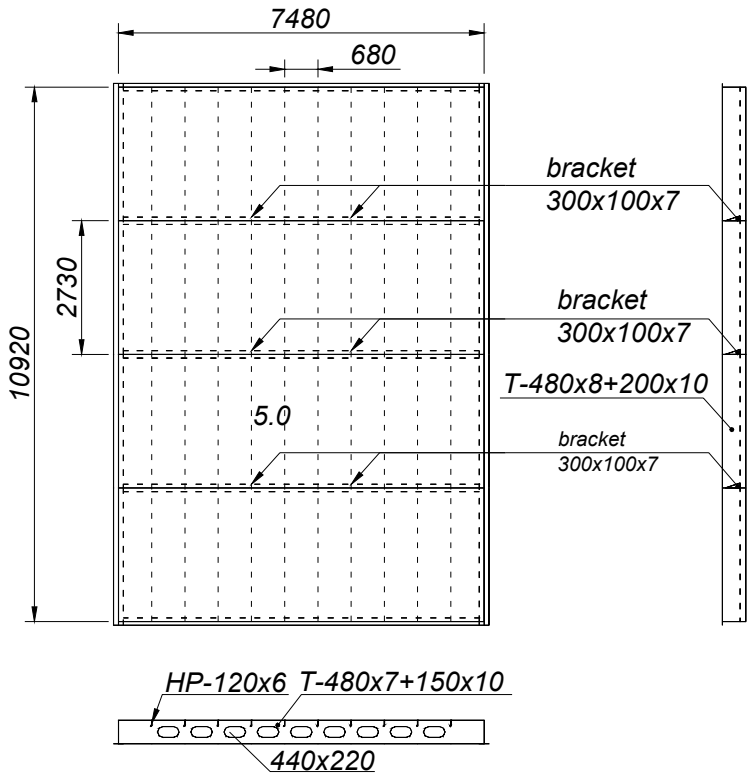

Figure 17. Geometry of structure A.

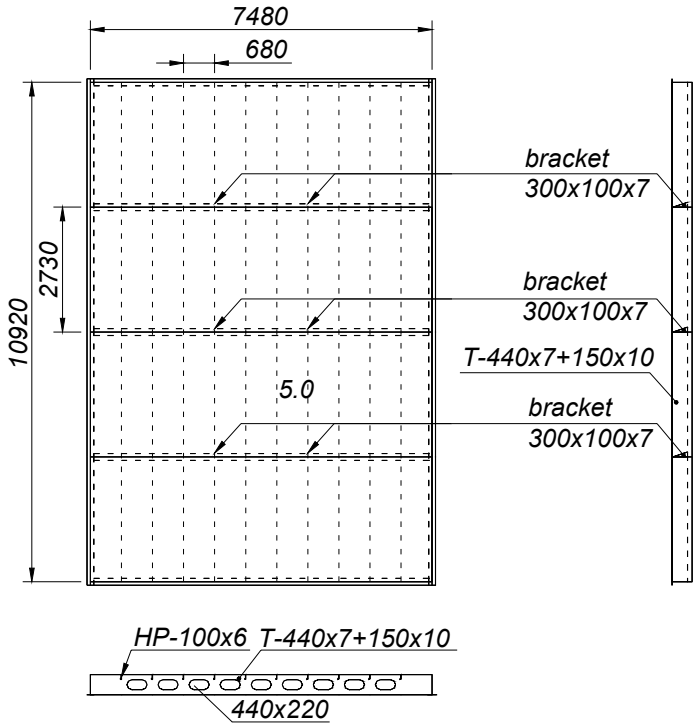

Figure 18. Geometry of structure B.

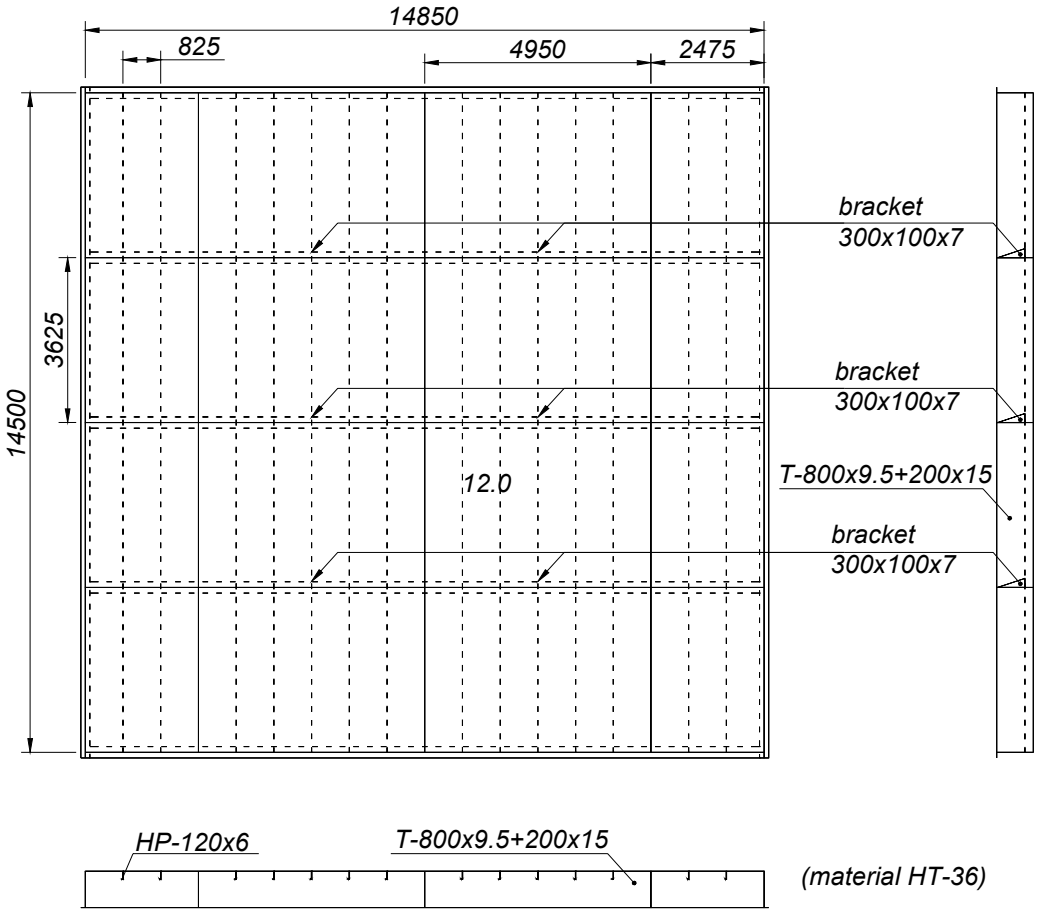

Figure 19. Geometry of structure C.

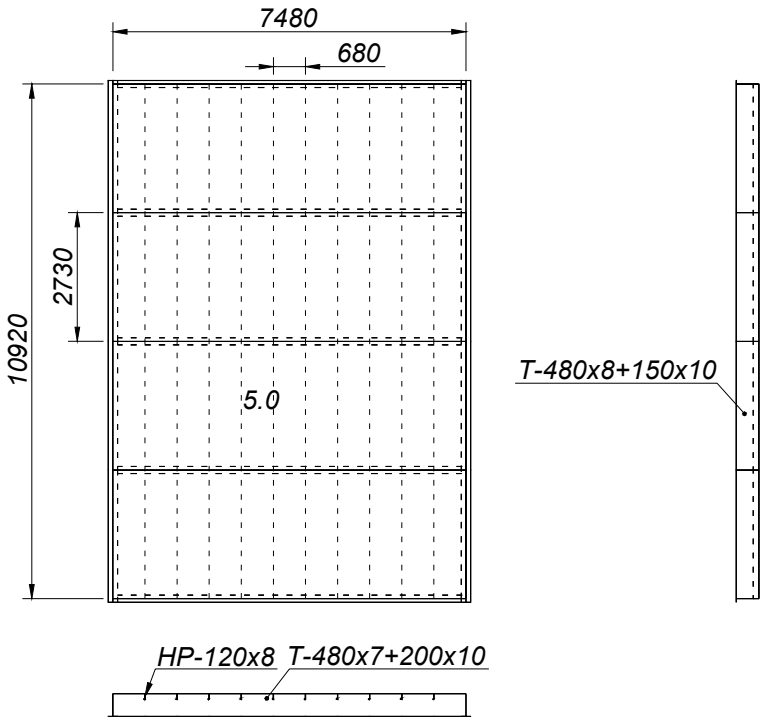

Figure 20. Geometry of structure D.

The analytical load-end shortening curves for stiffened panels were calculated using the equations given in reference [2]. The panel had to be divided into different structural members consisting of a plate with the breadth equal to the longitudinal spacing and of longitudinals or girders attached to this plate. The strain was considered as an input value. The average stress was calculated summing up the reaction forces from each member at a certain strain value and divided by the total cross-section area of the panel. Figure 21, Figure 22 and Figure 23 present the comparison of the averaged stress-strain curves calculated numerically and analytically. Plate buckling and the ultimate load for the panel derived from reference [11] are also presented. The results prove that the maximum load level and strength reduction are relatively well approximated with the analytic stress-strain curve formulas. The structural stiffness with the small strain values given by the analytical approach fits well into those obtained by the FE-method. However, the stiffness of structures A and B in the strain region between 0.05 and 0.1 was slightly higher in the case of the FE-method compared to that of the load-end shortening curves from reference [2]. This might be due to the difference between the boundary conditions used in the FE-analysis and those of the analytical approach. Also, the pillars could influence the averaged stress-strain relations. However, it can be concluded that the analytical approach provided sufficient accuracy for the

ultimate strength estimation of the structural panels used in passenger ships. The strength reduction of the panels was approximated within a maximum of 20 % discrepancy, compared to the FE-method.

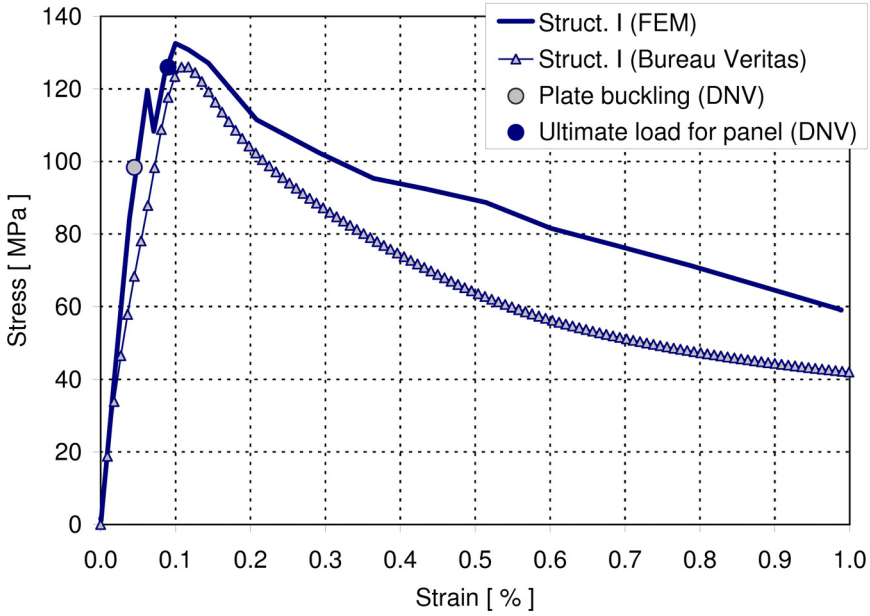

Figure 21. Comparison of the averaged analytical stress-strain and by the FE-method numerically calculated curve for structure A.

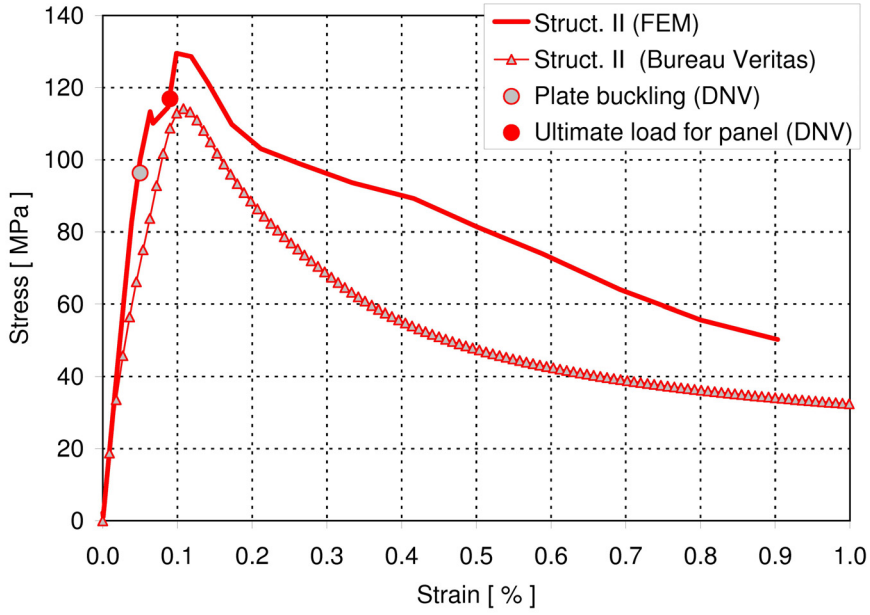

Figure 22. Comparison of the averaged analytical stress-strain and by the FE-method numerically calculated curve for structure B.

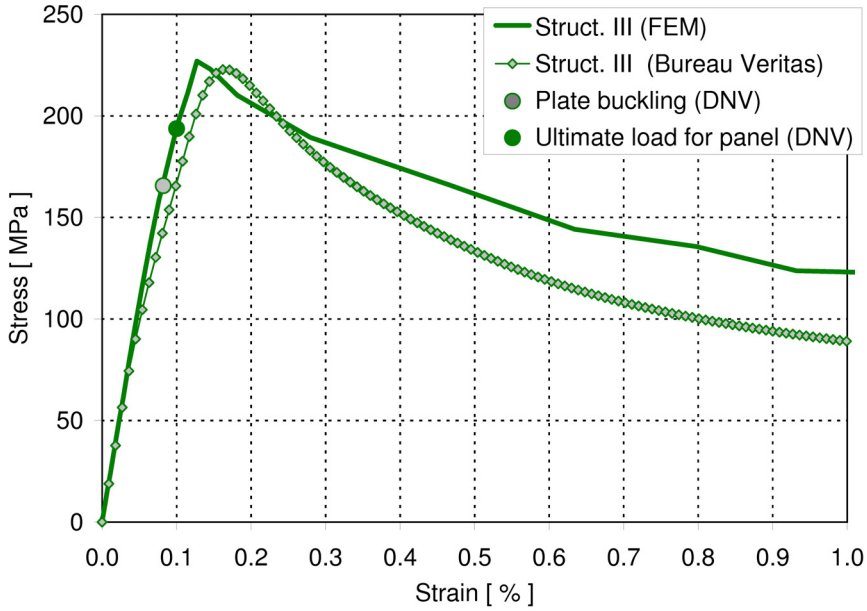

Figure 23. Comparison of the averaged analytical stress-strain and by the FE-method numerically calculated curve for structure C.

The comparison of axial stresses calculated for panel D in the case of tension-compression and compression-tension loading is presented in Figure 24 and Figure 25. In both load cases, panel behaviour is well estimated, allowing a possible reverse loading to take place in a realistic way. The compression-tension loading case indicates that the loading path can be well described with the cubic polynomial, see Figure 25.

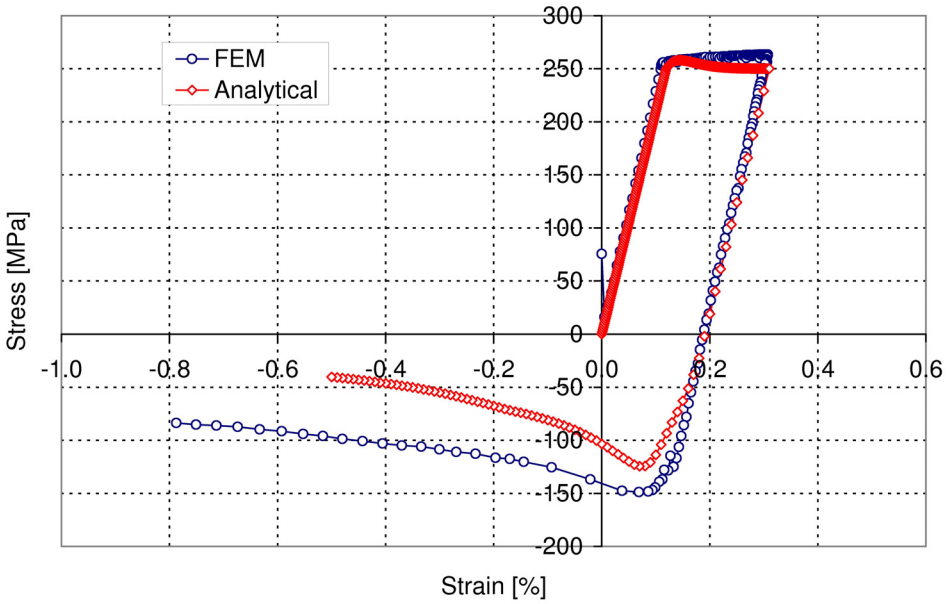

Figure 24. Panel stresses in tension-compression loading calculated with the FE-method and analytical equations.

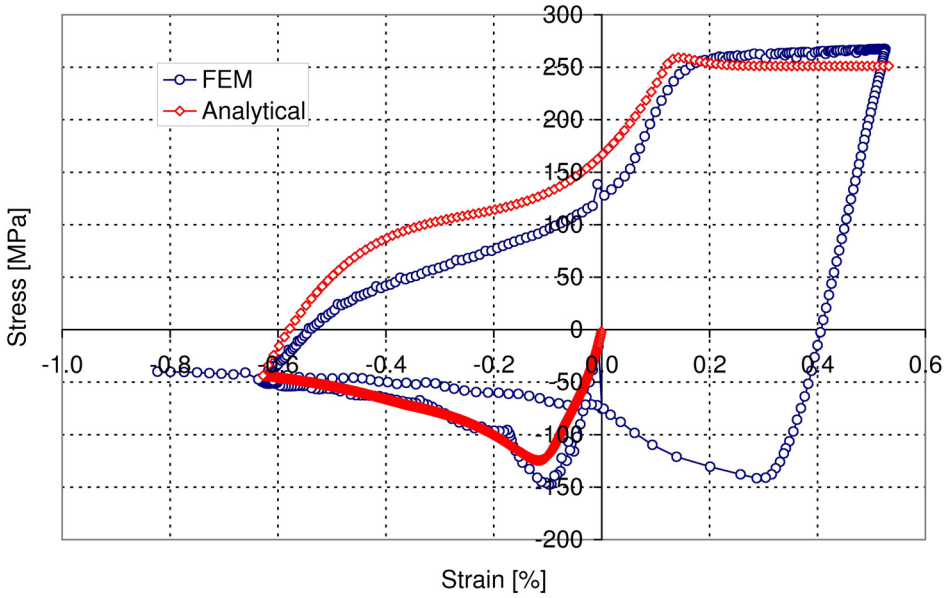

Figure 25. Panel stresses in compression-tension loading calculated with the FE-method and analytical equations.

3.3 TANGENT STIFFNESS FOR BENDING AND LONGITUDINAL ELONGATION

The approximation of tangent bending and axial stiffness of beams for the CB-method was done by integrating the normal stress from load-end shortening curves over the beam cross-section. The basic assumption is the linearly varying axial strain in the beam cross-section. According to the theory presented by Smith [35], the cross-section is divided into smaller structural members and for each member, the predefined load-end shortening curve is available, see Figure 26.

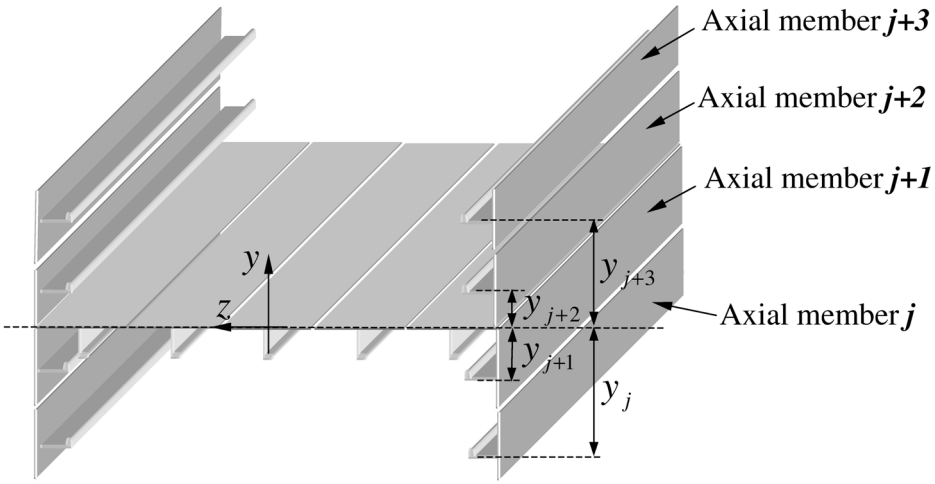

Figure 26. Cross-section of the of the beam divided into structural members.

The bending of the beam is based on the classical assumption that the cross-section of the beam remains plane during deformation. If the axial strain in the cross-section is known, then the tangent stiffness of each member of the cross-section can be directly obtained from load-end shortening curves as the vertical position of each structural member is fixed. The equations for tangent stiffness parameters for bending and axial elongation are presented in Appendix D. The tangent bending stiffness for the beam is

$$EI_{ii}^{t} = \int_{A} E_t y^2 \, dA = \sum_{k=1}^{m_i} E_{t,ik} \, y_k^2 \, A_{ik}, \tag{73}$$

where $E_{t,ik}$ is the tangent stiffness of member k in beam i, y_k is the co-ordinate of the strength member measured from the reference line, A_{ik} is the cross-section area of the member and m_i is the total number of members in beam i. In the same way, the axial stiffness is obtained

$$EA_{ii}^{t} = \int_{A} E_t \, dA = \sum_{k=1}^{m_i} E_{t,ik} A_{ik}. \tag{74}$$

The additional cross-term is needed in order to keep the co-ordinates of the beam's cross-section at the reference line

$$EX_{ii}^{t} = \int_{A} E_t y \, dA = \sum_{k=1}^{m_i} E_{t,ik} \, y_k \, A_{ik}. \tag{75}$$

The calculation procedure for the parameters of the tangent stiffness is quite simple. The beam has to be divided into strength members. Normal strain will vary also in the axial direction of each beam. Thus, the estimation of strain must be carried out in several cross-sections. Normally, the number of cross-section planes equals that of web frames. For very large structures, probably fewer cross-section planes are needed. The tangent stiffness E_t of each individual structural member was estimated using Eqs. (64)-(66), (69) or Eqs. (71) and (72), depending on the loading situation. After the tangent stiffness has been obtained for each individual structural member, the integration over the cross-section of the beam can be completed according to Eqs. (73)-(75).

3.4 TANGENT STIFFNESS FOR VERTICAL ELONGATION

The investigated structures describe the behaviour of side shells, longitudinal bulkheads and pillar lines. The vertical elongation stiffness was estimated for three different types of structures

shown in Figure 27, where openings could also be included. These structures are composed of vertically or longitudinally stiffened plate structures. The tangent stiffness for these structures was determined by summing up the effect of each structural member inside the web frame spacing. The applied load-end shortening curves are presented in Appendix E. The tangent stiffness for each member was calculated again using Eqs. (64)-(66), (69) or Eqs. (71) and (72), depending on the direction of the loading. The total value of the tangent stiffness is then the sum over each individual member. This tangent stiffness is defined per unit length. The vertical strain was estimated from the relative deflection δ^v divided by the height of the structure. It was assumed also that the window area did not contribute to the vertical deformation.

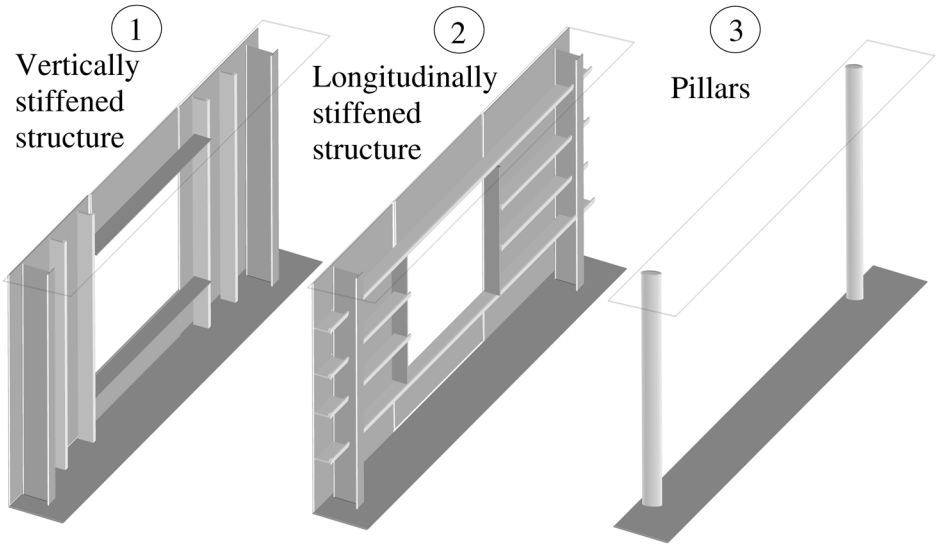

Figure 27. Different structures for the estimation of vertical stiffness.

3.5 TANGENT STIFFNESS FOR SHEAR COUPLING

3.5.1 Analytical formulation

Three different types of shear members were considered, similar to those presented in Figure 27. Both, vertically and longitudinally stiffened plate structures were described with the same structural model. It was assumed that these stiffened panels subjected to the shear loading would collapse due to two different failure modes, see Figure 28. In the case of large window openings, plate field between two openings tends to bend and the structure may collapse because of the formation of plastic hinges. This failure type was called as the collapse mode A. For small openings or if the openings are totally missing, failure can also occur due to the shear buckling of the stiffened plate field, marked as collapse mode B.

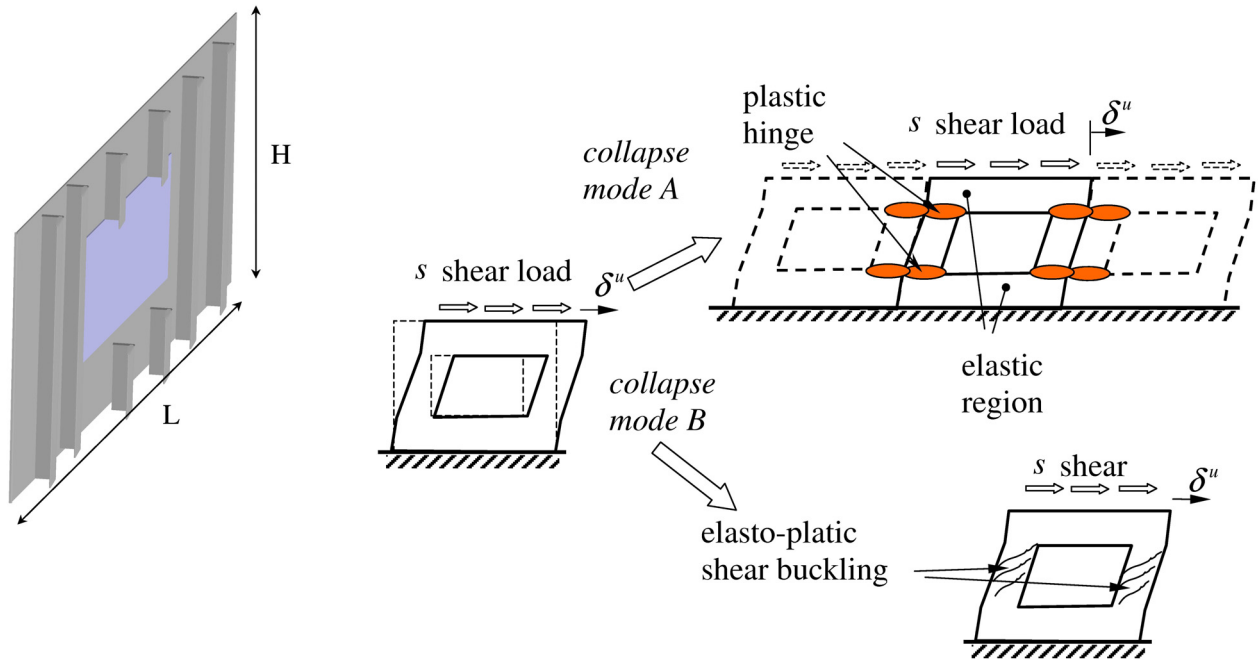

Figure 28. Shear stiffness definition for longitudinally or vertically stiffened shear members.

The shear member presented in Figure 28 was modelled so that the lower boundary of the structure was fixed and the shear force was applied on the upper boundary. It was assumed that the model could have two possible working stages, which were the elastic or post-ultimate stage. The shear member will deform due to the shear and also due to the bending, if the opening is included. In the elastic stage, the shear stiffness of the member per unit length is approximated as

$$T = \frac{1}{\frac{H_w L}{(L - L_w)tG} + \frac{(H - H_w)}{tG} + \frac{H_w^3 L}{12EI}}, \tag{76}$$

where H and L are the height and length of the shear member. Parameters H_w and L_w are the dimensions of the opening and I is the moment of inertia of the horizontal cross-section between two openings. A detailed presentation of Eq. (76) is given in Appendix F.

The maximum load carrying capacity of the shear member is determined by plate buckling or by plastic hinges. After this, the shear member moves from the elastic stage to the post-ultimate stage, which covers the post-buckling or the plastic hinge mechanism. Typical stress-strain curves for stiffened shear members are presented in Figure 29. Curve 1 corresponds to the shear buckling collapse typical of a side structure with a small opening or without any opening. Curve 2 describes the plastic hinge mechanism, which is typical of the side structure with a large opening. The shear collapse mode starts with the buckling and strength reduction may occur in the post-ultimate stage. The plastic hinge mechanism proceeds without strength reduction.

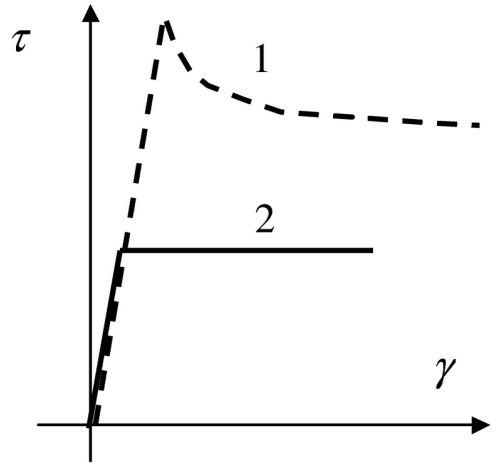

Figure 29. Sketch of collapse types for stiffened shear members. Number 1 describes the collapse due to shear buckling and number 2 presents the plastic hinge mechanism.

Due to the complex behaviour of the stiffened shear member, the shear flow s as a function of relative axial displacement δ^u is described with a continuous function. Thus, the shear flow is given

$$s = \frac{F_{ult}}{L} sign(\delta^u) \cdot \Phi \cdot \Phi_1, \tag{77}$$

where Φ and Φ_1 are the edge functions having the shape typical of stress-strain curves in shear. The term F_{ult}/L is the amplitude of edge functions and $sign(\delta^u)$ defines the sign of the shear flow. The edge function Φ is defined in Eq. (60), where now instead of relative strain ε_R, the relative displacement should be used δ_R. Thus,

$$\delta_R = \frac{\delta^u}{\delta_p^u}, \tag{78}$$

where δ_p^u is the displacement corresponding to the ultimate strength F_{ult}. Assuming that the structure stiffness T behaves elastically, the displacement δ_p^u becomes

$$\delta_p^u = F_{ult} T \,. \tag{79}$$

The edge function Φ_1 describes the strength reduction of the shear member beyond the ultimate point. Thus, based on the FE-analysis presented in Section 3.5.2, the edge function for strength reduction is expressed by

$$\Phi_1 = 1 - \frac{1}{5}\left(1 - e^{-|\delta_R| \cdot \frac{1}{10}}\right)^{\frac{n}{3}}. \tag{80}$$

Subscript 1 indicates the failure mode number 1. If this failure mode occurs, the edge function Φ_1 is included in Eq. (77). The ultimate strength depends on the failure modes based on plate buckling or plastic hinge. Therefore,

$$F_{ult} = \begin{cases} \tau_C t(L - L_w) & if \quad \tau_C t(L - L_w) \le \dfrac{2M_p}{H_w + 0.01} \\ \dfrac{2M_p}{H_w + 0.01} & if \quad \dfrac{2M_p}{H_w + 0.01} < \tau_C t(L - L_w) \end{cases}, \tag{81}$$

According to Paik [32], the ultimate shear stress τ_C for a stiffened panel is

$$\tau_C = \begin{cases} \tau_Y \left(1.324 \dfrac{\tau_E}{\tau_Y}\right) & if \quad \dfrac{\tau_E}{\tau_Y} < \dfrac{1}{2} \\ \tau_Y \left(0.039\left(\dfrac{\tau_E}{\tau_Y}\right)^3 - 0.274\left(\dfrac{\tau_E}{\tau_Y}\right)^2 + 0.676\dfrac{\tau_E}{\tau_Y} + 0.388\right) & if \quad 2 > \dfrac{\tau_E}{\tau_Y} \ge \dfrac{1}{2} \\ \tau_Y 0.956 & if \quad \dfrac{\tau_E}{\tau_Y} \ge 2 \end{cases}, \tag{82}$$

where τ_Y is the yield strength in shear defined by

$$\tau_Y = \frac{\sigma_Y}{\sqrt{3}} \tag{83}$$

and τ_E is the elastic buckling stress of the plate given by

$$\tau_E = 9.34\pi^2 \frac{E}{12\left(1 - \nu^2\right)}\left(\frac{t}{b}\right)^2. \tag{84}$$

Pillar members were described similarly to stiffened plate structures. However, the single allowable collapse mode is induced by the formation of plastic hinges. The deformation mode is shown in Figure 30. Therefore, Eq. (77) can also be used when the ultimate shear force is calculated from

$$F_{ult} = \frac{2M_p}{H}, \tag{85}$$

where M_p is the plastic moment of the cross-section of the pillar. The corresponding deflection is

$$\delta_p^u = \frac{M_p H^2}{6EI}. \tag{86}$$

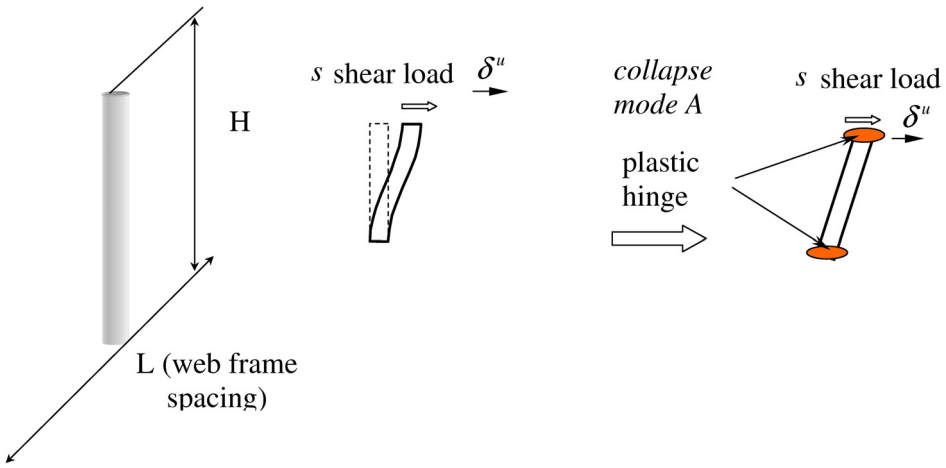

Figure 30. Definition of shear stiffness for a pillar member.

3.5.2 Effect of reverse loading in shear

Also, shear members may be reverse loaded during the strength analysis of the hull girder. It is difficult to detect when the reverse loading in shear, occurs but as structural members in axial loading included this kind of behaviour, the possibility of reverse loading of shear members was supplemented as well. Figure 31 presents a typical behaviour of the shear member in reverse loading. In initial loading, the shear member is acting according to Eq. (77), which can be presented simply as

$$s = g\left(\delta^u\right). \tag{87}$$

After the shear member reaches the ultimate strength, the strength capacity starts to reduce, marked as path 1 and 2 in Figure 31. At the end of the loading path, the shear member has a relative displacement equal to δ_t. The subsequent reverse loading will first unload the structure and then deform it in the direction opposite to that of initial loading. As the structure was loaded beyond the elastic limit, the initial path marked as 1 and 2 in Figure 31 will not be followed. Instead the elastic path marked as 3 in Figure 31 is followed whereupon path 4, which is the rest of the initial loading curve turned into the opposite direction, is chosen.

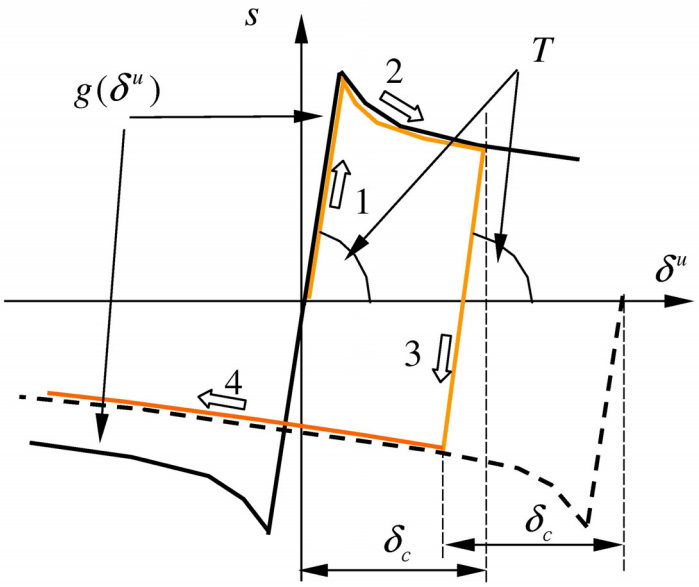

Figure 31. Sketch of the reverse loading of the shear member.

The calculation of the tangent stiffness for the shear member is divided into four parts where the difference depends on the loading or unloading direction. If the shear member is positively loaded and the next loading increment will be positive, then we have a condition, where $s \geq 0$ and $\Delta\delta^u \geq 0$. If this is the case, it has to be distinguished also whether there will be loading along the elastic or inelastic path. Thus, if $g(\delta_t + \delta_c) > s + T^t \Delta\delta^u$ and $\delta_c > 0$, the shear member will be loaded elastically and the shear stiffness is

$$T_c^t = T, \tag{88}$$

where T is obtained from Eq. (76), giving the initial shear stiffness of the structure. Otherwise, the structure will be loaded inelastically and the tangent shear stiffness and deformation parameter δ_t, counting deformations in a positive direction can be obtained as

$$\begin{cases} T^t = \dfrac{g\left[\delta^u + 2\left(\delta_c - \dfrac{g(\delta_c)}{T}\right) + \Delta\delta^u\right] - g\left[\delta^u + 2\left(\delta_c - \dfrac{g(\delta_c)}{T}\right)\right]}{\Delta\delta^u}. \\ \delta_t = \delta_t + \Delta\delta^u \end{cases} \tag{89}$$

If $s \geq 0$ and $\Delta\delta^u < 0$, the structure will be elastically unloaded and in that case stiffness is again determined by Eq. (88). The structure is loaded in the reversed direction if $s < 0$ and $\Delta\delta^u < 0$. Now once again it has to be determined whether the elastic or inelastic path will be used. If $-g(\delta_t + \delta_c) < s + T^t \Delta\delta^u$ and $\delta_t > 0$, the tangent shear stiffness is estimated according to Eq. (88).

Otherwise, the load path will be inelastic and tangent stiffness together with the deformation parameter is

$$\begin{cases} T^t = \dfrac{g\left[\delta^u - 2\left(\delta_t - \dfrac{g(\delta_t)}{T}\right) + \Delta\delta^u\right] - g\left[\delta^u - 2\left(\delta_t - \dfrac{g(\delta_t)}{T}\right)\right]}{\Delta\delta^u} \\ \delta_c = \delta_c + \left|\Delta\delta^u\right| \end{cases}. \tag{90}$$

If $s < 0$ and $\Delta\delta^u > 0$, elastic unloading occurs and stiffness is again estimated according to Eq. (88).

3.5.3 Validation with the 3D FE-method

For the validation, five different side structures were analysed. These were typical longitudinally stiffened bulkhead or side shell structures used in passenger ships. All the structures had a web frame spacing of $2700\,mm$ and a deck height of $2800\,mm$. The spacing between stiffeners was $700\,mm$. The web frame was composed of a web of $500\times7\,mm$ and of a flange of $200\times8\,mm$. Structure A is a typical bulkhead structure. The dimensions of the web frame for structure A are somewhat excessive, but the combination of plate thickness $5\,mm$ with bulb stiffeners $HP\,100\times6$ may be used for this purpose. Structure B describes a side or bulkhead structure, with a plate thickness of $8\,mm$ and stiffeners $HP\,120\times8$. Structure C is identical to version B, except the window opening with height $1400\,mm$ and length $1700\,mm$ is included. Also, structures D and E are similar, with a plating thickness of $10\,mm$, except the window opening is included in version D. The stiffeners in the case of D are bulb profiles of size $HP\,120\times8$ and in the case of E correspondingly $HP\,140\times8$. All of these structures are presented in Figure 32.

The calculations with the FE-method were conducted by applying pure shear loading on the structure. The structure was connected to two rigid decks, where the lower deck was fixed and the upper deck was moved longitudinally and kept straight. In order to reduce the effects of free boundaries, five web frames were modelled in a row at each FE-model.

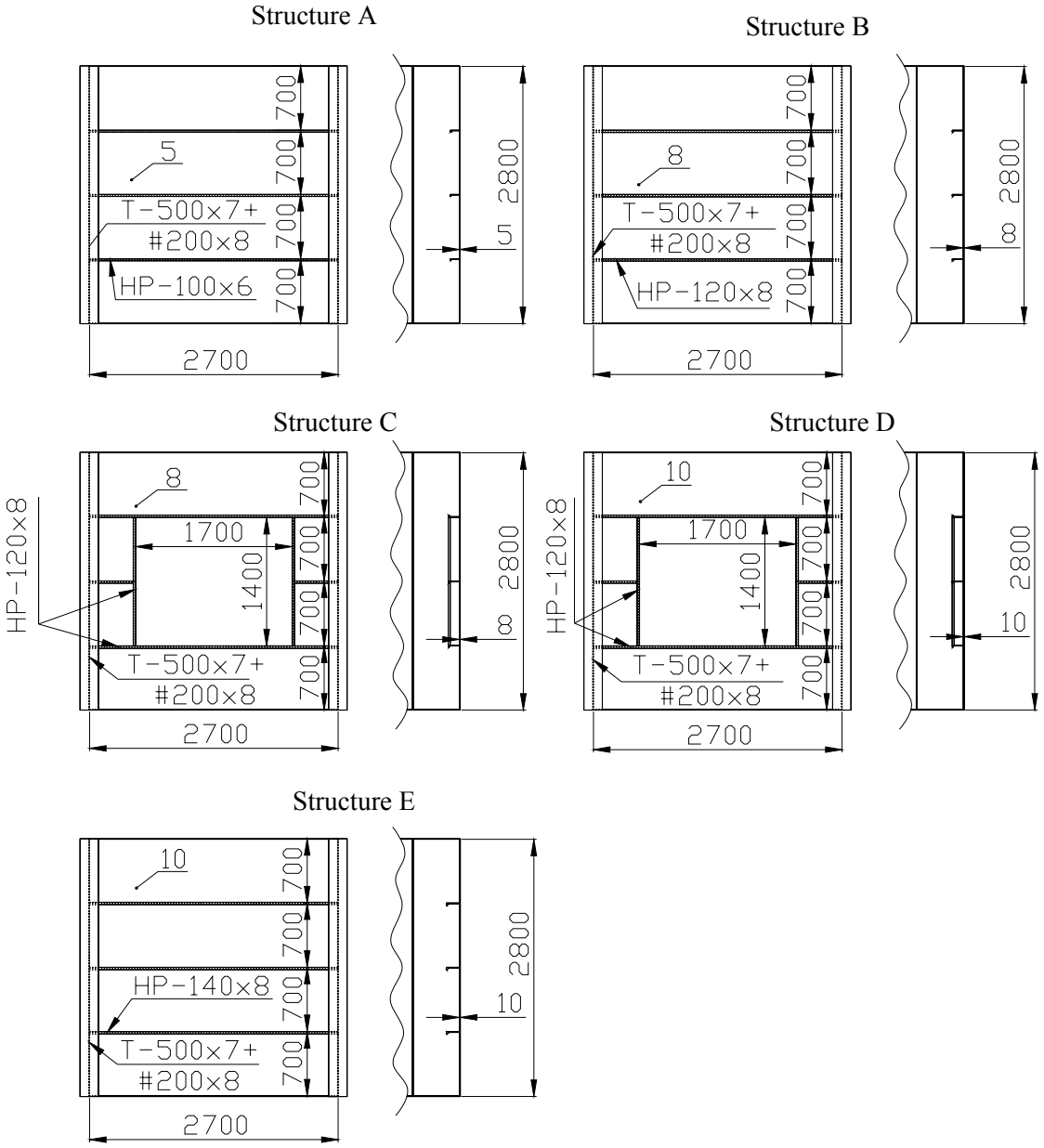

Figure 32. Side structures for validation with the FE-method.

The FE-analysis indicated that structures A, B and E collapsed due to elasto-plastic shear buckling, while the collapse of structures C and D was caused by the formation of plastic hinges. In the case of the shear buckling, a clear strength reduction could be observed, see Figure 33. The shear strength of the members without openings is very high up to buckling. After buckling, the reduction of strength was significant. However, in the case of the structure with an opening, structural collapse was caused by the formation of plastic hinges and after that the strength level remained constant. The elastic behaviour and ultimate strength of the shear members obtained with

analytical formulas corresponded well to the results of the FE-analysis, see Figure 33. For strength reduction, no analytic formulas were available, thus it was assumed that the strength reduction is 50 % for strength members without an opening.

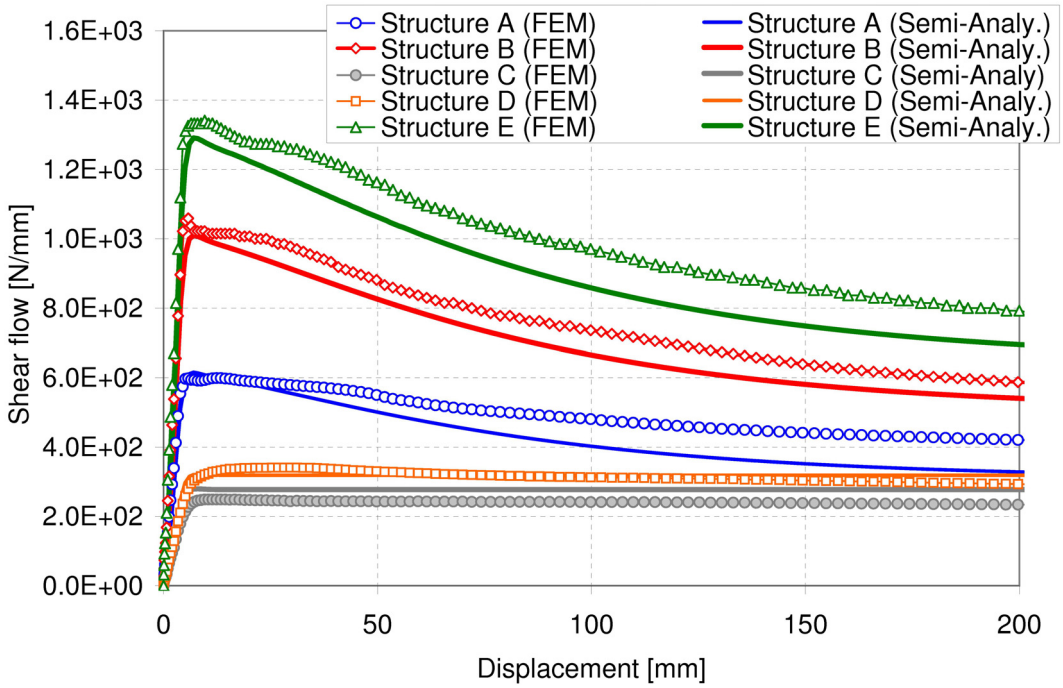

Figure 33. Force-displacement curves for structures A, B, C, D and E obtained by the FE-method and the semi-analytical approach.

Structure B was used also to validate the reverse loading effects. The analysis was done with the FE-method and the results were compared with the semi-analytical approach. For this purpose, the upper deck connected to the structure was displaced in the positive and negative horizontal direction with respect to the lower deck. In the first case, the maximum displacement of the upper deck was 80 mm and in the second case 150 mm. The validation shows that the reloading effects are well captured, see Figure 34. In the analytical approach, it is difficult to estimate stiffness in the unloading phase. As the FE-results show, the shear stiffness of the structure in unloading is two to three times smaller than the initial shear stiffness. This depends on the maximum displacement of the upper deck. However, it is not considered as a problem, as in reverse loading, the displacement in the starting direction is normally very small, which means also that the stiffness will be quite similar to the initial one.

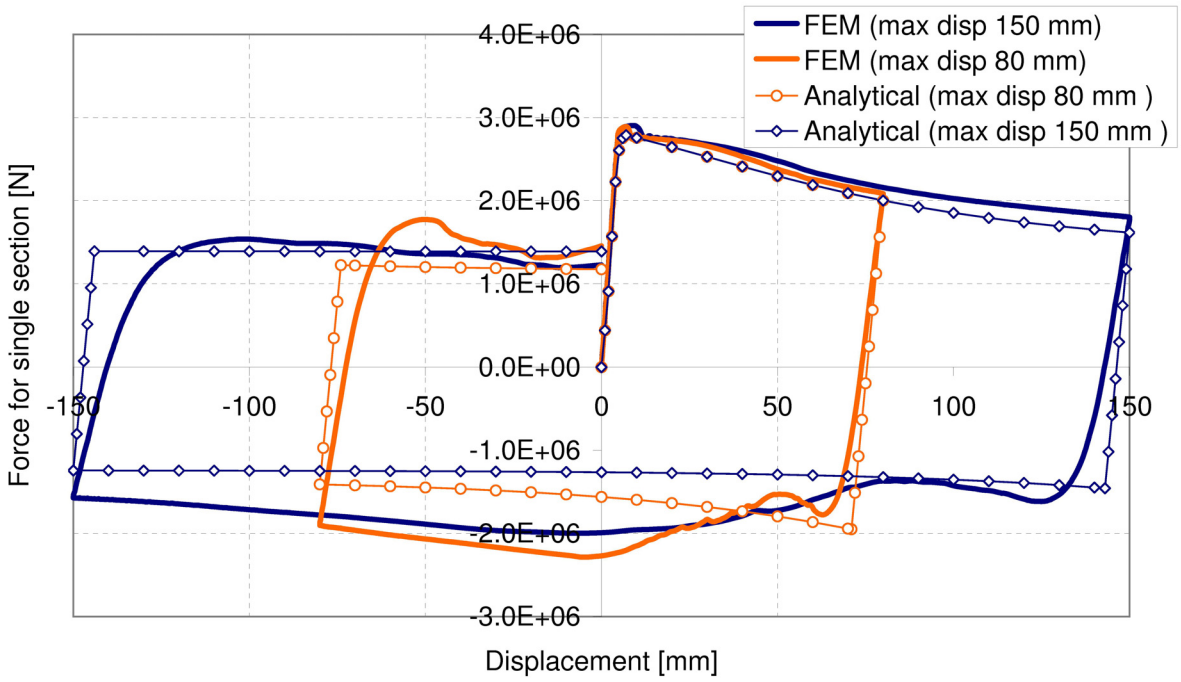

Figure 34. Structure B subjected to reverse shear loading.

3.6 DESCRIPTION OF THE CB-METHOD

In the present problem, quasi-static loading of the hull girder was used. The structural behaviour was non-linear. Geometrical non-linearity was not directly present, but still included through material behaviour described with averaged load-end shortening curves. Therefore, the structural strength might be reduced rapidly during loading. Thus, it was required to use a calculation procedure, which could control displacements and avoid their infinite increase in the post-collapse stage.

The Arc-length method is a suitable tool for solving problems where the response might decrease. Figure 35 presents a basic idea of the Arc-length method. Before each load increment, the direction of incremental displacements is estimated by calculating the tangent stiffness matrix D. An additional condition for the displacements is introduced by assuming that the length of the displacement vector cannot exceed predefined Δl during the load increment. Therefore, the load increment is automatically reduced when the incremental displacement vector tends to exceed the amplitude Δl. The equilibrium path is found when the required convergence at each load increment is reached. A detailed description of the method can be found presented in references Crisfield [9] and [10].

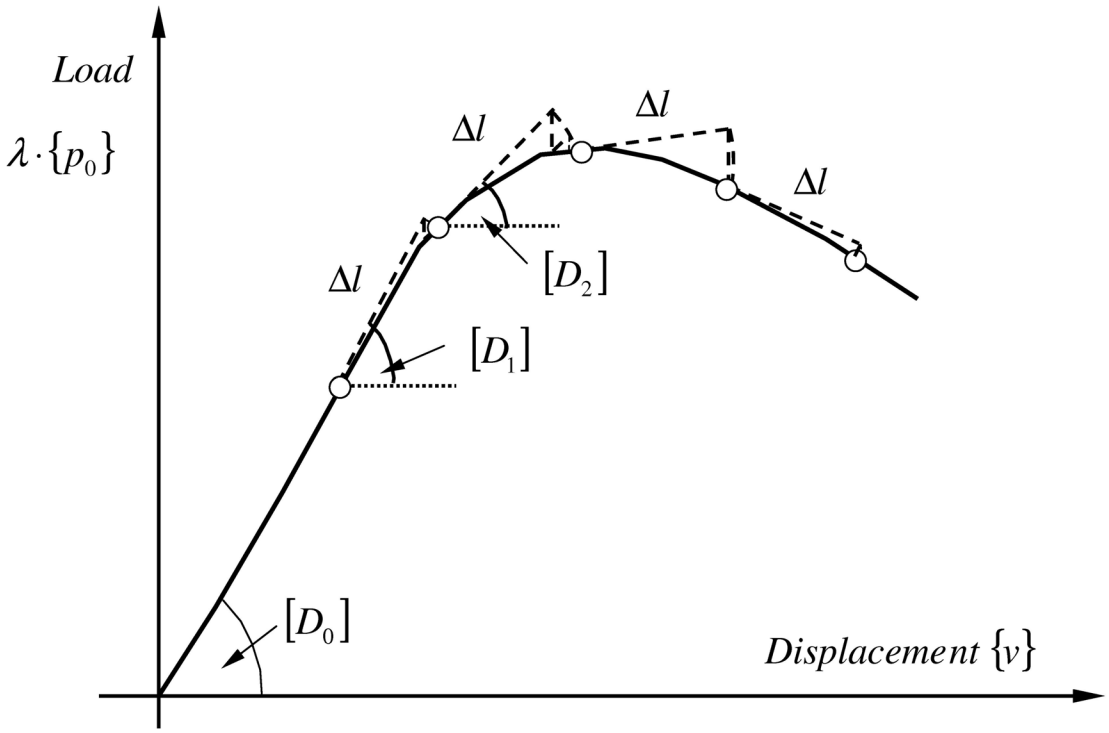

Figure 35. The arc-length method.

The flow chart of the CB-method is presented in Figure 36. The calculation started by reading the data from the input file, including the structural data of the hull girder. In the first stage, an initial load increment was assumed. Then the tangent stiffness matrix was calculated by using the cross-section data and analytically defined stress-strain curves. Thereafter, the new incremental displacement vector was approximated using the tangent stiffness matrix and initial loading. The calculation of internal forces and the equilibrium check indicated that a new iteration may be needed. If the equilibrium with a certain accuracy was not reached, the initial load increment would be modified and the equilibrium procedure would be repeated until the equilibrium point would be found. Now, the displacements and internal forces were updated and thus, a new bending moment value for the hull girder was calculated. The loop of this calculation procedure was repeated until a clear strength reduction of the hull girder was achieved. Finally, the ultimate moment could be defined from the response curve.

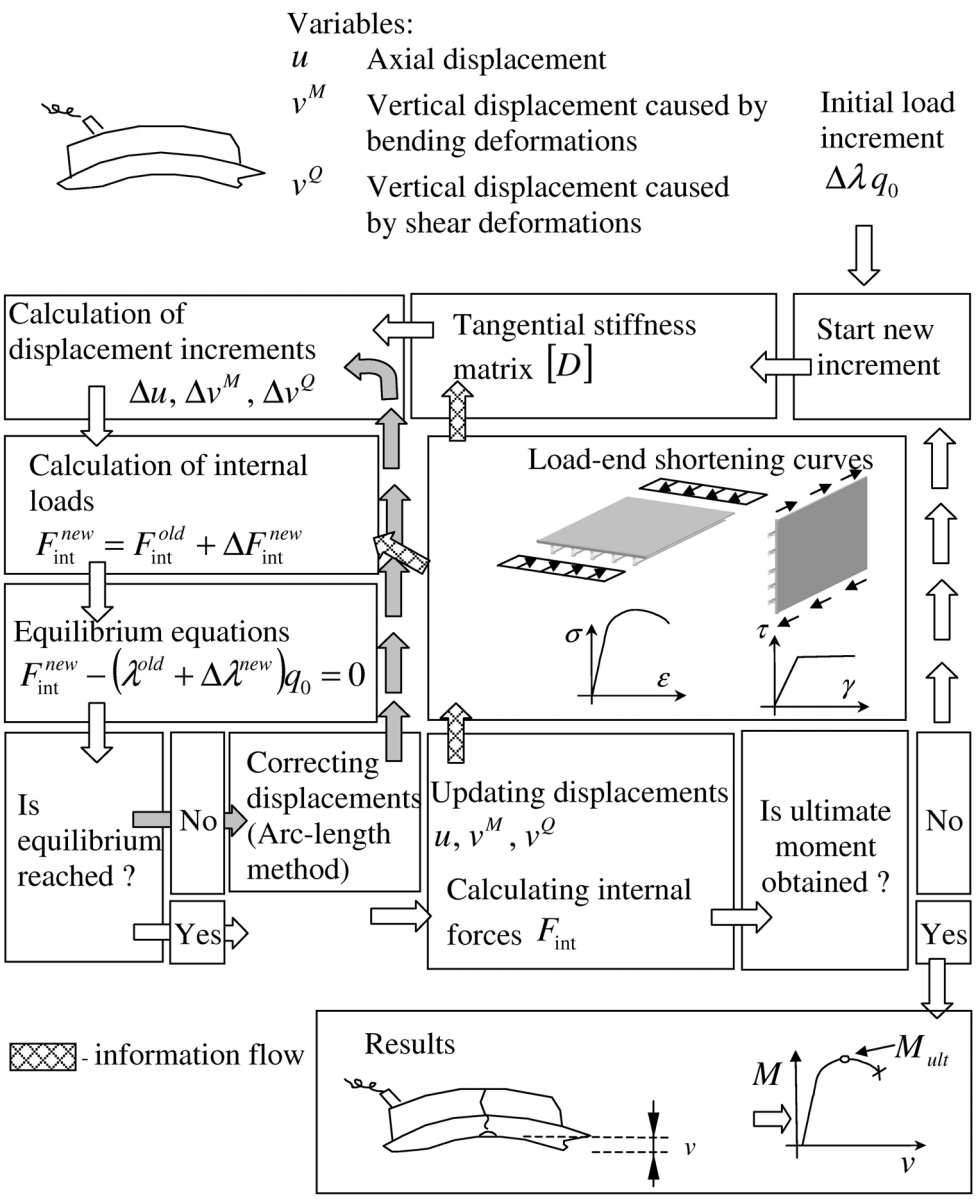

Figure 36. Flow chart of the CB-method.

In order to calculate the integrals used in the tangent stiffness matrix and equilibrium equations, the numerical integration over the beam length has to be conducted. For that, the hull girder was divided into transverse sections with the length of web frame spacing. The present integration scheme assumes that the functions are varying slowly between web frames. Therefore, it was possible to calculate the integral by summing the integrants.

4 CASE STUDIES

4.1 DOWLING'S BOX GIRDER

To demonstrate the validity of the CB-method, the calculated results were compared with the experimental test results received by Dowling et al. [13]. In those tests, several steel box girders were loaded with a point load or with the pure bending moment up to the ultimate strength. These structures can be considered as tanker type ship structures because they are composed of the upper and lower flange connected by two side webs. Therefore, the effects common to passenger ships with multi-layer decks were absent, but the comparison was intended to verify the calculation routine of the CB-method.

It was decided to use the test results conducted for model No. 2. During the tests, the force and displacements were measured. Some difficulties with the comparison were caused by the fact that in the structure significant residual stresses and initial deflections existed. These effects were not included in the load-end shortening curves. In order to consider these effects, the yield stress of the material was reduced.

4.1.1 Tested structure

The structure is shown in Figure 37. It consists of a box-type cross-section where the upper and lower flange have a thickness of $4.88\,mm$. Both plate fields are stiffened with four L shape stiffeners. The stiffeners have a web height of $50.8\,mm$, a flange breadth of $15.9\,mm$ and a thickness for the web and flange of $4.8\,mm$. Spacing for web frames is $787.4\,mm$. The structure is loaded with the constant moment all over the length of the structure up to collapse. The present loading condition can be called as sagging loading. The deflection was measured at the middle of the structure with respect to the first and fourth web frame.

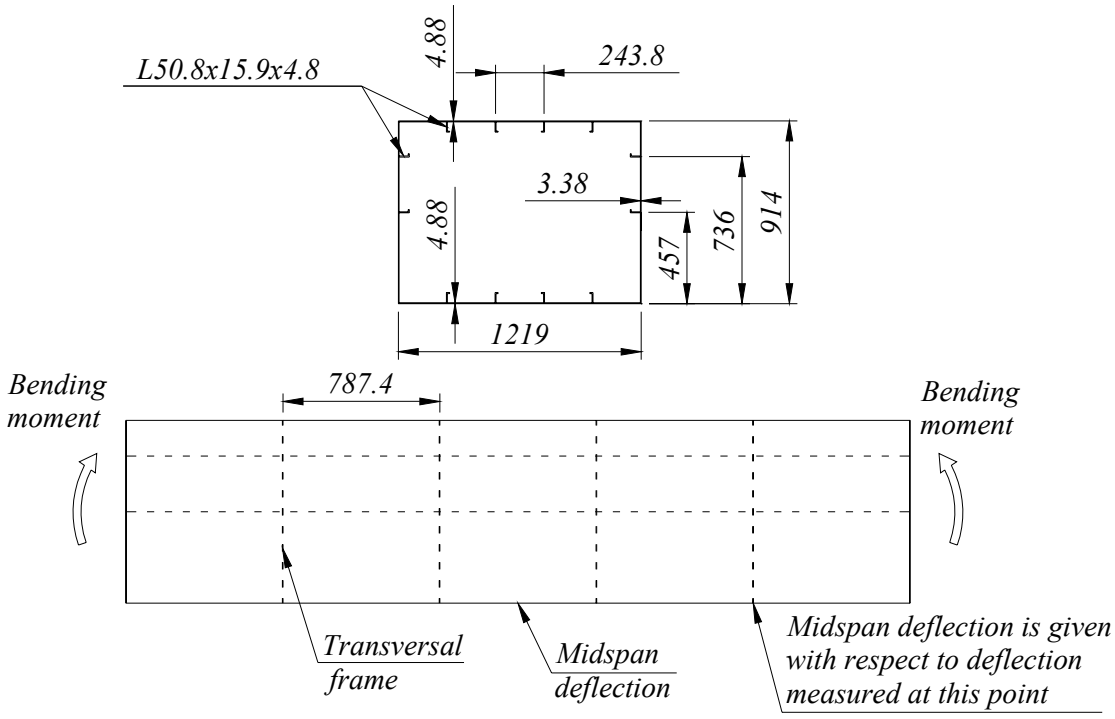

Figure 37. Box girder with dimensions. Drown based in the picture taken from reference Dowling et. al. [13]

The influence of residual stresses and initial deflections is crucial for the flange in compression. Therefore, the strength reduction of the compression flange was obtained by reducing the yield stress of the material. According to the test, the upper flange will fail at the stress value $205.4\ MPa$. Based on load-end shortening curves used in the CB-method, the failure stress for the stiffened panel was $228.0\ MPa$. The same load value at failure of the panel can be obtained, if the yield stress $232.0\ MPa$ is used instead of $276.5\ MPa$. The material parameters are given in Table 2.

Table 2. Properties of box girder.

Component	Dimensions (mm)	σ_y for structure (MPa)	E for structure (MPa)	σ_y for CB model (MPa)	E for CB model (MPa)
Upper flange	4.88	298.0	$208.5 \cdot 10^3$	276.5	$205.3 \cdot 10^3$
Lower flange	4.88	298.0	$208.5 \cdot 10^3$	276.5	$205.3 \cdot 10^3$
Web	3.38	211.6	$216.2 \cdot 10^3$	276.5	$205.3 \cdot 10^3$
Upper Stiffeners	$50.8 \times 15.9 \times 4.8L$	276.5	$191.5 \cdot 10^3$	232.5	$205.3 \cdot 10^3$
Other Stiffeners	$50.8 \times 15.9 \times 4.8L$	276.5	$191.5 \cdot 10^3$	276.5	$205.3 \cdot 10^3$

In the CB-method, the only loading possibility was the distributed load. Therefore, the loading condition similar to the test load was obtained using a longer test structure. The total length of the structure was taken 99 times the web frame spacing and the loading had a cosine shape. In this case, in the middle of the structure within 5 web frames, the bending moment value stayed almost constant and thus, the structure behaved similar to that of the test structure.

4.1.2 3D FEM analysis

The finite element for a steel box girder was analysed with the LS-DYNA FE-code. The structure was modelled in the same way as the structure used in the experiment. Four node shell elements were used in the FE-model. The residual stresses and initial deflections were included. According to the tests, see reference [13], the value for residual stresses was taken as 56 MPa of the compression in upper flange plate and 208 MPa of the tension in upper flange stiffeners. For the FE-model, the initial deflection of 2.3 mm downwards was used for the plate field of the upper flange. Heading to the side, the deflection was reduced linearly down to zero at the position of the webs. The load was increased in time, but the loading speed was taken so small that the kinetic energy of the structure did not exceed 5 % of the internal energy. The structural behaviour is shown at various load levels in Figure 38.

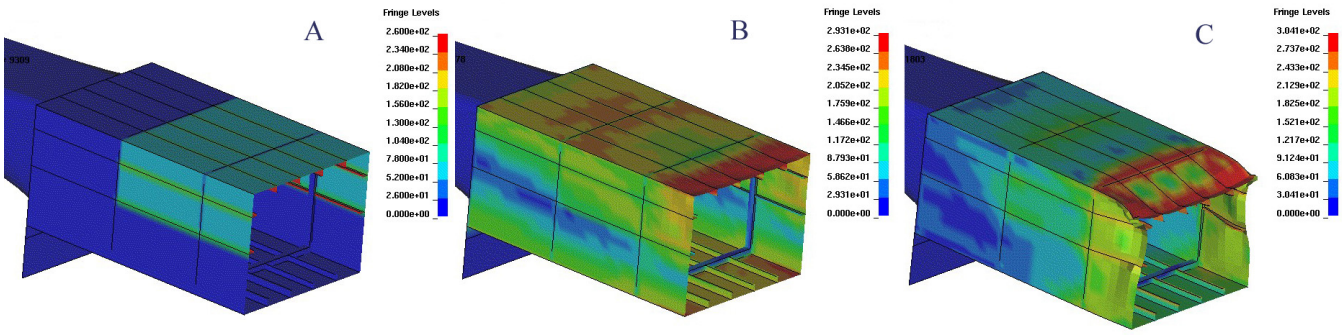

Figure 38. FE-model of a steel box girder. A) Initial state of the structure, B) Structure after plate failure, D) Structure after collapse.

4.1.3 Comparison

The curves of the moment as a function of the deflection are shown in Figure 39. The ultimate moment obtained in the test was 1550 kNm and the CB and FE-method gave 1650 kNm and 1730 kNm, respectively. The reason for the overestimates by the FE-method with the ultimate

strength of 11% may be due to the poor quality of the element mesh. This is indicated also by the shape of the FE-response curve at the collapse point, which differs clearly from that of the tests. Also, the longitudinal stiffeners may be too stiff in tripping and therefore the total panel strength was increased. Obviously, the FE-results can be improved by using more elements in the longitudinal stiffeners.

The difference between the CB-method and the test result was approximately 7 %, which is a good result. The fact that the moment curve by the CB-method and that of the tests are reduced with the same slope indicates that the post-collapse behaviour can be well described by the CB-method. The higher collapse strength in the case of the CB-method depends on the accuracy of the applied load-end shortening curves. The test result and the FE-analysis show that the CB-method can be well applied for the estimation of the ultimate strength of box-type structures.

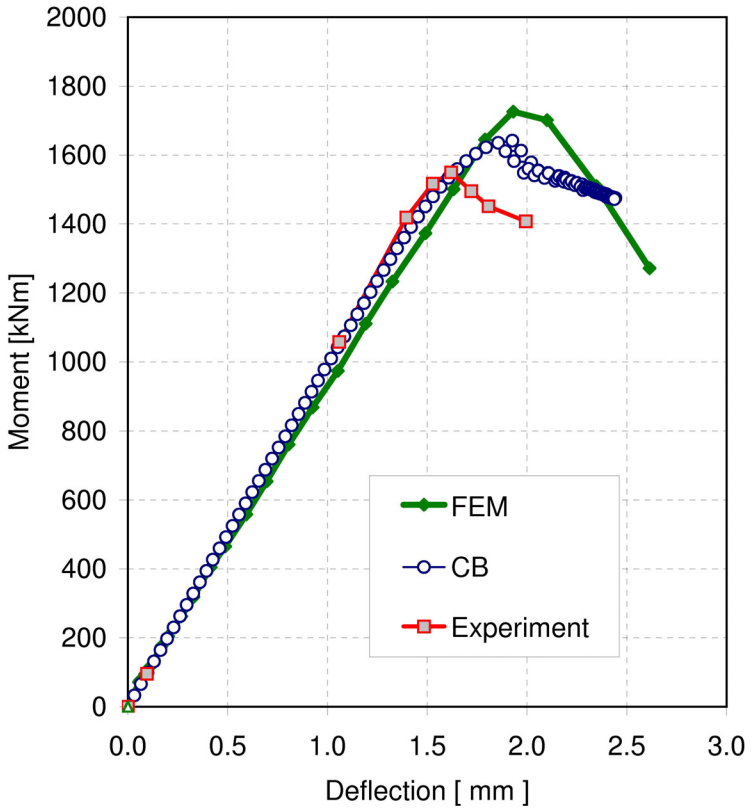

Figure 39. Moment-deflection curves of the steel box girder produced by experiment, the CB-method and the FE-method.

4.2 POST-PANAMAX PASSENGER SHIP

In order to test the applicability of the CB-method for a passenger ship with a modern layout, a post-Panamax type ship was analysed. The structure was considered as a prismatic beam with a

length of 273 m. The use of a prismatic beam compared to a non-prismatic one reveals the ultimate strength phenomenon in the hull girder more explicitly. The layout of the midship section is given in Figure 40. The analysis was focused on the prismatic hull girder, thus structural dimensions were based on the values of the midship section. The distributed load with a cosine shape was applied on the hull girder ensuring self-balance. This load described also well that required by Classification Societies, as the maximum value of the bending moment was at the midship and that of shear force at a quarter length measured from the ends.

4.2.1 Structure

The considered post-Panamax passenger ship has thirteen decks, a double bottom and a recess for lifeboats. According to the design, the web frame spacing is taken as $2730\,mm$. The uppermost deck is a box structure giving additional strength for the global bending of the hull girder. The lower decks are supported by pillars and by the side shell. In the superstructure, the longitudinal bulkhead is situated at a distance of $4000\,mm$ from the centre line. It starts from the 6^{th} deck and continues up to the 12^{th} deck and is vertically supported by the pillar line. The side plating of the superstructure has large openings with dimensions 2200×2100 mm starting from the 6^{th} deck. The ship has also twenty transverse watertight bulkheads up to the 4^{th} deck and six fire bulkheads from the 4^{th} deck to the uppermost deck.

In the structure, the shear load is designed to be carried by the side shell between the baseline and the 4^{th} deck and above it by the plating in the recess space between the 4^{th} and 6^{th} deck. Above it, the shear load is carried by the plating of the 6^{th} deck and by the longitudinal bulkhead between the 6^{th} and 11^{th} deck. All of those structural members transferring the shear flow are presented in Figure 40 where the path leading the shear flow is marked by ABCDEF. The thickness of the external shell plating is $16\,mm$ in the bottom area and $10\,mm$ between the 2^{nd} and 4^{th} deck. The thickness of the side shell in the recess area is 6 mm. Deck plating thickness is generally $5\,mm$ except the first three decks, where the thickness of deck plating is gradually increased from 5 to $7.5\,mm$. The longitudinal bulkhead has a plate thickness of $6\,mm$. For the stiffening of decks and longitudinal bulkheads, $HP100$ profiles are used. Most of the decks have longitudinal deck girders with a web of $480\times8\,mm$ and a flange of $200\times10\,mm$.

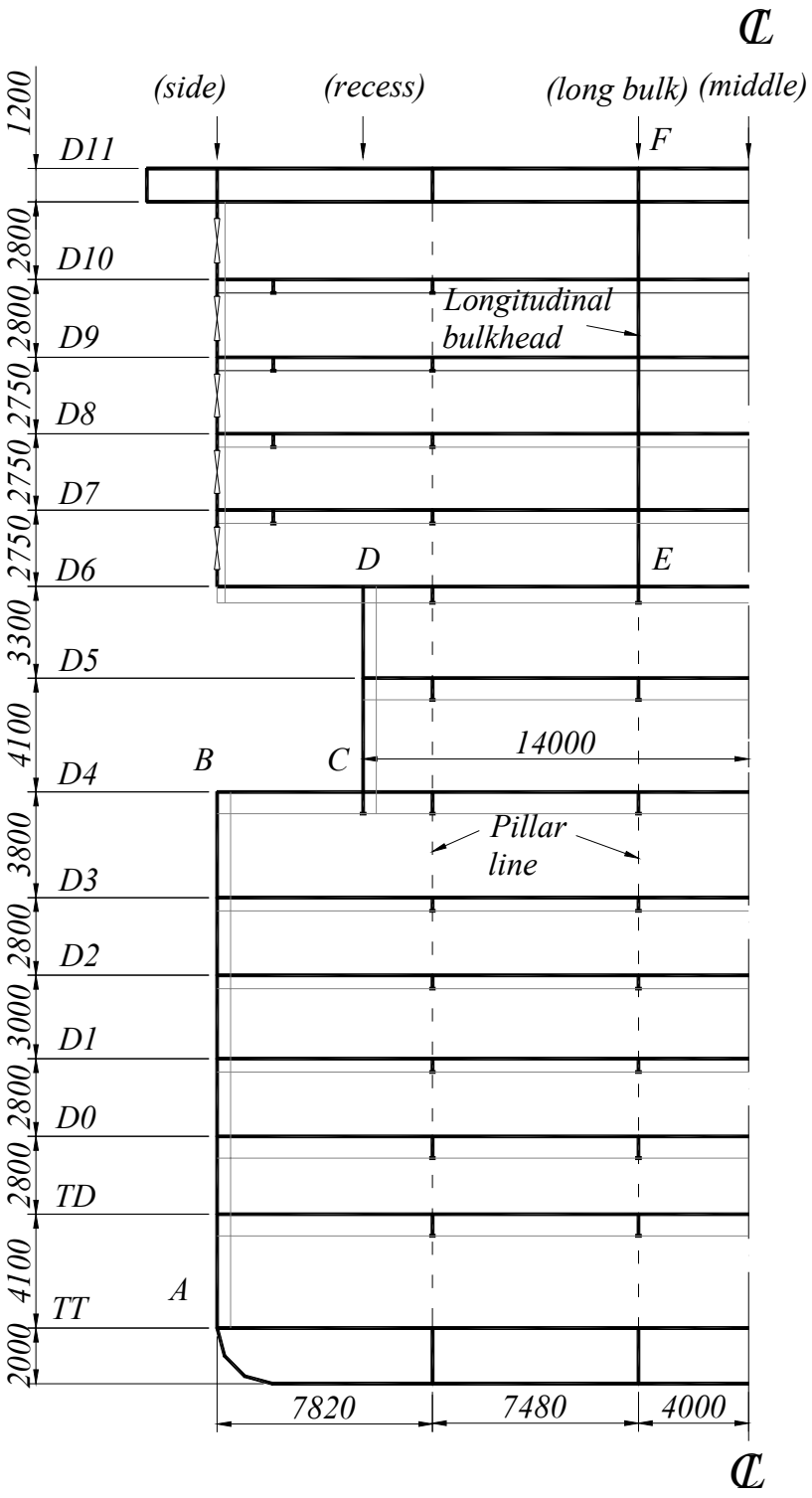

Figure 40. Layout of the midship section for the post-Panamax passenger ship.

4.2.2 3D FEM analysis

The non-linear FE-analysis for the post-Panamax passenger ship was conducted with the LS-DYNA FE-code. The 3D FE-model had a total of about 1,300,000 four-node thin shell elements and 170,000 two-node beam elements. The critical question for a large FE-model is the smallest element size, the element type and the total number of elements used in the model. It is clear that too small element size increases rapidly the need of memory capacity and calculation time. On the other hand, rough mesh in critical areas will produce a model that is too stiff, causing unrealistically high ultimate strength.

The mesh size problem of the hull girder was divided into two sub problems. The first one was related to longitudinal structures under normal stress, and the second one to that under shear stress. In order to model the longitudinal structural elements correctly, the test analyses were carried out for typical deck structures. In those analyses, deck structures were compressed by moving the boundaries, while the corresponding reaction force was calculated, giving as a result, the load-end shortening curve for each structure. The deck consisted of one large longitudinal girder, four longitudinals and a plating. Dimensions were chosen as $5\,mm$ for deck plating with $HP\,100$, bulb profile having a spacing of $680\,mm$. The longitudinal girder was taken as T-profile with $480\,mm \times 8\,mm$ for the web and $200\,mm \times 10\,mm$ for the flange. The first FE model had very dense mesh, which was not adequate for the global model. This model had nine four-node shell elements for the plate between longitudinals. For the longitudinal deck girder, six shell elements for the web and four shell elements for the flange were used. The stiffeners were modelled using four shell elements. The bulb region of the stiffener was modelled with a single shell element with linearly changing thickness. All the other models contained less dense mesh, which enabled us to save calculation time when using them in the global model. In Figure 41 the results from various simulations are presented.

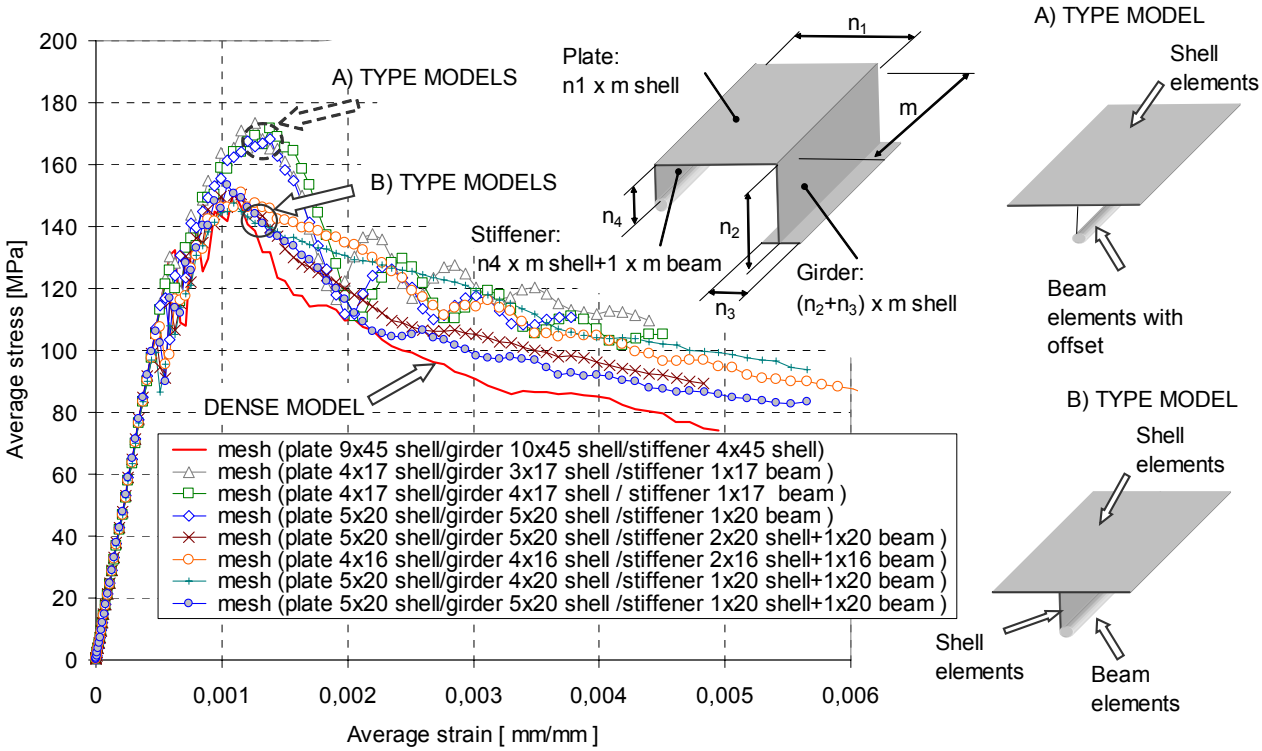

Figure 41. Comparison of various stiffened plate models in axial compression.

An important conclusion from these analyses is that to simulate proper collapse, at least four shell elements have to be used for plating between stiffeners. The longitudinals can be modelled using a one shell element for the web and a one beam element for the bulb. Figure 41 reveals that longitudinals, which are modelled as a single beam with offset, are clearly overestimating the ultimate strength. The reason for this is probably the effect of tripping, as in the case of A type models, the tripping is missing. An adequate mesh size will need 5×20 shell elements in the plate strip and 5×20 shell elements in the girder, of which 3×20 shell elements are applied in the web and 2×20 in the flange. Thus, for longitudinals, 20 shell and beam elements are required. This kind of dense mesh has to be used at the midship, as the axial collapse of stiffened panels is most likely to occur.

The second problem was related to structures under shear loading, like longitudinal bulkheads, side structures and decks, for instance, parts BC and DE in Figure 40. These structural elements had to be modelled such that the shear buckling of the stiffened plate structure could be possible. However, the mesh density described above may enable also the formation of shear buckling. Therefore, at the midship, the mesh density determined according to the test calculations could be considered sufficient also for side structures. However, for the structures carrying the shear load, the mesh density has to be the same all over the ship length, as the collapse induced by shear buckling can spread all over the ship length when the loading increases.

Therefore, 5x20 elements in the plate bounded by longitudinal stiffeners and transverse web frames were used for the hull girder mesh. However, this type of dense mesh could not be used everywhere in the model, as problem size might grow quickly beyond the computer capacity. Therefore, only critical regions where the collapse was expected were refined. Due to the shape of loading, it was assumed that the maximum normal stresses were expected at the midship. Therefore, the midship area inside the seven web frames was refined. In Figure 42 the area marked with letter B presents the midship region where the mesh was refined. The ship structure suffers also from relatively high shear stresses in the region $L/4$ and $3L/4$, where the shear force has maximum values. The high shear stress combined with the normal stress might cause shear failure, which can start with a lower load value than axial failure amidships. Therefore, the same element density was used in the areas marked with letter A and B, see Figure 42.

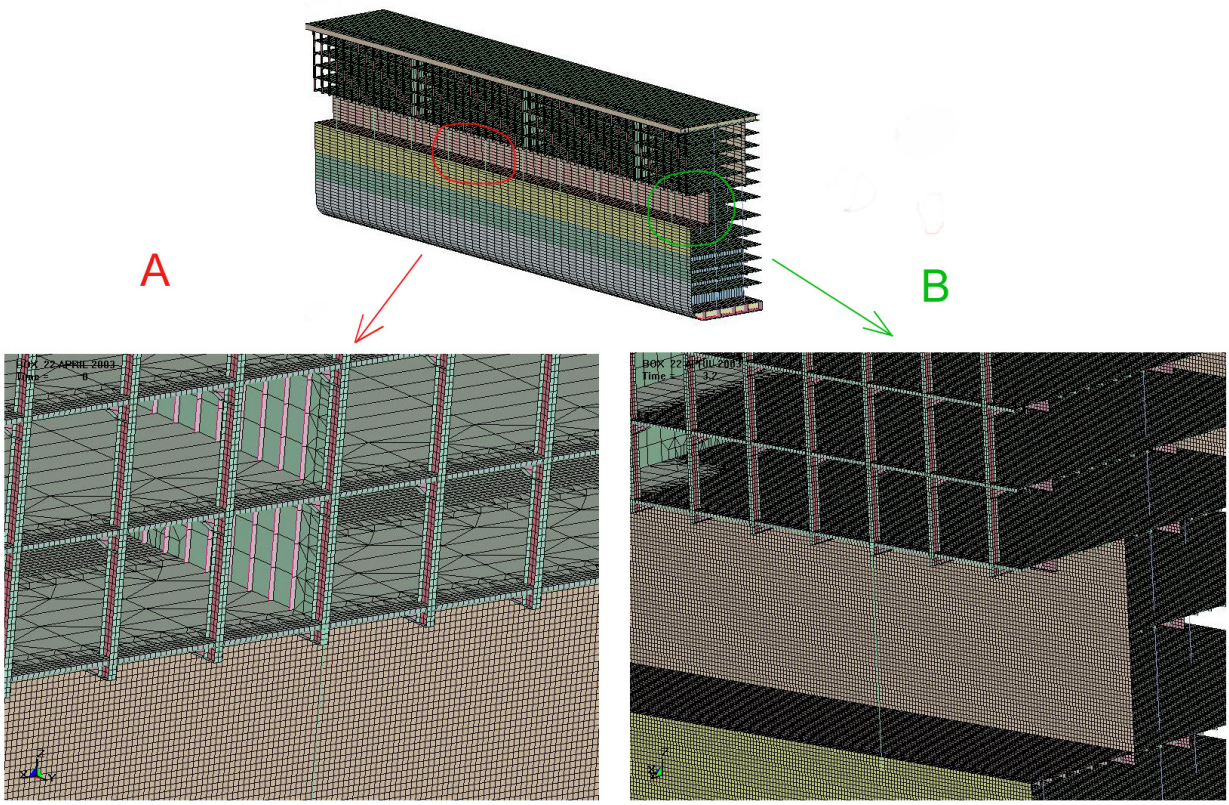

Figure 42. Mesh density for different model areas.

The FE-model was a quarter model, where the symmetric boundary conditions were used at the midship and at the centreline. As axial collapse at the midship was expected, the applied boundary conditions could prevent anti-symmetric collapse modes in axial structural components. However, it was assume that their effect is small. The loading of the hull girder was considered as a line load, see Figure 43.

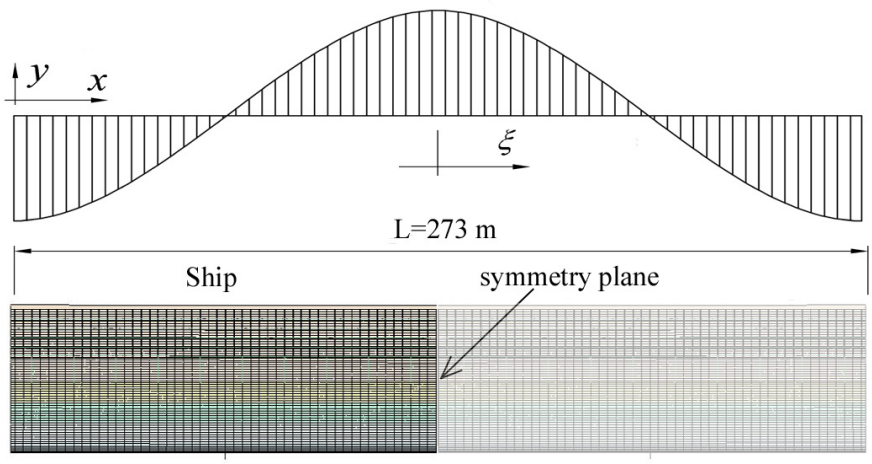

Figure 43. Loading for a ship beam.

The distributed line load was applied as pressure on the ship bottom. During the simulation the load shape was fixed and the load amplitude was gradually increased. As the explicit LS-DYNA code enables only dynamic analysis, loading speed was again taken so small that the kinetic energy of the structure would not exceed five percent of the internal energy. The moment amidships were calculated from the normal stresses by a simple routine. Stress values for each element were obtained from the database created by the FE-code. The summation of element stresses multiplied by element areas and positions will give the value for the moment at each time step. Similarly, the FE-database gives the maximum deflection of the hull girder at each time step.

4.2.3 Analysis with the CB-method

The midship section of the hull girder was divided into beams for the CB-analysis. The geometry of the section was complicated and due to this the mixed coupling between beams had to be used. The division of the section to the beams is shown in Figure 44, where the numbering starts from the bottom beam. The total number of the beams was 25. The beam marked with number one consists of double bottom and two lowest decks, as the continuous side plating is so thick there that the shear effect can be neglected. Thus, further division will not improve the results. The rest of the midship section was divided into two or three beams per deck, as there the shear flow follows two different paths. Normally, the pillars had so small shear stiffness that their influence on the shear flow could be neglected. The number sets with small letters, separated by a comma define the coupling numbering. For each beam, six shape functions were used, giving the total number of degrees of freedom (DOF) in the CB-model as 450.

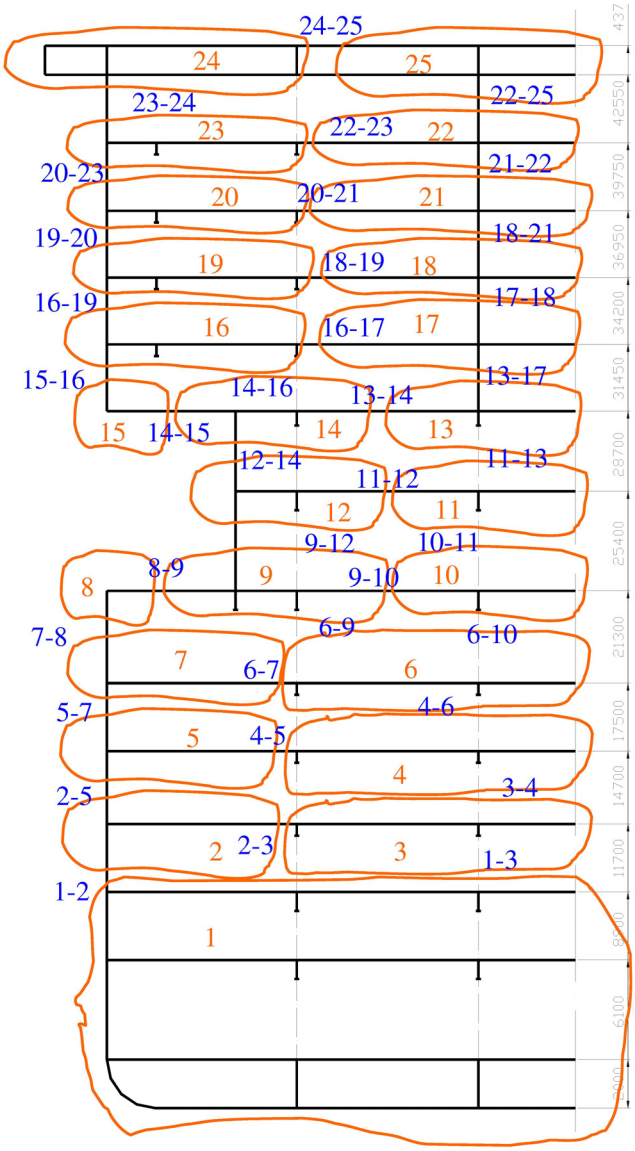

Figure 44. Set of beams for a post-Panamax passenger ship.

4.2.4 Comparison of results

In the sagging loading condition, the upper decks are in compression and the bottom structure is in tension. The loading path and failure modes are shown in Figure 45 and Figure 46. Structural failure started with shear buckling at the recess area at $x = L/4$, at the same time elastic buckling of the upper decks at the midship occurred, marked as 1 and 2 in Figure 45 and Figure 46. At the next face, the upper decks failed, marked as number 3. Due to this, the slope of the moment-deflection curve changed rapidly. The ultimate strength was reached when the failure progressed to the 3rd deck, marked as number 4 in Figure 45 and Figure 46. The ultimate moment value of the hull girder in sagging was $8.3 \cdot 10^6$ *kNm*.

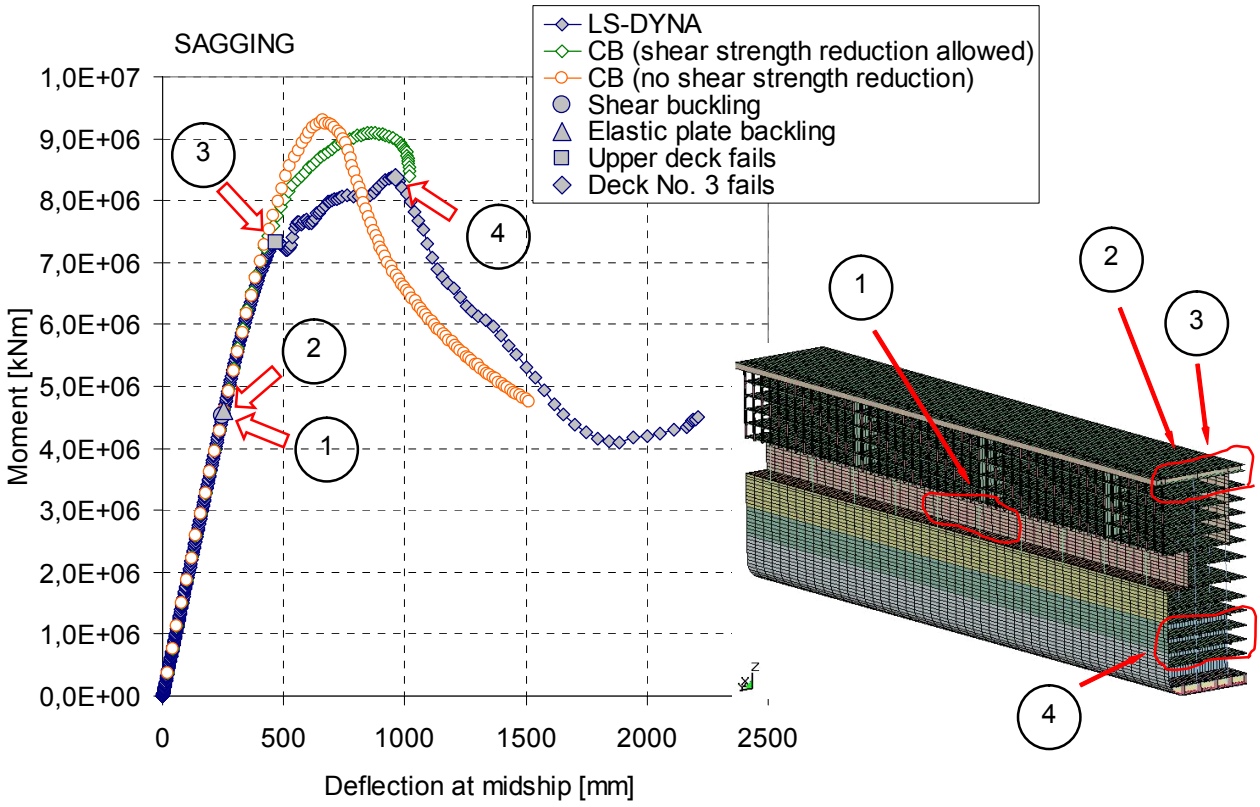

Figure 45. Moment-deflection curves under sagging loading.

The CB-method gave an estimation of the ultimate moment $9.0 \cdot 10^6$ *kNm*. The correlation between the results calculated with the FE-method and with the CB-method is good. It is important to point out that after the failure of the upper deck, marked as number 3, structural stiffness was reduced remarkably. At this face, the ultimate shear strength of stiffened plating at the recess area was also reached. The CB-method was able to estimate this strength change only where the shear member included also strength reduction, see the green curve in Figure 45.

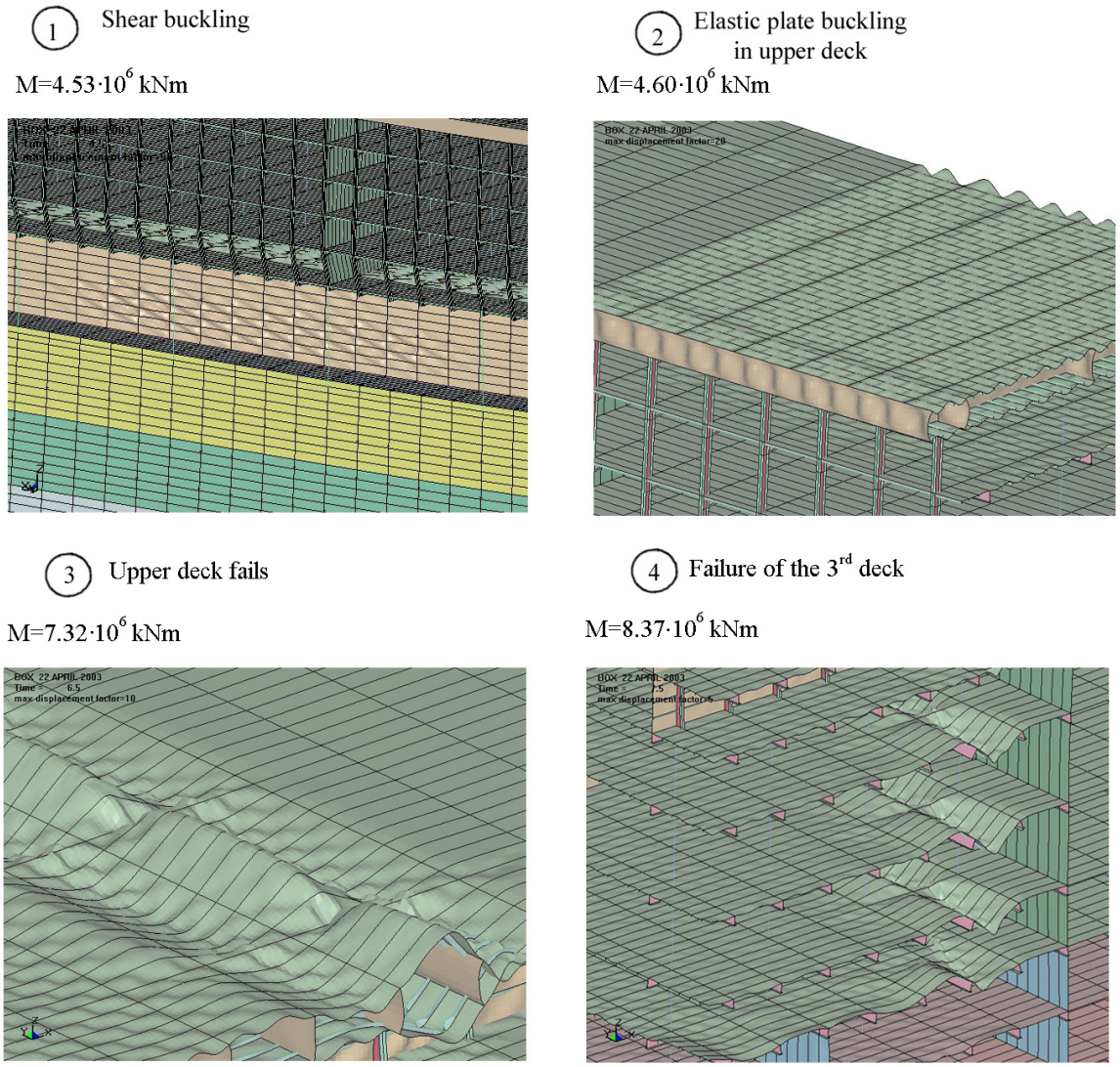

Figure 46. Failure modes of hull girder in sagging loading produced by the FE-analysis.

The behaviour of the hull girder in the post collapse stage was well estimated also with the CB-method. The results by the FE-method presented in Figure 45 show that a tremendous strength reduction of the hull girder occurred. The same behaviour was obtained by the CB-method. The fact that the CB-method overestimated the ultimate strength might be caused by the fact that the normal stress was not considered for the shear strength estimation of panels.

In the hogging case, the upper decks are in tension and bottom structures in compression. The upper decks can carry significantly more load in tension than in compression due to the slenderness of the structural elements. Therefore, the shear failure in the recess area occurred much earlier compared to the compression failure in the longitudinal bulkhead at the midship. These failure modes are marked with numbers 1 and 2 in Figure 47 and Figure 48. It might be difficult to

understand why the compression failure occurs in the bulkhead at the midship, marked with number 2 in Figure 47. This could be explained by the fact that as a result of the shear failure of the recess, the normal stresses could not be transferred from the hull to the superstructure. Therefore, they both bent independently and the lower part of the superstructure could reach the compression stress sufficient for panel collapse earlier than the bottom structure.

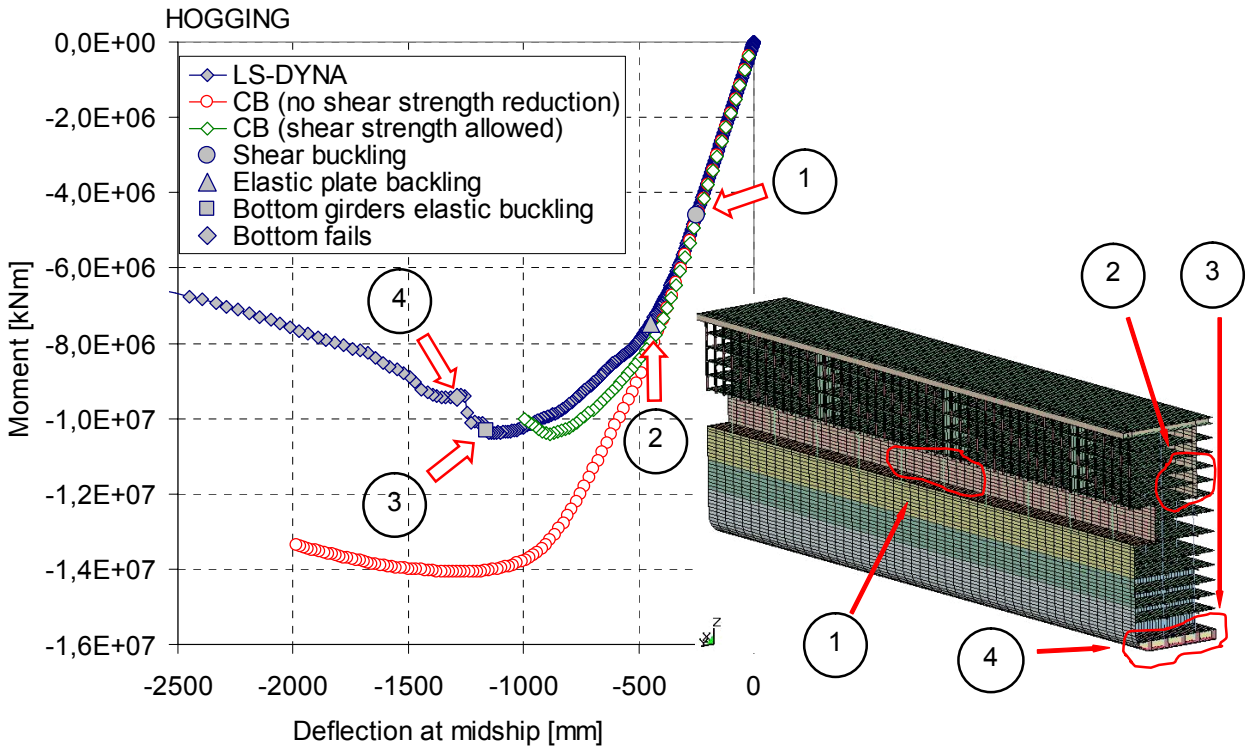

Figure 47. Moment-deflection curves under hogging loading.

Load increase resulted in the bottom girders buckling in the elastic compression mode, marked with number 3 in Figure 47 and Figure 48. At that point, the ultimate strength of the structure was reached. Finally, the whole bottom structure collapsed, causing the reduction of the bending moment.

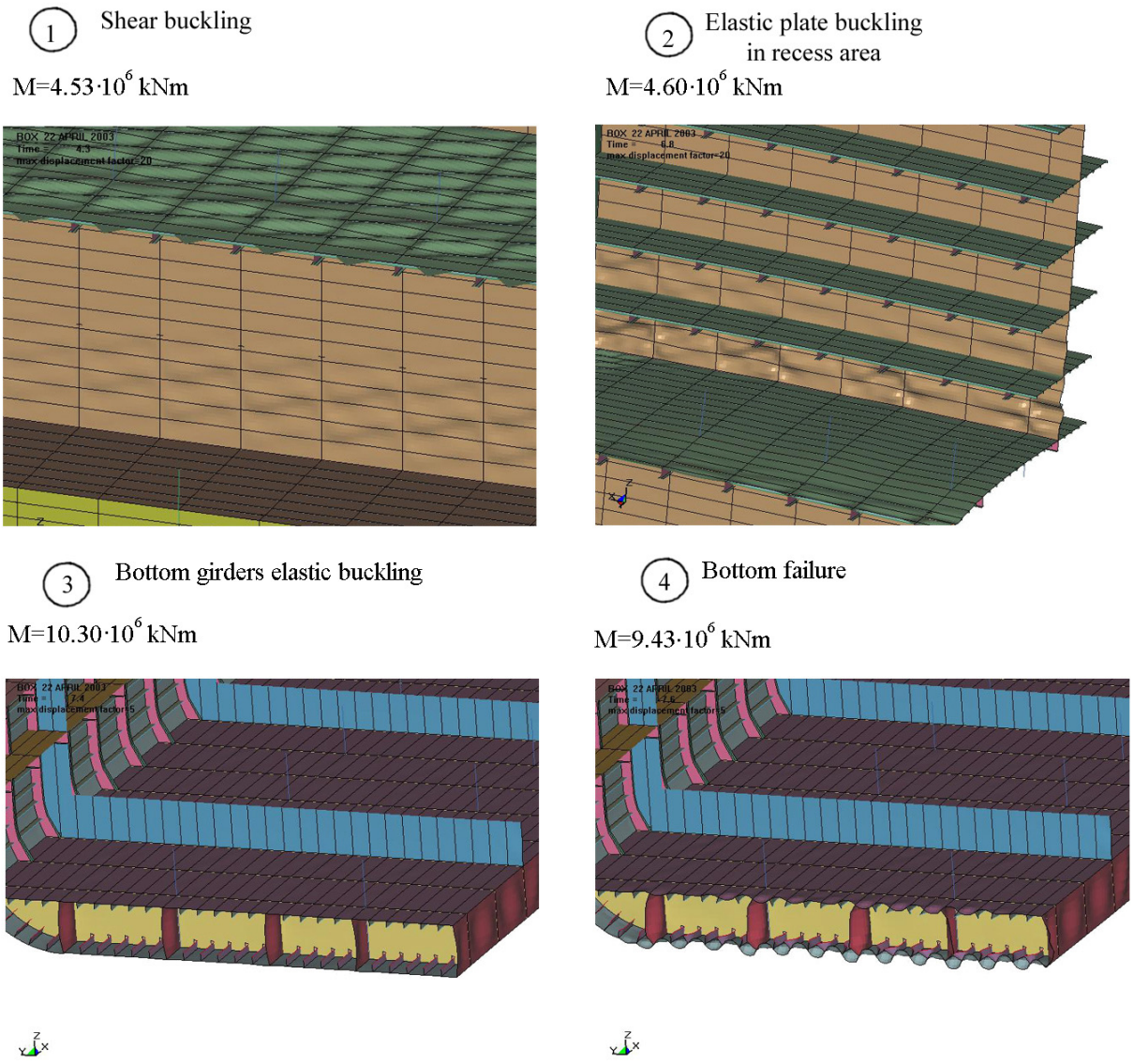

Figure 48. Failure modes of hull girder in hogging loading.

The results of the CB-method indicated that the strength reduction of shear members had a tremendous effect on the ultimate strength of the hull girder. When this reduction was considered, the moment-displacement curves obtained with the CB-method coincided with those by the FE-method. If the shear strength reduction was not allowed, the CB-method produced almost 40% higher moment value. This effect could be again explained by a situation where the superstructure and hull bend separately.

The comparison of stresses amidships probably provides the best understanding about the structural behaviour obtained by different calculation methods. The normal stresses in the sagging condition were calculated for the deflection $v = 135\,mm$. The CB-method followed well that of the FE-method before the shear buckling occurred, see Figure 45. For the deflection $v = 230\,mm$,

stresses in the lower part of the hull girder still matched well, but those in the upper part had some discrepancy. This was caused by too high shear stiffness in the recess area in the case of the CB-method. The fact that the shear stiffness was too high might be due to the fact that in the case of the shear buckling of the side structure, the effect of the normal stress was not taken into account. During the load increase, the situation improved as the upper decks collapsed and thereafter had a small influence on the equilibrium, see Figure 49. The similarity between the stresses produced by the FE- and CB-method was remarkable. The normal stresses in the ultimate stage for the deflection $v = 962\,mm$, shown in Figure 50, showed clearly that the load-end shortening curves used in the CB-method had not responded to the real situation. For example, the longitudinal girders in the 2nd deck produced high stress values in the case of large strains. In the ultimate stage, the result obtained by the FE-method indicated that the neutral axis had drifted almost 5 m downwards from the initial position. This phenomenon was not so strong in the case of the CB-method.

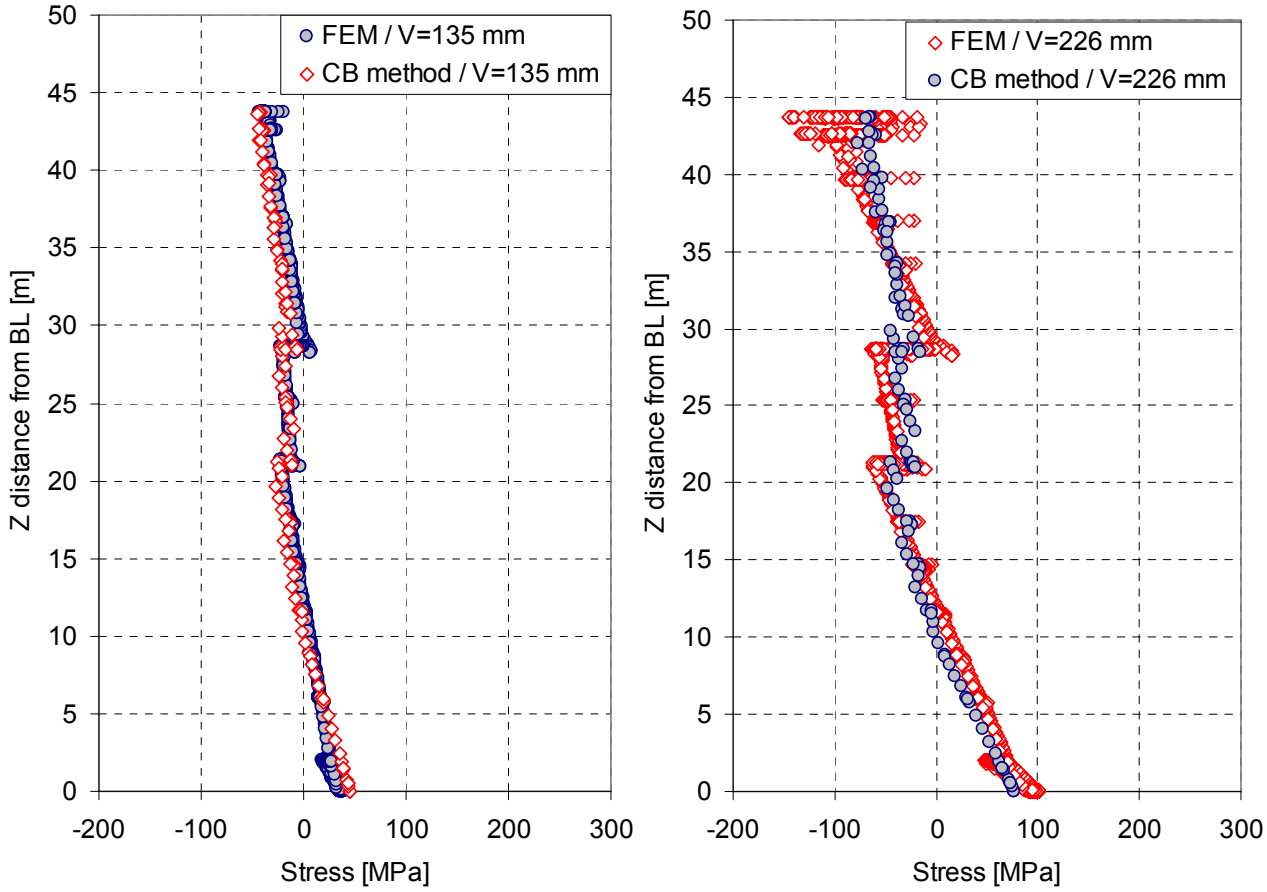

Figure 49. Stress distributions at the midship section in the sagging case with the beam deflection $V = 135\,mm$ and $V = 226\,mm$, respectively.

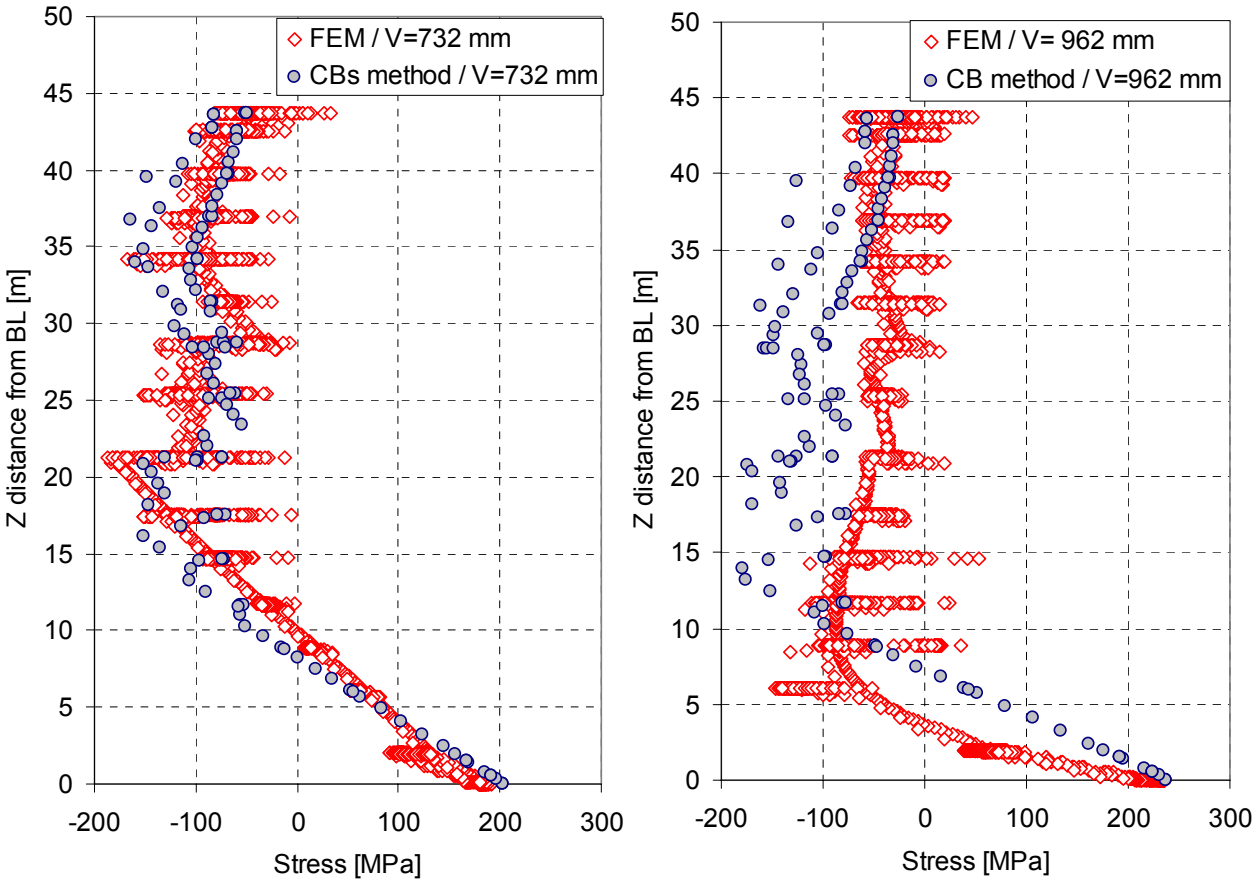

Figure 50. Stress distributions at the midship section in the sagging case with the beam deflection $V = 732\ mm$ and $V = 962\ mm$, respectively.

The shifting of the neutral axis is a factor that indicates that the reverse loading in the structural members is possible. The member located in the tension zone might encounter compression instead of tension after the shift of the neutral axis. This fact can be observed from Figure 50 where the distance of the neutral axis from the base line changed from 12 m to 9 m, when the bending moment value had increased from $6.0 \cdot 10^6\ kNm$ to $8.2 \cdot 10^6\ kNm$.

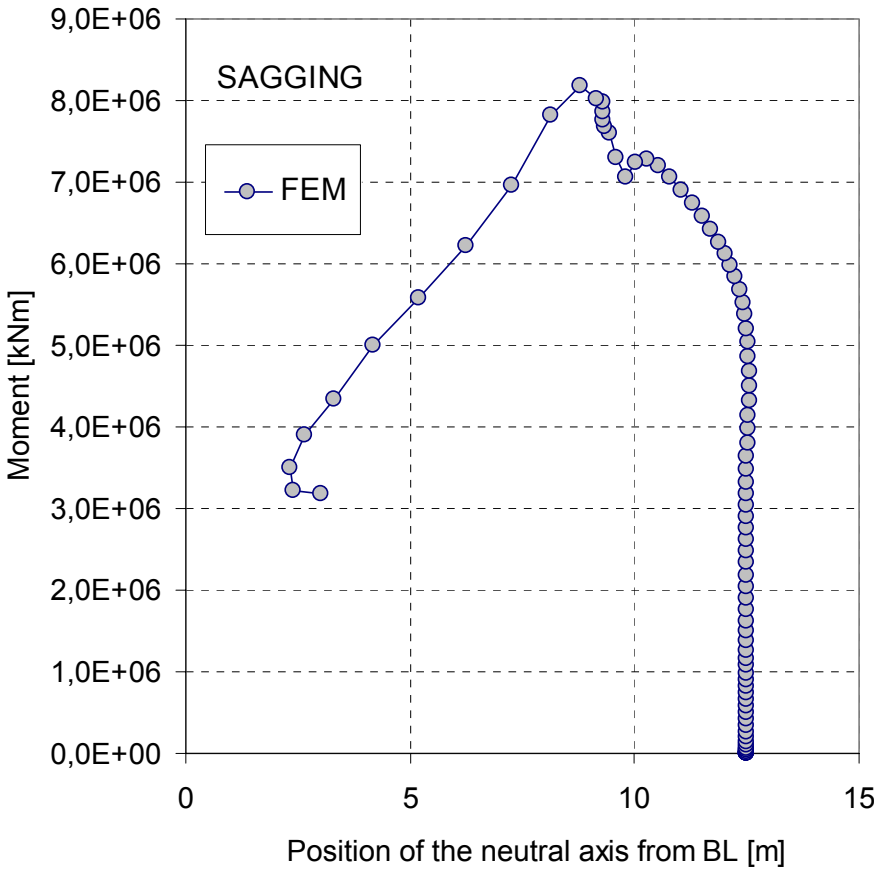

Figure 51. Position of the neutral axis measured from baseline.

5 DISCUSSION

The ultimate moment values of the hull girder for the post-Panamax passenger ship obtained by the FE- and CB-method are presented in Figure 52. The comparison of the ultimate moment values can give several interesting results. First of all, the correlation of the results is excellent, proving that the CB-method is applicable to the analyses of the ultimate strength for passenger ships when the hull girder is considered to be prismatic. In the case of passenger ship, the ultimate strength in the hogging loading is about 25 % higher than that of in sagging loading, see Figure 52.

The shear strength reduction of stiffened panels after the shear buckling is an important issue since it has a substantial influence on the ultimate strength of the hull girder. The results by the CB-method given in Figure 52 show that the ultimate moment of the hull girder in hogging loading drops drastically, almost 30 percent, when the shear strength reduction is taken into account. This causes strong separation of the superstructure from the hull, especially in the hogging loading. In the phase of initial loading, the hull girder behaves more or less like a single structure but after reaching the ultimate strength, both structural units tend to bend as individual beams.

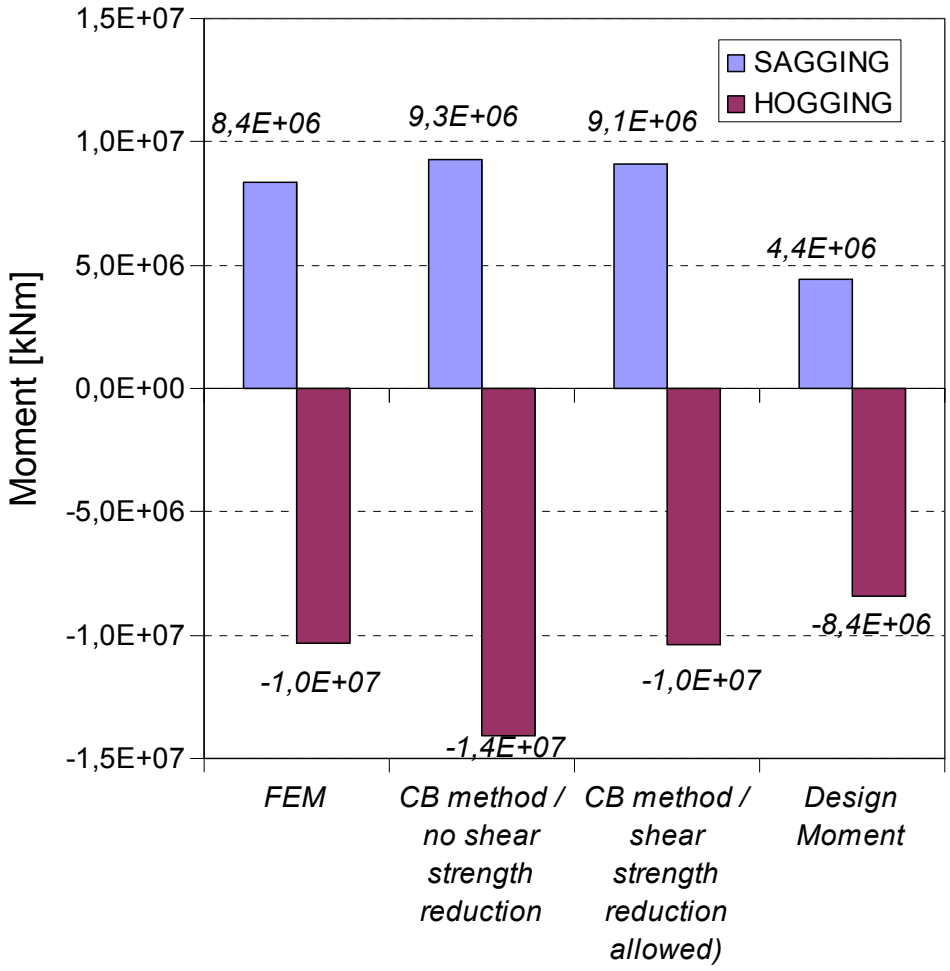

Figure 52. Results of ultimate strength analyses compared to design loads for the prismatic hull girder of the post-Panamax passenger ship.

It is important to compare the results with the design loads given by the Classification Societies. For this comparison, DNV rules [11] were used. According to the rules, the design moment consists of the sum of the bending moments of still water and the wave. The passenger ships are always in the hogging conditions in still water, where buoyancy force is concentrated at the midship area due to the low block coefficient and the weight of the ship is more equally distributed. However, it must be recognised that the lightweight of the ship plays a more important role than deadweight. During the construction process, a need for large cut outs near amidships exists, causing the neutralisation of the stresses induced by still water loading. Thus, the total bending moment in the sagging loading condition is calculated assuming zero value for the bending moment of still water. Naturally, in the hogging loading condition, the maximum value of the bending moment of the hogging still water is applied. Based on this, the design moments for sagging and hogging are presented in Figure 52. The comparison of the results shows that the ratio between the ultimate and design moment is about 1.75 for the sagging condition and 1.2 for the hogging condition. The comparison of this design moment value in hogging to the moment-deflection curve in Figure 47 reveals that the buckling

process had started below the design moment. This exceptional result was due to the selected approach of the analysis based on the assumption of the prismatic hull girder. Thus, the local structural strengthening for instance in the areas having high shear stresses was excluded.

The results reported recently [34] on the bending moment of the hull girder for passenger ships in a damaged condition indicate that the bending moment of still water in sagging may also appear in the accidental loading case based on SOLAS rules.

6 CONCLUSIONS

The coupled beams method is a useful tool to estimate the ultimate strength of the hull girder in the case of passenger ships with a multi-deck superstructure. This method is based on an assumption that the ship structure can be modelled as a set of coupled beams. In this work, the theory of the non-linear CB-method was developed and presented. The essential innovation in the method is the modelling of the coupling between beams in the hull girder with non-linear springs described with the load-displacement curves. Special emphasis was put on the springs carrying shear loading, called as shear members. All the coupling members as well as beams are capable of considering the non-linear effects caused by material plasticity or the loss of stability.

The load-end shortening curves of the structural members used in the beams were validated with the 3D FE-analysis for the deck structures typical of a passenger ship. The analysis proved clearly that the formulas from the literature are well applicable. A special semi-analytic model of the load-displacement curves for the coupling members in shear with opening options was created. There, the shear strength reduction included in the load-displacement curves proved to play an important role in the ultimate strength of the hull girder, especially in hogging loading. Additionally, the possibility of reverse loading included as the FE-analyses of the hull girder revealed that this might give a significant contribution to the normal stresses of the hull girder close to the ultimate stage. The different reverse loading schemes based on the analytic formulas were validated with the FE-analysis.

In this thesis, the CB-method was applied to the prismatic hull girder of a post-Panamax ship. The ultimate strength of the hull girder was estimated both in sagging and hogging loading. The Arc-length approach used in the CB-method made it possible to clearly distinguish the ultimate stage of the hull girder. This fact can be seen from the load-deflection curves, especially in the area where the load level starts to reduce after reaching the ultimate point. Also, the CB-method enables one to estimate the deflections, axial displacements and normal stresses in the hull girder.

The non-linear FE-method offered an excellent possibility to validate the CB-method and also to improve the understanding of the collapse process of the hull girder. A quarter FE-model of the hull girder was used for this purpose. In order to optimise the calculation time, an intensive suitability study of the finite element mesh was carried out. Based on this, the configuration and proper element size for the plating and stiffeners were determined. It was assumed that the critical area for the global FE-model was the midship region, as a maximum bending moment occurs there. Furthermore, the longitudinal bulkhead and side structures based on the mesh suitability analysis were refined all over the ship length, as the shear collapse might have a major influence.

The ultimate strength of the prismatic hull girder in the case of the post-Panamax passenger ship was estimated with the CB-method and with the FE-method. According to the CB method, the ultimate bending moment in sagging was $9.1 \cdot 10^6\ kNm$, which is 9 % higher than that according to the FE-method - $8.4 \cdot 10^6\ kNm$. In the hogging condition, the ultimate strength values are almost the same, having only around 1 % difference. By the CB-method, the value of the ultimate bending moment was $10.4 \cdot 10^6\ kNm$ and by the FE-method $10.3 \cdot 10^6\ kNm$, correspondingly. Slight differences in stresses and deflections could be observed after the first non-linear effects. However, the stresses, deflections, and ultimate load can be well estimated with the CB-method, enabling the use of the method in the concept stage of the ship project.

On the basis of the results obtained by the FE- and CB-method, the failure process of the hull girder could be described in detail. In the sagging loading, the structural failure starts with the shear collapse of the recess area and at the same time, the elastic buckling of the upper decks takes place. The ultimate strength is reached when the failure progresses down to the lower decks. In the hogging loading, the first failure is induced by the shear buckling at the recess area situated at a quarter length from both ends. Thereafter, shear collapse progresses towards the midship section, causing the separation of the hull and the superstructure. Next, the longitudinal bulkhead will collapse due to the combination of the normal and shear stress. Finally, the ultimate strength is reached when the bottom structure fails. The results related to the failure modes show clearly that the shear strength of the longitudinal bulkheads and side structures plays a very important role. The 3D FE-analysis also revealed that the strength increase effect of the transverse bulkheads on the hull girder is small. However, the transverse bulkheads might initiate a failure at the joint between the bulkhead and the hull girder. This behaviour can be clearly seen in hogging where the collapse started at the transverse bulkhead.

In the present study, a validation was carried out for a single ship. To acquire more reliable knowledge, several ships with various midship sections should be investigated. Also, the tests in a small-scale could produce valuable validation data.

The CB-method proved to be a useful tool for the estimation of the ultimate strength in the case of passenger ships with a multi-deck superstructure. This method offers an accuracy below 15 %. The main advantage of the CB-method is that it saves time. The input model for the prismatic ship was done for the CB-method within one day, when for the 3D FE-method, the modelling time was up to one month. Also, the calculation time was much shorter for the CB-method. Instead of 12 days, using a two processor PC, FE-calculations by the CB-analysis were carried out within 10-15 minutes using a normal PC.

The theory of the CB-method developed in this thesis enables one to analyse in principle the ultimate strength for a non-prismatic ship structure with structural discontinuities. However, a thorough validation must be carried out before the non-prismatic approach can be applied in design work. It would be advantageous to understand the effect of the bow and aft part of the ship on the ultimate strength.

REFERENCES

[1] Bai Y, Bendiksen E and Tendrup Pedersen P. Collapse analysis of ship hulls. Marine structures 6, 1993, pp. 485-507.

[2] Bureau Veritas. Rules for Classification of Steel Ships. Edition December 2003.

[3] Beghin D, Jastrzebski T and Taczala M. Result - A computer code for evaluation of the ultimate longitudinal strength of hull girder. Proceedings of PRADS 95; the 6th International Symposium on Practical Design of Ships and Mobile Units, Vol. 2, 1995, pp. 832-843.

[4] Bleich HH. Nonlinear distribution of bending stresses due to distortion of the cross section. J. Applied Mechanics, Vol. 20, 1952, p. 95.

[5] Caldwell JB. The effect of superstructure on the longitudinal strength of ships. Trans. Instit. Nav, Archit., March, 1957.

[6] Caldwell JB. Ultimate longitudinal Strength, Trans RINA, Vol.107, 1965, pp.411-430.

[7] Chapman JC. The interaction between a ship and a long superstructure. T.I.N.A. Vol. 99, 1957, p. 618.

[8] Crawford L. Theory of long ships' superstructures. Trans. Soc. Nav. Archit., N.Y., Vol. 58, 1950, p. 693.

[9] Crisfield MA. Non-Linear Finite Element Analysis of Solids and Structures. Vol 1. John Willey & Sons, West Sussex, England, 1991.

[10] Crisfield MA. A fast incremental/iterative solution procedure that handles "Snap-through". Computers & Structures, Vol. 13, 1981, pp 55-62

[11] Det Norske Veritas. Rules for Classification of Ships. Part 3, Ch. 1, Hull structural design ships with length 100 meters and above. Norway, January 2004.

[12] Dow RS. Testing and analysis of 1/3-scale welded steel frigate model. Proceedings of International Conference on Advances in Marine Structures. Dunfermline, Scotland, 1991, pp. 749-773.

[13] Dowling PJ, Chatterjee S, Frieze PA, Moolani FM. The experimental and predicted collapse behaviour of rectangular stiffened steel box girders. Int Conference on Steel Box Girder Bridges, Institute of Civil Engineers, London, 1973.

[14] Fransman J. The influence of passenger ship superstructures on the response of the hull girder. Trans. RINA ,1988.

[15] Gere JM and Timoshenko SP. Mechanics of Materials: Third Edition. PWS-KENT Publishing Company, Boston, 1990, pp. 693-694.

[16] Gordo JM and Guedes Soares C. Approximate methods to evaluate the hull girder collapse strength. Marine structures, Vol 9, no 3-4, 1996, pp. 449-470.

[17] Gordo JM, Guedes Soares C and Faulkner D. Approximate assessment of the ultimate longitudinal strength of the hull girder. Journal of Ship Research Vol. 40, no. 1, 1996, pp.60-69.

[18] Hovgaard W. A new theory of the distribution of shearing stresses in riveted and welded connections and its application to discontinuities in the structure of ship, Trans. RINA, 1931, p. 108.

[19] Johnson AJ. Stresses in deckhouse and superstructure. T.I.N.A. Vol. 99, 1957, p. 634.

[20] Kutt LM, Piaszczyk CM and Chen YK. Evaluation of longitudinal ultimate strength of various ship hull configurations. SNAME Trans., Vol. 93, 1985, pp.33-55.

[21] Mansour AE, Yang JM and Thayamballi A. An experimental investigation of ship hull ultimate strength. SNAME Trans., Vol. 98, 1990, 411-439.

[22] Muckle W. The Influence of proportions on the behavior of partial superstructures constructed of aluminum alloy. Trans. RINA 1955, pp. 435-494.

[23] Naar H, Varsta P and Kujala P. A theory of coupled beams for strength assessment of passenger ships. Marine Structures, Vol.17, 2004, pp. 590-611.

[24] Nishihara S. Ultimate longitudinal strength of mid-ship cross-section. Naval Architecture and Ocean Engineering, Vol.22, no. 1, 1984, pp. 200-214.

[25] de Oliveira JG. Hull-deck Interaction. Chapter 3 in Ship Structural Design Concepts, Second Cycle, editor JH. Evans, Cornell Maritime Press, USA, 1983, p. 160-278.

[26] Ostapenko A. Strength of ship hull girders under moment, shear and torque. Proceedings of the SSC-SNAME Symposium on External Loads Response, Arlington, U.S.A., 1981, pp.149-166.

[27] Paik JK and Mansour AE. A simple formulation for predicting the Ultimate strength of ships. Journal of Marine Science and Tecnology 1, 1995, 52-62.

[28] Paik JK and Lee DH. Ultimate longitudinal strength-based safety and reliability assessment of ship's hull girder. Journal of the Society of Naval Architects of Japan, Vol. 168, 1990, pp. 395-407.

[29] Paik JK. Ultimate longitudinal strength-based safety and reliability assessment of ship's hull girder (2nd rteport)-stiffened hull structure. Journal of the Society of Naval Architects of Japan, Vol. 169, 1991, pp. 403-414.

[30] Paik JK, Kim DH, Bong HS, Kim MS and Han SK. Deterministic and probabilistic safety evaluation for a new double-hull tanker with transverseless system. SNAME Trans., Vol. 100, 1992, pp. 173-198.

[31] Paik JK. Ultimate hull girder strength analysis using Idealised Structural Unit Method: A case study for double hull girder with transverseless system. Proceedings of PRADS 92; the 5th International Symposium on Practical Design of Ships and Mobile Units, Vol. 2, 1992, pp. 745-763.

[32] Paik JK and Thayamballi AK. Ultimate Limit State Design of Steel Plated Structures, John Wiley and Sons, Chichester, U.K, 2003

[33] Reckling KA. Behaviour of box girders under bending and shear. Proceedings of ISSC 79. Paris, 1979, pp. II.2.46-II.2.49.

[34] Tagg R and Akbar R. Structural survivability of a modern passenger ship, Marine Technology, Vol. 41, No. 1, 2004, pp. 22-30.

[35] Smith CS. Influence of local compressive failure on ultimate longitudinal strength of a ship's hull. Proc. Int. Symp. on Practical Design in Shipbuilding, Tokyo, Japan, 1977, 73-79.

[36] Terazava K, Yagi J. The effect of superstructure on the strength of ship. J Soc Nav Archit Jpn 1957; 100, 101, 1958; 102,103, 1959, Vol. 105, 1960, Vol. 106

[37] Ueda Y, Rashed SMH and Paik JK. Plate and stiffened plate units of the idealised structural unit method – under inplane loading. Journal of the Society of Naval Architects of Japan, Vol. 156, 1984, pp. 366-376. (in Japanese).

[38] Vasta J. Lessons learned from full-scale ship structural tests. SNAME Trans., Vol. 66, 1958, pp. 165-243

[39] Yamakoshi M. On the stiffness factor of deck structure supported with transverse bulkheads. *Report of S.S.C. of Japan*, 1959.

[40] Yao T and Nikolov PI. Progressive collapse analyses of a ship's hull under longitudinal bending, Journal of the Society of Naval Architects of Japan, Vol. 170, 1991, pp. 449-461.

APPENDIX A EQUILIBRIUM EQUATIONS OF THE BEAM IN INCREMENTAL FORM

The equation of longitudinal equilibrium for a single beam can be presented also as

$$\frac{\partial}{\partial x}(N_i)+\sum_{j=1}^{n} s_{ij}=0\,. \qquad \textbf{(A.1)}$$

The incremental relation describes the change of axial force ΔN_i when the shear flows Δs_{ij} will change. For incremental relation it has to be assumed that the shear flows are independent from each other. Therefore, the derivation of Eq. **(A.1)** with respect to shear flow s_{i1} and multiplication with increment Δs_{i1} results

$$\frac{\partial}{\partial x}\left(\frac{\partial N_i}{\partial s_{i1}}\right)\Delta s_{i1}+\frac{\partial s_{i1}}{\partial s_{i1}}\Delta s_{i1}=0\,. \qquad \textbf{(A.2)}$$

The number of shear flows per single beam can be in maximum equal to n and due to this the total number of equations is equal to n either. All these equations can be summed and thus

$$\frac{\partial}{\partial x}\left(\sum_{j=1}^{n}\frac{\partial N_i}{\partial s_{ij}}\Delta s_{ij}\right)+\sum_{j=1}^{n}\frac{\partial s_{ij}}{\partial s_{ij}}\Delta s_{ij}=0\,. \qquad \textbf{(A.3)}$$

The left part from the expression located in brackets is the axial force increment ΔN_i and due to this Eq. (A.3) gets

$$\frac{\partial}{\partial x}(\Delta N_i)+\sum_{j=1}^{n}\Delta s_{ij}=0\,, \qquad \textbf{(A.4)}$$

which is the incremental form of the longitudinal equilibrium equation. All other equilibrium equations can be derived in a similar way.

APPENDIX B TANGENT STIFFNESS MATRIX

According to Galerkin's method the equilibrium equations are transferred to functional form. Multiplying the equilibrium equations with the weight functions and integrating all over the length the functional form can be achieved. Doing so the axial equilibrium equation is modified as

$$\int_{-1}^{1} u_i \frac{\partial \Delta N_i}{\partial x} d\xi + \int_{-1}^{1} u_i \sum_{j=1}^{n} \Delta s_{ij} d\xi = 0\,, \tag{B.1}$$

where u_i is the unknown axial displacement vector considered as weight function. Similarly the equation describing vertical force equilibrium is

$$\int_{-1}^{1} v_i^Q \frac{\partial \Delta Q_i}{\partial x} d\xi + \int_{-1}^{1} v_i^Q \sum_{j=1}^{n} \Delta p_{i,j} d\xi = \int_{-1}^{1} v_i^Q \Delta\lambda \cdot q_i d\xi\,, \tag{B.2}$$

where v_i^Q is the weight function. Also incremental moment equilibrium results as

$$\int_{-1}^{1} v_i^M \frac{\partial}{\partial x}\left(\frac{\partial \Delta M_i}{\partial x} + \sum_{j=1}^{n} C_{ij} \cdot \Delta s_{ij} \right) d\xi + \int_{-1}^{1} v_i^M \sum_{j=1}^{n} \Delta p_{ij} d\xi = \int_{-1}^{1} v_i^M \Delta\lambda \cdot q_i d\xi\,, \tag{B.3}$$

where v_i^M is corresponding weight function. The first term in Eq. (B.1) can be integrate by parts and gives

$$u_i \Delta N_i \Big|_{-1}^{1} + (-1) \int_{-1}^{1} \frac{\partial u_i}{\partial x} \Delta N_i d\xi + \int_{-1}^{1} u_i \sum_{j=1}^{n} \Delta s_{ij} d\xi = 0\,. \tag{B.4}$$

The equation (B.2) can be rewritten after integration as

$$v_i^Q \Delta Q_i \Big|_{-1}^{1} + (-1) \int_{-1}^{1} \frac{\partial v_i^Q}{\partial x} \Delta Q_i d\xi + \int_{-1}^{1} v_i^Q \sum_{j=1}^{n} \Delta p_{ij} d\xi = \int_{-1}^{1} v_i^Q \Delta\lambda \cdot q_i d\xi \tag{B.5}$$

and Eq. (B.3) as

$$\begin{aligned} & v_i^M \left(\frac{\partial \Delta M_i}{\partial x} + \sum_{j=1}^{n} C_{ij} \cdot \Delta s_{ij} \right) \Bigg|_{-1}^{1} + (-1) \frac{\partial v_i^M}{\partial x} \Delta M_i \Bigg|_{-1}^{1} + \int_{-1}^{1} \frac{\partial^2 v_i^M}{\partial x^2} \Delta M_i d\xi + \\ & + (-1) \int_{-1}^{1} \frac{\partial v_i^M}{\partial x} \sum_{j=1}^{n} C_{ij} \cdot \Delta s_{ij} d\xi + \int_{-1}^{1} v_i^M \sum_{j=1}^{n} \Delta p_{ij} d\xi = \int_{-1}^{1} v_i^M \Delta\lambda \cdot q_i d\xi, \end{aligned} \tag{B.6}$$

If the boundary conditions are taken into account the Eqs. (B.4), (B.5) and (B.6), will result

$$(-1) \int_{-1}^{1} \frac{\partial u_i}{\partial x} \Delta N_i d\xi + \int_{-1}^{1} u_i \sum_{j=1}^{n} \Delta s_{ij} d\xi = 0\,, \tag{B.7}$$

$$(-1) \int_{-1}^{1} \frac{\partial v_i^Q}{\partial x} \Delta Q_i d\xi + \int_{-1}^{1} v_i^Q \sum_{j=1}^{n} \Delta p_{ij} d\xi = \int_{-1}^{1} v_i^Q \Delta\lambda \cdot q_i d\xi \tag{B.8}$$

and

$$\int_{-1}^{1} \frac{\partial^2 v_i^M}{\partial x^2} \Delta M_i d\xi + (-1) \int_{-1}^{1} \frac{\partial v_i^M}{\partial x} \sum_{j=1}^{n} C_{ij} \cdot \Delta s_{ij} d\xi + \int_{-1}^{1} v_i^M \sum_{j=1}^{n} \Delta p_{ij} d\xi = \int_{-1}^{1} v_i^M \Delta\lambda \cdot q_i d\xi \,. \qquad \text{(B.9)}$$

Before the coupling forces $\Delta p_{i,j}$ and $\Delta s_{i,j}$ can be substituted into equilibrium equations they have to rearranged so that the unknown variables can be easily separated. Therefore, the suitable form for summations terms has to be found. By introducing matrices

$$T_{ij}^{A,t} = \begin{cases} -T_{ij}^t & if \quad j \neq i \\ \sum_{k=1}^{n} T_{ik}^t & if \quad j = i \end{cases}, \qquad \text{(B.10)}$$

$$T_{ij}^{B,t} = \begin{cases} T_{ij}^t C_{ij} & if \quad j \neq i \\ \sum_{k=1}^{n} T_{ik}^t C_{ik} & if \quad j = i \end{cases} \qquad \text{(B.11)}$$

and

$$T_{ij}^{C,t} = \begin{cases} -T_{ij}^t C_{ij} C_{ji} & if \quad j \neq i \\ \sum_{k=1}^{n} T_{ik}^t (C_{ik})^2 & if \quad j = i \end{cases}, \qquad \text{(B.12)}$$

the following summation terms can be written

$$\sum_{j=1}^{n} \Delta s_{ij} = (-1) \sum_{j=1}^{n} T_{ij}^{A,t} \Delta u_j + \sum_{j=1}^{n} \left(T_{ij}^{B,t}\right)^T \frac{\partial \Delta v_j^M}{\partial x} \qquad \text{(B.13)}$$

and

$$\sum_{j=1}^{n} C_{ij} \Delta s_{ij} = (-1) \sum_{j=1}^{n} T_{ij}^{B,t} \Delta u_j + \sum_{j=1}^{n} T_{ij}^{C,t} \frac{\partial \Delta v_j^M}{\partial x} \,. \qquad \text{(B.14)}$$

In the same way by introducing the matrix

$$K_{ij}^{A,t} = \begin{cases} -K_{ij}^t & if \quad j \neq i \\ \sum_{k=1}^{n} K_{ik}^t & if \quad j = i \end{cases} \qquad \text{(B.15)}$$

the summation term consisting vertical coupling force is rearranged.

$$\sum_{j=1}^{n} \Delta p_{ij} = (-1) \sum_{j=1}^{n} K_{ij}^{A,t} \Delta v_j^M + (-1) \sum_{j=1}^{n} K_{ij}^{A,t} \Delta v_j^Q \,. \qquad \text{(B.16)}$$

The final set of equilibrium equations can be obtained by substituting Eqs. (13), (14), (17) and (B.13), (B.14), (B.16) into Eqs. (B.7), (B.8), (B.9). Thereafter,

$$\int_{-1}^{1}\frac{\partial u_i}{\partial x}EA_{ii}^{t}\frac{\partial \Delta u_i}{\partial x}d\xi+(-1)\int_{-1}^{1}\frac{\partial u_i}{\partial x}EX_{ii}^{t}\frac{\partial^2 \Delta v_i^M}{\partial x^2}d\xi+\int_{-1}^{1}u_i\sum_{j=1}^{n}T_{ij}^{A,t}\Delta u_j d\xi+$$
$$+(-1)\int_{-1}^{1}u_i\sum_{j=1}^{n}\left(T_{ij}^{B,t}\right)^T\frac{\partial \Delta v_j^M}{\partial x}d\xi=0, \tag{B.17}$$

$$\int_{-1}^{1}\frac{\partial v_i^Q}{\partial x}GA_{ii}^{S,t}\cdot\frac{\partial \Delta v_i^Q}{\partial x}d\xi+\int_{-1}^{1}v_i^Q\sum_{j=1}^{n}K_{ij}^{A,t}\Delta v_j^M d\xi+\int_{-1}^{1}v_i^Q\sum_{j=1}^{n}K_{ij}^{A,t}\Delta v_j^Q d\xi=$$
$$=(-1)\int_{-1}^{1}v_i^Q\Delta\lambda\cdot q_i d\xi \tag{B.18}$$

and

$$\int_{-1}^{1}\frac{\partial^2 v_i^M}{\partial x^2}EI_{ii}^{t}\frac{\partial^2 \Delta v_i^M}{\partial x^2}d\xi+(-1)\int_{-1}^{1}\frac{\partial^2 v_i^M}{\partial x^2}EX_{ii}^{t}\frac{\partial \Delta u_i}{\partial x}d\xi+$$
$$+(-1)\int_{-1}^{1}\frac{\partial v_i^M}{\partial x}\sum_{j=1}^{n}T_{ij}^{B,t}\Delta u_j d\xi+\int_{-1}^{1}\frac{\partial v_i^M}{\partial x}\sum_{j=1}^{n}T_{ij}^{C,t}\frac{\partial \Delta v_j^M}{\partial x}d\xi+$$
$$+\int_{-1}^{1}v_i^M\sum_{j=1}^{n}K_{ij}^{A,t}\Delta v_j^Q d\xi+\int_{-1}^{1}v_i^M\sum_{j=1}^{n}K_{ij}^{A,t}\Delta v_j^M d\xi=$$
$$=(-1)\int_{-1}^{1}v_i^M\Delta\lambda\cdot q_i d\xi \tag{B.19}$$

Above presented equations are written for beam number i. In case of n beams the total set of equations can be given in matrix form as

$$\int_{-1}^{1}\left\{\frac{\partial u}{\partial x}\right\}^T\left[EA^t\right]\left\{\frac{\partial \Delta u}{\partial x}\right\}d\xi+(-1)\int_{-1}^{1}\left\{\frac{\partial u}{\partial x}\right\}^T\left[EX^t\right]\left\{\frac{\partial^2 \Delta v^M}{\partial x^2}\right\}d\xi+\int_{-1}^{1}\{u\}^T\left[T^{A,t}\right]\{\Delta u\}d\xi+$$
$$+(-1)\int_{-1}^{1}\{u\}^T\left[T^{B,t}\right]^T\left\{\frac{\partial \Delta v^M}{\partial x}\right\}d\xi=0, \tag{B.20}$$

$$\int_{-1}^{1}\left\{\frac{\partial v^Q}{\partial x}\right\}^T\left[GA^{S,t}\right]\left\{\frac{\partial \Delta v^Q}{\partial x}\right\}d\xi+\int_{-1}^{1}\left\{v^Q\right\}^T\left[K^{A,t}\right]\{\Delta v^M\}d\xi+\int_{-1}^{1}\left\{v^Q\right\}^T\left[K^{A,t}\right]\{\Delta v^Q\}d\xi=$$
$$=(-1)\int_{-1}^{1}\left\{v^Q\right\}^T\Delta\lambda\cdot\{q\}d\xi \tag{B.21}$$

and

$$\int_{-1}^{1}\left\{\frac{\partial^2 v^M}{\partial x^2}\right\}^T\left[EI^t\right]\left\{\frac{\partial^2 \Delta v^M}{\partial x^2}\right\}d\xi+(-1)\int_{-1}^{1}\left\{\frac{\partial^2 v^M}{\partial x^2}\right\}^T\left[EX^t\right]\left\{\frac{\partial \Delta u}{\partial x}\right\}d\xi+$$
$$+(-1)\int_{-1}^{1}\left\{\frac{\partial v^M}{\partial x}\right\}^T\left[T^{B,t}\right]\{\Delta u\}d\xi+\int_{-1}^{1}\left\{\frac{\partial v^M}{\partial x}\right\}^T\left[T^{C,t}\right]\left\{\frac{\partial \Delta v^M}{\partial x}\right\}d\xi+ \tag{B.22}$$
$$+\int_{-1}^{1}\{v^M\}^T\left[K^{A,t}\right]\{\Delta v^Q\}d\xi+\int_{-1}^{1}\{v^M\}^T\left[K^{A,t}\right]\{\Delta v^M\}d\xi=$$
$$=(-1)\int_{-1}^{1}\{v^M\}\Delta\lambda\{q\}d\xi.$$

The unknown variables are approximated as linear combination of known functions $B(\xi)_1 \ldots B(\xi)_m$ and unknown constants $\Delta c_1 \ldots \Delta c_m$. Therefore, the displacement increments are given as

$$\{\Delta u\}=[B_u]\{\Delta c^u\}, \tag{B.23}$$

$$\{\Delta v^Q\}=[B_v^Q]\{\Delta c_v^Q\} \tag{B.24}$$

and

$$\{\Delta v^M\}=[B_v^M]\{\Delta c_v^M\}. \tag{B.25}$$

The tangent stiffness matrix for the total system is obtained by substituting the Eqs. (B.23) - (B.25) into equilibrium equations (B.20) - (B.22). Doing so we obtain

$$\begin{bmatrix} D_{11} & D_{12} & 0 \\ D_{12}{}^T & D_{22} & D_{23} \\ 0 & D_{23}{}^T & D_{33} \end{bmatrix}\begin{Bmatrix} \Delta c_u \\ \Delta c_v^M \\ \Delta c_v^Q \end{Bmatrix}=\Delta\lambda\begin{Bmatrix} 0 \\ F^M \\ F^Q \end{Bmatrix}, \tag{B.26}$$

where

$$[D_{11}]=\int_{-1}^{1}\frac{\partial}{\partial x}[B_u]^T\left[EA^t\right]\frac{\partial}{\partial x}[B_u]d\xi+\int_{-1}^{1}[B_u]^T\left[T^{A,t}\right][B_u]d\xi, \tag{B.27}$$

$$[D_{12}]=(-1)\int_{-1}^{1}\frac{\partial}{\partial x}[B_u]^T\left[EX^t\right]\frac{\partial^2}{\partial x^2}\left[B_v^M\right]d\xi+(-1)\int_{-1}^{1}[B_u]^T\left[T^{B,t}\right]^T\frac{\partial}{\partial x}\left[B_v^M\right]d\xi, \tag{B.28}$$

$$[D_{22}]=\int_{-1}^{1}\frac{\partial^2}{\partial x^2}\left[B_v^M\right]^T\left[EI^t\right]\frac{\partial^2}{\partial x^2}\left[B_v^M\right]d\xi+\int_{-1}^{1}\frac{\partial}{\partial x}\left[B_v^M\right]^T\left[T^{C,t}\right]\frac{\partial}{\partial x}\left[B_v^M\right]d\xi+$$
$$+\int_{-1}^{1}\left[B_v^M\right]^T\left[K^{A,t}\right]\left[B_v^M\right]d\xi, \tag{B.29}$$

$$[D_{23}] = \int_{-1}^{1} [B_v^M]^T [K^{A,t}][B_v^Q] d\xi \,, \tag{B.30}$$

$$[D_{33}] = \int_{-1}^{1} \frac{\partial}{\partial x}[B_v^Q]^T [GA^{S,t}] \frac{\partial}{\partial x}[B_v^Q] d\xi + \int_{-1}^{1} [B_v^Q]^T [K^t][B_v^Q] d\xi \tag{B.31}$$

are the sub-matrices and

$$\{F^M\} = (-1)\int_{-1}^{1} [B_v^M]\{q\} d\xi \,, \tag{B.32}$$

$$\{F^Q\} = (-1)\int_{-1}^{1} [B_v^Q]\{q\} d\xi \tag{B.33}$$

are the sub-vectors.

APPENDIX C EQUILIBRIUM EQUATIONS FOR TOTAL SYSTEM

The final shape of equilibrium equations used in solution correction is given as

$$\begin{Bmatrix} F_1^A \\ F_2^A \\ F_3^A \end{Bmatrix} + \begin{Bmatrix} F_1^B \\ F_2^B \\ F_3^B \end{Bmatrix} = (\lambda + \Delta\lambda) \begin{Bmatrix} 0 \\ F^M \\ F^Q \end{Bmatrix}, \tag{C.1}$$

where

$$F_1^A = \int_{-1}^{1} \frac{\partial}{\partial x}[B_u]^T \{N + \Delta N\} d\xi \,, \tag{C.2}$$

$$F_2^A = (-1)\int_{-1}^{1} \frac{\partial^2}{\partial x^2}[B_v^M]^T \{M + \Delta M\} d\xi \,, \tag{C.3}$$

$$F_3^A = (-1)\int_{-1}^{1} \frac{\partial}{\partial x}[B_v^Q]^T \{Q + \Delta Q\} d\xi \tag{C.4}$$

and

$$F_1^B = (-1)\int_{-1}^{1} [B_u]^T \{S + \Delta S\} d\xi \,, \tag{C.5}$$

$$F_2^B = \int_{-1}^{1} \frac{\partial}{\partial x} \left[B_v^M\right]^T \left\{S^C + \Delta S^C\right\} d\xi + (-1)\int_{-1}^{1} \left[B_v^M\right]^T \{P + \Delta P\} d\xi \,, \tag{C.6}$$

$$F_3^B = (-1)\int_{-1}^{1} \left[B_v^Q\right]^T \{P + \Delta P\} d\xi \,. \tag{C.7}$$

APPENDIX D TANGENT STIFFNESS FOR BENDING AND LONGITUDINAL ELONGATION

According to Crisfield [9] the axial displacement in a beam cross-section can be estimated as

$$u(x,y) = u_0 - y\frac{\partial v}{\partial x}, \tag{D.1}$$

where u_0 is the axial displacement of the beam measured at reference line. For small displacements we can assume that the axial deformation in beam is obtained as

$$\varepsilon_x = \frac{\partial u(x,y)}{\partial x} = \frac{\partial u_0}{\partial x} - y\frac{\partial^2 v}{\partial x^2} \,. \tag{D.2}$$

By considering Eq. (62) and assuming that previous Eq. can be presented also in an incremental forma the relation between the increase of normal stress and displacement can be obtained. Hereafter the axial displacement u_0 defined at reference line is marked as u instead and doing so

$$\Delta\sigma_x = E_t\left(\frac{\partial \Delta u_0}{\partial x} - y\frac{\partial^2 \Delta v}{\partial x^2}\right). \tag{D.3}$$

Now also internal force increments ΔN and ΔM can be estimated on the bases of normal stress as follows

$$\Delta N = \int_A \Delta\sigma_x dA = \int_A E_t dA\, \frac{\partial \Delta u}{\partial x} + (-1)\int_A E_t y dA\, \frac{\partial^2 \Delta v}{\partial x^2} \tag{D.4}$$

and

$$\Delta M = -\int_A \Delta\sigma_x y dA = \int_A E_t y dA \frac{\partial \Delta u_0}{\partial x} + (-1)\int_A y^2 dA \frac{\partial^2 \Delta v}{\partial x^2}. \quad \text{(D.5)}$$

The comparison of Eqs. (76) and (82) with Eqs. (13) and (14) gives the following definitions for tangent stiffness parameters defining bending and axial elongation of beam. Thus

$$EA^t = \int_A E_t dA \ , \quad \text{(D.6)}$$

$$EI^t = \int_A E_t y dA \quad \text{(D.7)}$$

and

$$EX^t = \int_A E_t y dA \ . \quad \text{(D.8)}$$

APPENDIX E LOAD-END SHORTENING CURVES

According to reference [2] the equation describing the load-end shortening curve for the elasto-plastic collapse of hard corners in tension and in compression and longitudinally or transversally stiffened plate in tension is to be obtained from the following formula:

$$\sigma_{CR0} = \Phi\sigma_Y . \quad \text{(E.1)}$$

The stiffened plate member is composed of stiffener to it attached plate strip. According to assumptions the stiffened plate member can collapse due to beam column buckling described with Euler column buckling stress, due to torsional buckling or due to web local buckling of ordinary stiffener. The relevant collapse mode is chosen as one of three above mentioned collapse modes where the mode with minimum stress value will occur.

The equation describing the load-end shortening curve for the beam column buckling of ordinary stiffeners composing the hull girder transverse section is to be obtained from the following formula:

$$\sigma_{CR1} = \Phi\sigma_{C1}\frac{A_S + b_e t}{A_S + bt}, \quad \text{(E.2)}$$

where Φ is the edge function defined in (60), σ_{C1} is the critical stress, b_e is the effective breath of the attached shell plating, b is the stiffeners spacing and t is the thickness of plating. The critical stress can be determined from equation

$$\sigma_{C1} = \begin{cases} \dfrac{\sigma_{E1}}{\varepsilon_R} & if \quad \sigma_{E1} \le \dfrac{\sigma_Y}{2}\varepsilon_R \\ \sigma_Y\left(1 - \dfrac{\Phi\sigma_Y\varepsilon_R}{4\sigma_{E1}}\right) & if \quad \sigma_{E1} > \dfrac{\sigma_Y}{2}\varepsilon_R \end{cases}, \tag{E.3}$$

where σ_{E1} is the Euler buckling stress which is defined as

$$\sigma_{E1} = \pi^2 E \frac{I_E}{A_E l^2}, \tag{E.4}$$

where I_E is net moment of inertia of ordinary stiffeners with attached shell plating of with b_{e1}, A_E is the net sectional area of ordinary stiffeners with attached shell plating of with b_e and l is the span of stiffener. By defining the plate slenderness parameter

$$\beta_e = \frac{b}{t}\sqrt{\frac{\varepsilon_R\sigma_Y}{E}} \tag{E.5}$$

it is possible to calculate the effective breadth for net moment of inertia and sectional area. The effective breadth for net moment of inertia of ordinary stiffeners with attached plating is defined as

$$b_{e1} = \begin{cases} \dfrac{b}{\beta_e} & if \quad \beta_e > 1.0 \\ b & if \quad \beta_e \le 1.0 \end{cases}. \tag{E.6}$$

The effective breadth for net sectional area of ordinary stiffeners with attached plating is defined as

$$b_e = b \cdot g. \tag{E.7}$$

where

$$g = \begin{cases} \left(\dfrac{2.25}{\beta_e} - \dfrac{1.25}{\beta_e^{\,2}}\right) & if \quad \beta_e > 1.25 \\ 1 & if \quad \beta_e \le 1.25 \end{cases}. \tag{E.8}$$

The equation describing the load-end shortening curve for the lateral-flexural buckling of ordinary stiffeners composing the hull girder transverse section is to be obtained according to the following formula

$$\sigma_{CR2} = \Phi \frac{A_S \sigma_{C2} + bt\sigma_{CP}}{A_S + bt}, \tag{E.9}$$

where σ_{C2} is the critical stress which is defined according to Eq. (E.3) where σ_{E1} is replaced by Euler torsional buckling stress σ_{E2}. The stress σ_{CP} in Eq. (E.9) is the buckling stress of attached plating, which is given as

$$\sigma_{CP} = \sigma_Y \cdot g\,. \tag{E.10}$$

According to theory the Euler torsional buckling stress can be estimated as

$$\sigma_{E2} = \frac{\pi^2 E I_w}{I_p L^2}\left(\frac{K_C}{m^2} + m^2\right) + 0.358E\frac{I_t}{I_p}, \tag{E.11}$$

where I_w is net sectorial moment of inertia of the stiffener about its connection to the attached plating and can be calculated for various members like for flat bars:

$$I_w = \frac{h_w{}^3 t_w{}^3}{36}, \tag{E.12}$$

for T-sections:

$$I_w = \frac{t_f b_f{}^3 h_w{}^2}{12} \tag{E.13}$$

and for angles or bulb sections:

$$I_w = \frac{b_f{}^3 h_w{}^2}{12(b_f + h_w)^2}\left[t_f b_f{}^2 + 2b_f h_w + 4h_w{}^2 + 3t_w b_f h_w\right]. \tag{E.14}$$

The parameters t_f and t_w define the flange and web plate thickness and b_f and h_w are the breadth of the flange plate and the height of the web plate.

The net polar moment of inertia I_p of the stiffener about its connection to the attached plating can be calculated for flat bars as:

$$I_p = \frac{h_w{}^3 t_w}{3} \tag{E.15}$$

and for stiffeners with face plate:

$$I_p = \frac{h_w{}^3 t_w}{3} + h_w{}^2 b_f t_f\,. \tag{E.16}$$

The St. Venant's net moment of inertia I_t of the stiffener used in Eq. (E.11) and consisting no attached plating, can be estimated for flat bars as:

$$I_t = \frac{h_w t_w^{\ 3}}{3} \tag{E.17}$$

and for stiffeners with flange:

$$I_t = \frac{1}{3}\left[h_w t_w^{\ 3} + b_f t_f^{\ 3}\left(1 - 0.63\frac{t_f}{b_f}\right)\right]. \tag{E.18}$$

The parameter m in Euler torsional buckling stress equation is the number of half waves is to be taken equal to the integer number such that

$$m^2(m-1)^2 \le K_C < m^2(m+1)^2, \tag{E.19}$$

where

$$K_C = \frac{C_0 L^4}{\pi^2 E I_w}, \tag{E.20}$$

where C_0 is the stiffness of the attached plating and is calculated as

$$C_0 = \frac{Et^3}{2.73b}. \tag{E.21}$$

The equation describing the load-end shortening curve for the web local buckling of flanged ordinary stiffeners composing the hull girder transverse section is to be obtained from the following formula:

$$\sigma_{CR3} = \Phi\sigma_Y \frac{b_e t + h_{we} t_w + b_f t_f}{bt + h_w t_w + b_f t_f}, \tag{E.22}$$

where h_{we} is the effective height of the web given as

$$h_{we} = \begin{cases} h_w\left(\dfrac{2.25}{\beta_e} - \dfrac{1.25}{\beta_e^{\ 2}}\right) & if \quad \beta_w > 1.25 \\ h_w & if \quad \beta_w \le 1.25 \end{cases}, \tag{E.23}$$

where

$$\beta_w = 10^3 \frac{h_w}{t_w}\sqrt{\frac{\varepsilon_R \sigma_Y}{E}}. \tag{E.24}$$

The equation describing the load-end shortening curve for the web local buckling of flat bar ordinary stiffeners composing the hull girder transverse section is to be obtained from the following formula:

$$\sigma_{CR4} = \Phi \frac{bt\sigma_{CP} + h_w t_w \sigma_{C4}}{bt + h_w t_w}, \tag{E.25}$$

where σ_{C4} is the critical buckling stress for stiffener web and can be calculated from Eq. (E.3) where instead of buckling stress σ_{E4} the local Euler buckling stress has to be used. This buckling stress is obtained as

$$\sigma_{E4} = 160 \cdot 10^3 \left(\frac{t_w}{h_w} \right)^2. \tag{E.26}$$

The equation describing the load-end shortening curve for the buckling of transversely stiffened panels composing the hull girder transverse section is to be obtained from the following formula:

$$\sigma_{CR5} = \Phi \sigma_Y \left[\frac{b}{l} \left(\frac{2.25}{\beta_e} - \frac{1.25}{\beta_e^2} \right) + 0.1 \left(1 - \frac{b}{L} \right) \left(1 + \frac{1}{\beta_e^2} \right)^2 \right]. \tag{E.27}$$

APPENDIX F TANGENT STIFFNESS FOR SHEAR COUPLING

It is assumed that the shear member can function in two possible modes, which are the elastic mode and post-buckling mode. In order to model the behaviour both modes have to be described analytically. In the present appendix the elastic behaviour is under consideration. It can be supposed that the elastic behaviour is cleared when the shear stiffness is successfully determined. The stiffened plate field with the opening is presented in Figure 53. This plate structure is working as coupling member between two deck structures moving in a parallel direction with respect to each other. Therefore the shear force, is applied on the upper boundary and the lower boundary is clamped to ground. Stiffeners are not directly considered as there shear stiffness is very small compared to stiffness of the plate. According to assumption three deformation fields are present in member denoted as 1, 2 and 3 in Figure 53.

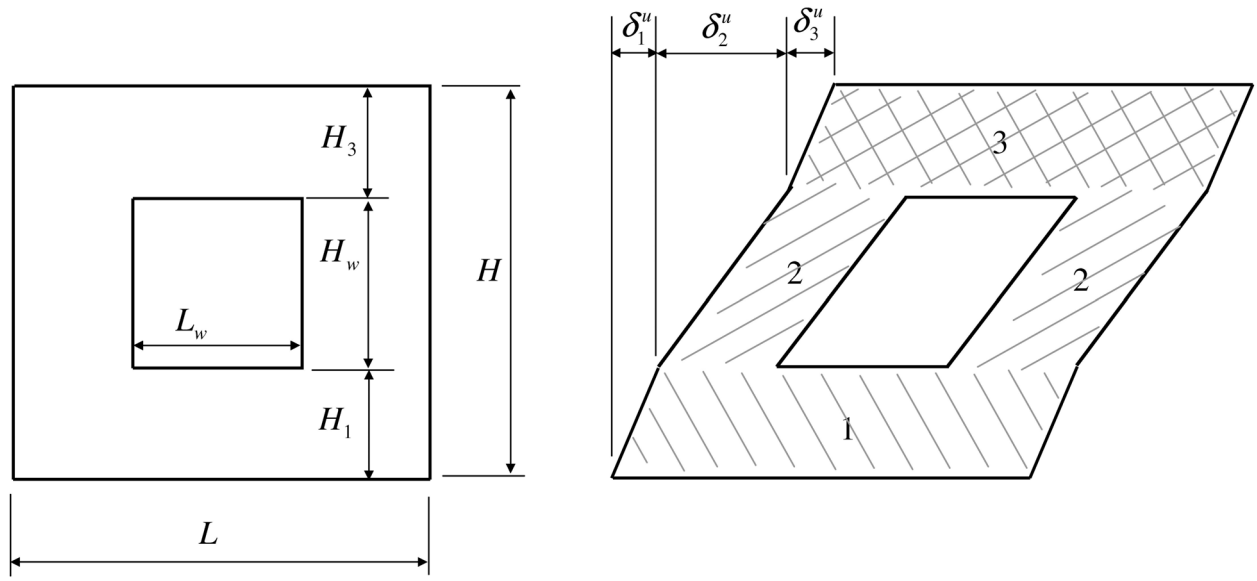

Figure 53. Deformation mode of the shear member.

The shear stiffness per unit length is defined as

$$T = \frac{s}{\delta_u} \ , \tag{F.1}$$

where s is the shear flow acting as a shear force per unit length in upper boundary of the member and δ_u is the total displacement of the upper boundary with respect to the lower boundary. Each plate field has to carry the same load but the deformations will be different. The shear deformation in field 1 is therefore estimated as

$$\gamma_1 = \frac{\delta_1^u}{H_1} \ , \ \gamma_2 = \frac{\delta_2^u}{H_w} \text{ and } \gamma_3 = \frac{\delta_3^u}{H_3} \tag{F.2}$$

The same shear force F^s is producing deformations in regions 1, 2 and 3 and therefore the following relations can be presented for those deformation regions

$$\frac{F^s}{Lt} = G\gamma_1 = G\frac{\delta_1^u}{H_1} \ , \ \frac{F^s}{(L-L_w)t} = G\gamma_2 = G\frac{\delta_2^u}{H_w} \text{ and } \frac{F^s}{Lt} = G\gamma_3 = G\frac{\delta_3^u}{H_3} \tag{F.3}$$

where G is the shear modulus of the plate material and t is the plate thickness. All the other parameters are defined in Figure 53. In case when the window opening is very large the region 2 becomes narrow and therefore this region could additionally have a bending deformation mode, which is producing additional displacement δ_b^u equal to

$$\delta_b^u = \frac{F^s H_w^{\,3}}{12EI} \ , \tag{F.4}$$

where E is the elastic modulus and I is the moment of inertia of the cross-section obtained by cutting the area between window openings. For this moment of inertia all vertical members like stiffeners and girders placed between window boundaries have to be considered together with plating. The total displacement δ^u can be now determined using relations defined in (F.3) and in (F.4). Thus

$$\delta^u = \left(\frac{H_1}{GLt} + \frac{H_w^{\,3}}{12EI} + \frac{H_w}{G(L-L_w)t} + \frac{H_3}{GLt} \right) F^s \ , \tag{F.5}$$

Thereafter, by using Eqs. (F.5) and (F.1) the shear stiffness per unit length can be determined as

$$T = \frac{1}{\dfrac{H-H_w}{Gt} + \dfrac{H_w^{\,3} L}{12EI} + \dfrac{H_w L}{G(L-L_w)t}} \ . \tag{F.6}$$

ISBN 951-22-8028-0
ISBN 951-22-8029-9 (PDF)
ISSN 1795-2239
ISSN 1795-4584 (PDF)